วิธีการบรรเทาการเพิ่มขึ้นของแรงดันภายใต้ภาวะแรงดันไม่ได้ดุลสำหรับระบบผลิตไฟฟ้าจากเซลล์แสงอาทิตย์แบบเชื่อมต่อกับโครงข่ายไฟฟ้า

นางสาวลีซอง เอือง

วิทยานิพนธ์นี้เป็นส่วนหนึ่งของการศึกษาตามหลักสูตรปริญญาวิศวกรรมศาสตรมหาบัณฑิต
สาขาวิชาวิศวกรรมไฟฟ้า ภาควิชาวิศวกรรมไฟฟ้า
คณะวิศวกรรมศาสตร์ จุฬาลงกรณ์มหาวิทยาลัย
ปีการศึกษา 2558

A Voltage Rise Mitigation Strategy under Voltage Unbalance for a Grid-Connected Photovoltaic System

Miss Lysorng Oeng

A Thesis Submitted in Partial Fulfillment of the Requirements
for the Degree of Master of Engineering Program in Electrical Engineering
Department of Electrical Engineering
Faculty of Engineering
Chulalongkorn University
Academic Year 2015

Thesis Title	A Voltage Rise Mitigation Strategy under Voltage Unbalance for a Grid-Connected Photovoltaic System
By	Miss Lysorng Oeng
Field of Study	Electrical Engineering
Thesis Advisor	Assistant Professor Somboon Sangwongwanich, D. Eng.

Accepted by the Faculty of Engineering, Chulalongkorn University in Partial Fulfillment of the Requirements for the Master's Degree

.....Dean of the Faculty of Engineering
(Associate Professor Supot Teachavorasinskun, D. Eng.)

THESIS COMMITTEE

.....Chairman
(Assistant Professor Surapong Suwankawin, Ph.D.)
.....Thesis Advisor
(Assistant Professor Somboon Sangwongwanich, D. Eng.)
.....External Examiner
(Sompob Polmai, Ph.D.)

ลีซอง เอือง : วิธีการบรรเทาการเพิ่มขึ้นของแรงดันภายใต้ภาวะแรงดันไม่ได้ดุลสำหรับระบบผลิตไฟฟ้าจากเซลล์แสงอาทิตย์แบบเชื่อมต่อกับโครงข่ายไฟฟ้า (A Voltage Rise Mitigation Strategy under Voltage Unbalance for a Grid-Connected Photovoltaic System) อ.ที่ปรึกษาวิทยานิพนธ์หลัก: ผศ. ดร.สมบูรณ์ แสงวงค์วาณิชย์, 99 หน้า.

ปัญหาหลักของแหล่งผลิตไฟฟ้าจากเซลล์แสงอาทิตย์ที่แพร่หลายมากขึ้นคือการเพิ่มขึ้นของแรงดันเนื่องจากการจ่ายกำลังไฟฟ้าจากระบบผลิตไฟฟ้าจากเซลล์แสงอาทิตย์เข้าสู่โครงข่ายไฟฟ้า นอกจากนี้จากการสังเกตโดยทั่วไปยังพบว่าแรงดันที่จุดเชื่อมต่อร่วม (point of common coupling; PCC) มักจะไม่ได้ดุลเนื่องจากโหลดในระบบไฟฟ้าไม่สมดุล สำหรับวิธีที่ได้รับความนิยมในการแก้ไขปัญหาการเพิ่มขึ้นของแรงดันคือการฉีดกำลังรีแอกทีฟเพื่อปรับตัวประกอบกำลัง อย่างไรก็ตามวิธีนี้ไม่เหมาะสมในเชิงเศรษฐศาสตร์ เนื่องจากเจ้าของแหล่งผลิตไฟฟ้าจากเซลล์แสงอาทิตย์อาจมีค่าใช้จ่ายในการฉีดกำลังรีแอกทีฟให้กับการไฟฟ้า ในส่วนของปัญหาแรงดันไม่ได้ดุลนั้น งานวิจัยเพื่อการชดเชยแรงดันไม่ได้ดุลปกติมีจุดประสงค์เพื่อปรับปรุงคุณภาพกำลังไฟฟ้าเพียงอย่างเดียวโดยไม่ได้พิจารณาว่าแรงดันไม่ได้ดุลไม่มีความสัมพันธ์กับปัญหาการเพิ่มขึ้นของแรงดันแต่อย่างใด ดังนั้นโดยทั่วไปการแก้ปัญหาการเพิ่มขึ้นของแรงดันและปัญหาแรงดันไม่ได้ดุลในระบบไฟฟ้าจะพิจารณาแยกอิสระจากกัน

วิทยานิพนธ์ฉบับนี้จะแสดงให้เห็นว่า โดยปกติแล้วแรงดันไม่ได้ดุลส่งผลอย่างมีนัยสำคัญต่อค่าสูงสุดของแรงดันระหว่างสายซึ่งใช้เป็นเกณฑ์บ่งบอกถึงการเพิ่มขึ้นของแรงดันหรือแรงดันเกิน ดังนั้นการเพิ่มขึ้นของแรงดันเกินขีดจำกัดจึงมีสาเหตุมาจากสองปัจจัยได้แก่ การไหลย้อนของกำลังไฟฟ้า (reverse power flow) และแรงดันไม่ได้ดุล จากปัจจัยข้างต้นวิทยานิพนธ์นี้จึงนำเสนอการแก้ไขปัญหาแรงดันเพิ่มขึ้นในระบบโดยเสนอให้ชดเชยแรงดันไม่ได้ดุลด้วยการฉีดกระแสลำดับลบ (negative-sequence current) เพื่อลดค่าสูงสุดของแรงดันระหว่างสายเป็นอันดันแรก หากแรงดันในระบบสามารถกลับสู่ภายใต้ขีดจำกัดได้ก็ไม่ต้องดำเนินมาตรการใดๆ เพิ่มเติม แต่หากแรงดันยังคงสูงเกินขีดจำกัดอยู่ จึงค่อยใช้การฉีดกำลังรีแอกทีฟและ/หรือการลดทอนกำลังจริงตามจำเป็นในการแก้ไขปัญหาแรงดันเพิ่มขึ้นต่อไป

ภาควิชา วิศวกรรมไฟฟ้า ลายมือชื่อนิสิต .....

สาขาวิชา วิศวกรรมไฟฟ้า ลายมือชื่อ อ.ที่ปรึกษาหลัก .....

ปีการศึกษา 2558

5770528621 : MAJOR ELECTRICAL ENGINEERING
KEYWORDS: GRID-CONNECTED PHOTOVOLTAIC INVERTER, UNBALANCED VOLTAGE, VOLTAGE RISE, NEGATIVE SEQUENCE CURRENT INJECTION, REACTIVE CURRENT, POWER CURTAILMENT

LYSORNG OENG: A Voltage Rise Mitigation Strategy under Voltage Unbalance for a Grid-Connected Photovoltaic System. ADVISOR: ASST. PROF. SOMBOON SANGWONGWANICH, D. Eng., 99 pp.

The voltage rise due to the injection of power from a photovoltaic (PV) system into the power system network is a major problem for high penetration of PV generation. It is also observed that the voltages at the point of common coupling (PCC) are usually unbalanced due to the unbalanced loads in the system. One popular method to solve the voltage rise problem is by injection of reactive power to adjust the power factor. However, this is uneconomic because the PV owner may be charged by the utility for the injected reactive power. On the other hand, although some works have been done on unbalanced voltage compensation, their objective is purely to improve the power quality and has nothing to do with the voltage rise problem. Therefore, in general, the voltage rise and voltage unbalance are treated as two unrelated issues.

In this thesis, it will be revealed that voltage unbalance usually contributes significantly to the maximum line-to-line voltage which is the criterion for voltage rise or overvoltage. Therefore, the voltage rise over the limit is in fact caused by two factors; the reverse power flow and the voltage unbalance. With this understanding, it is proposed in this thesis that cancellation of voltage unbalance by negative-sequence current injection should be done first to reduce the maximum line-to-line voltage. And if this measure helps to bring the voltage back within the limit, then no further action is needed. Otherwise, additional reactive power injection and/or active power curtailment may be necessary.

Department: Electrical Engineering Student's Signature .....
Field of Study: Electrical Engineering Advisor's Signature .....
Academic Year: 2015

ACKNOWLEDGEMENTS

This thesis work has been carried out during the year 2014-2016 in Power Electronic Research Laboratory (PERL), Department of Electrical Engineering, Chulalongkorn University. The supervisor of the thesis is Assistant Professor Dr. Somboon Sangwongwanich to whom I would like to express my sincere gratitude. Without his guidance; support; encouragement, and valuable contributions, this work could not have been done successfully.

The financial support provided by ASEAN University Network/ Southeast Asia Engineering Education Development Network (AUN/SEED-Net) Program of Japan International Cooperation Agency(JICA) is gratefully appreciated.

My sincere thanks go to the committee of the thesis examination including Assistant Professor Dr. Surapong Suwankawin and Dr. Sompob Polmai for their valuable time, comments, suggestions and discussions in order to fulfill my work. Additionally, I would like to thank to all of my friends in Power Electronic Research Laboratory for their encouragement and kind help during my research work.

Finally, I would like to express my gratitude to my family for their unconditional love and support during my studies and throughout my whole life.

CONTENTS

Page

Page

LIST OF TABLES

LIST OF FIGURES

1 Introduction

1.1 Background and Motivation

The rising price and limitation of conventional energy such as fossil fuels, and the environmental impacts due to the emission of carbon dioxide have brought to the use of renewable resources such as solar and wind energy. The renewable resources, however, widely depend on the geographical areas and local conditions. In Thailand, the solar energy has gained more interest than the wind energy, and there are a lot of researches focusing on it.

The integration of renewable energy into the conventional grids is mostly done at the distribution level. Renewable energy and conventional grid are usually coupled via the power converter interface. There are three main objectives for utilization of power converters, i.e., grid-forming, grid-feeding and grid-supporting. The connection of renewable energy into the distribution system may bring some problems such as voltage rise, increased harmonic distortion, and frequency deviation. These issues can cause severe problems on equipment [1], or can lead to unintentional trip of a power generator. Grid codes have been introduced in several countries in order to prevent the aforementioned problems [2]. In the case of Thailand, the maximum limit of the voltage rise is set at 5% in normal operation and 10% in emergency operation in order to prevent unpredicted problems [3]. On the other hand, the allowable threshold for unbalanced voltage has been limited to 2% in the low voltage system and to 1.8% in the medium voltage distribution system [3].

Voltage rise and voltage unbalance are often considered as the most severe problems in the power system with integration of renewable energy. Numerous studies have been done focusing on the mitigation of voltage rise and reduction of voltage unbalance for high penetration of PV systems. Some typical strategies to solve the voltage rise and voltage unbalance are briefly reviewed in the following paragraphs.

The tap position control of the automatic voltage regulator (AVR) or on-load tap changer (OLTC) as shown in Fig. 1 can be used to maintain the voltage within the acceptable range [4]. However, it might take up to several minutes to regulate the voltage due to the slow mechanism of the tap changer. Moreover, frequent use of the tap-change mechanism could reduce the life time of the transformer.

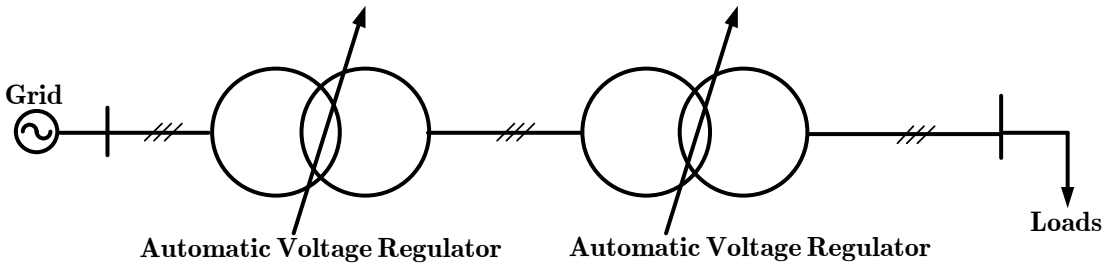

Fig. 1. Voltage control in a distribution feeder.

Reactive power control in Fig. 2 is the popular and effective method for solving voltage rise problem [4, 5]. The reactive power injection can be used to successfully bring the voltage into the limit without reducing the production of the active power from PV farms, unless the capacity of inverter is insufficient for compensation. However, the PV owner may be charged by the utility for the injection of the reactive power into the system. Apart from the injection of reactive power, power curtailment is another alternative solution [3, 6] to reduce the overvoltage. The active power curtailment seems to be very attractive because it could reduce overvoltage effectively. It is, however, an undesirable method for the PV owner, because the reduction of power means loss of the revenue. Therefore, it is preferable if the voltage rise problem can be alleviated by a controller which avoids as much as possible the injection of reactive power and power curtailment.

Fig. 2. Reactive power injection and power curtailment from a PV system.

Battery storage can also be used to store the excess energy from the PV, which, as a consequence, results in voltage reduction at the bus. This concept is attractive since PV owners can generate more revenue. However, the high cost of the battery storage system is the main obstacle to commercialization of this concept. Batteries of electric vehicles [5] have also been considered for this purpose, but the practical realization does not yet exist.

It should be mentioned that the techniques for mitigation of voltage rise problem proposed so far are for the balanced system [3-7]. However, in the real power system,

a certain amount of voltage unbalance always exists. When the voltage is unbalanced, the line-to-line voltages are not equal and this may increase the voltage rise in the system. The fact that voltage unbalance affects voltage rise has never been taken into consideration so far by most researchers. In general, the voltage rise and the voltage unbalance are treated as two unrelated issues. Although there are some researches which discuss the unbalanced voltage compensation [1, 8-12], their sole purpose is to cancel the unbalanced voltage in order to improve power quality rather than to reduce the voltage rise.

The main topic studied in this thesis will be the mitigation of voltage rise due to the integration of PV systems into the distribution system under unbalanced voltage condition. To the author's knowledge, there are no researches that analyze quantitatively the impact of unbalanced voltages over the magnitude of line-to-line voltages and investigate how this worsens the voltage rise problem. It will be shown in this thesis that the voltage unbalance usually contributes significantly to the maximum line-to-line voltage which is the criterion for voltage rise or overvoltage. Therefore, the voltage rise over the limit is in fact caused by two factors, i.e., the reverse power flow and the voltage unbalance. With this understanding, it will be proposed in this thesis that cancellation of voltage unbalance by negative-sequence current injection should be done first to reduce the maximum line-to-line voltage. And if this measure helps to bring the voltage back within the limit, then no further action is needed. Otherwise, additional (positive-sequence) reactive power injection or active power curtailment may be necessary.

1.2 Objectives and scope of study

There are three main objectives in this research work:

- To analyze quantitatively the relationship between voltage rise and unbalanced voltage
- To analyze the effects of negative-sequence current injection on active and reactive power metering
- To propose a strategy to mitigate voltage rise under unbalanced voltage condition at the point of common coupling (PCC) of PV, which prioritizes the unbalanced voltage compensation in coordination with the reactive power injection and power curtailment. The overall control strategy can be divided into three steps as follows:
  - Step 1: Injection of current in negative sequence
  - Step 2: Injection of reactive power in positive sequence

- Step 3: Power curtailment

The proposed strategy will be implemented in MATLAB/Simulink. It will be then applied on an MV distribution network at Mae Hong Son area, whose system is depicted in Fig. 3. It consists of a 100km distribution line, two AVR transformers, three-phase balanced loads, single-phase unbalanced loads, and a 4-MW PV plant.

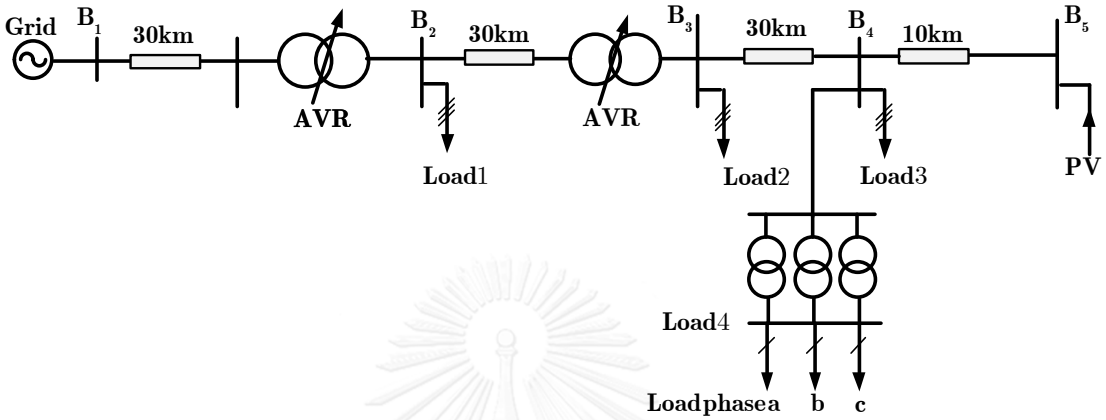

Fig. 3. System diagram of a distribution feeder in Mae Hong Son area.

1.3 Main contribution

The main contribution of this research is to develop three controllers for mitigating voltage rise in a three-phase unbalance system with the presence of a photovoltaic system. The first controller, which is the main part of the work, compensates the negative sequence voltage by injecting negative sequence current. This controller helps to reduce the PCC voltage with little effects on the active and reactive power, because the small value of negative sequence voltage will produce small active and reactive power in the negative sequence although the negative sequence current may be appreciable. The second controller injects the reactive power in positive sequence aiming to reduce the voltage at the PCC. The capability of this controller is limited by the size of inverter connecting the PV generation to the grid. If the inverter is oversized compared to the PV generation capacity, the voltage rise can be significantly mitigated. Finally, the third controller functions to curtail the active power from the PV as the last measure to suppress the voltage rise, which is an unwanted method viewed from the PV owner. However, it is an unavoidable method if all other methods fail to bring the voltage back within the acceptable limit.

1.4 Outline of thesis

This thesis is structured into 7 chapters:

Chapter 1 describes the background knowledge of the voltage rise and voltage unbalance problem and also the motivation toward this research work. The objectives and scope of study are also defined in this chapter.

Chapter 2 gives an overview on the existing strategies for voltage rise and voltage unbalance mitigation. The methods to solve the voltage rise problem based on the reactive power injection and on the active power curtailment are explained in detail.

Chapter 3 focuses on theoretical analysis that proves the relationship between the unbalanced voltage and the voltage rise, which is the basis for developing the controller for voltage rise mitigation. The second part of the chapter will explain the benefit of this method of negative sequence current injection on power metering. The chapter is finished with the simulation result in order to justify the theoretical analysis.

Chapter 4 is dedicated to the development of the first controller which is based on the injection of negative sequence current for voltage rise reduction. The simplified model of the distribution network is introduced in order to design the controller's gains, which are then tested with the real model of the distribution network. Time simulation and phasor simulation are considered for studying the behavior of controller both in steady-state and transient conditions.

Chapter 5 focuses on the second controller which injects the reactive current in positive sequence for reducing voltage rise. Both time and phasor simulation are considered. The behavior of the system is examined when the first controller described in chapter 4 is integrated with this second controller in order to work in parallel to suppress voltage rise.

Chapter 6 describes the development of the third controller which curtails the active power from the PV for voltage rise reduction. The three controllers are then combined together, and its capability of solving voltage rise problem is examined.

This thesis ends with the conclusions and outlooks in Chapter 7.

2 Overview of voltage rise and voltage unbalance mitigation

2.1 Voltage rise mitigation

Voltage rise can be mitigated in many ways with different pros and cons. For example, increasing the size of conductors or adding a new parallel line can reduce the voltage rise. However, this method will increase the investment cost due to the changing of distribution feeders. The voltage rise also can be reduced by regulating the voltage at some parts of the substations or at some points of the feeder. Adjusting the tap of an MV/LV transformer or using automatic voltage regulator (AVR) will also help to manage the voltage along the feeder. In addition, controlling the loads (demand response) by adding more loads along the feeder when the power from PV highly increased will help to suppress the voltage rise too. A part from the above methods, the voltage can also be lowered by allowing the generator to absorb reactive power, installing passive or active reactive power on the feeders, tailoring active power from PV, or installing energy storages [13].

2.1.1 Reactive power method (Q method)

Usually, the inverter for PV is sized at 10% higher than the rated capacity of the PV [14, 15]. This extra current capacity can be used to support the reactive power of the PV generation to be within a predetermined power factor (PF) limit. The amount of reactive power Q injected into the grid is limited in a way to obtain a minimum of 0.95 power factor in LV system and 0.9 power factor in MV system.

The autonomous regulation of voltage deviation by the Q method is much faster and gets more interest than some other methods. There are several methods to supply reactive power such as fixed reactive power, fixed power factor, $\cos\varphi(P)$ and $Q(U)$ methods [16-18].

- Fixed Q method needs some investigation on the voltage rise at each bus of the system. In general, this static reactive power provision will set the power factor (PF) of the buses nearby the transformer higher than those which are far from the transformer, as shown in Fig. 4 [18].

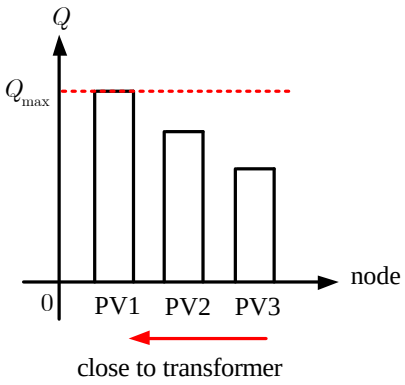

Fig. 4. Reactive power method by using fixed Q method

- In the fixed power factor method as shown in Fig. 5, the inverter will always absorb reactive power which is proportional to the active power as depicted in Eq. (1)-(2). When the PV farm generates small amount of active power, the reactive power will be also small. Therefore, the grid voltage will not increase too much. However, the unnecessary supply of reactive power will create more power losses in the system. Therefore, $\cos\varphi(P)$ method has been proposed to prevent this case from occurring.

$$\tan\theta = \frac{Q}{P} \tag{1}$$

$$\Rightarrow Q = P \times \tan\theta \tag{2}$$

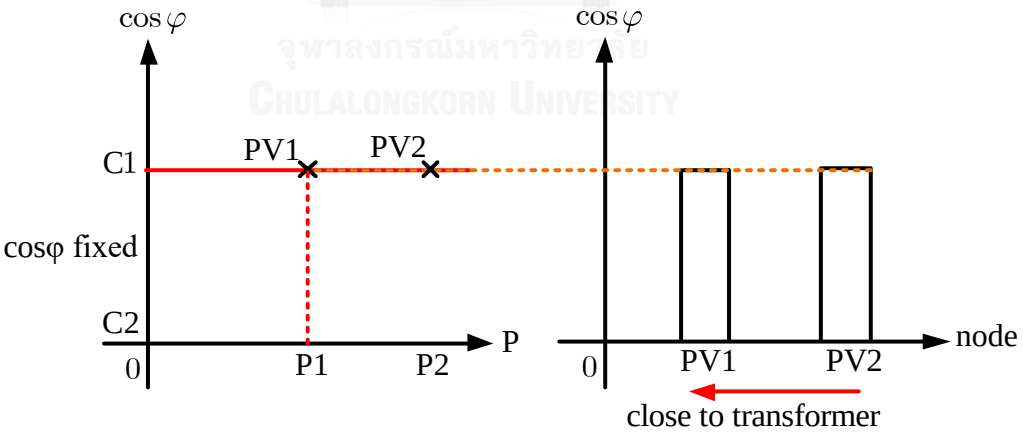

Fig. 5. Reactive power method by using $\cos\varphi$ fixed method

- $\cos\varphi(P)$, PF is a function of active power as shown in Fig. 6. This method controls the power factor based on the real power P as explained in Eq. (3) [19]. This means that the voltage rise varies depending on the power injection from the PV regardless of the load flow in the system.

$$\cos\varphi = \begin{cases} C_1 & P < P_1 \\ \dfrac{C_1 - C_2}{P_1 - P_2} \cdot (P - P_1) + C_1 & P_1 \le P \le P_2 \\ C_2 & P > P_2 \end{cases} \quad (3)$$

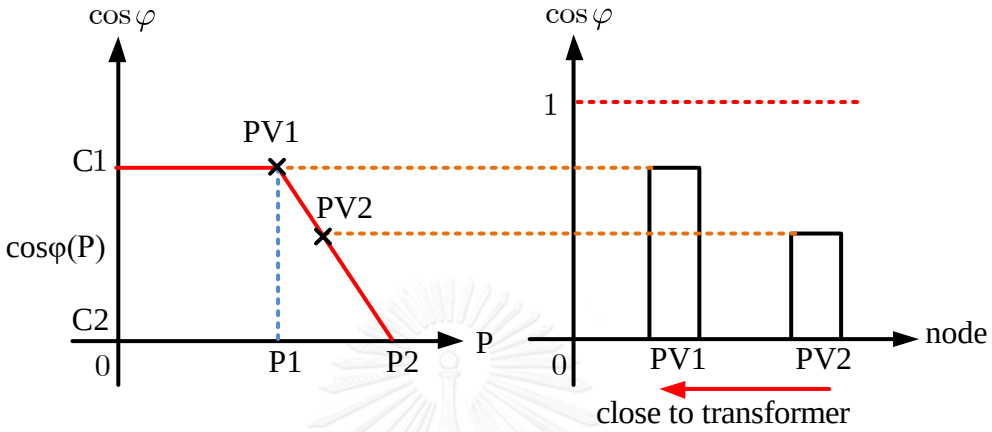

Fig. 6. Reactive power method by using $\cos\varphi(P)$ method

- $Q(U)$ method controls the reactive power based on the voltage at point of common coupling. Fig. 7 depicts the principle of such method. The characteristic of Q(U) method is defined by tuning the voltages at U_1 and U_2, U_3 and U_4 as shown in Eq. (4). With this method, there is no reactive power generation when the voltage at PCC is in the acceptable range. Therefore, the reactive power will be generated only when the voltage is under or over the limitation.

$$Q = \begin{cases} Q_{\max} & U < U_1 \\ \dfrac{Q_{\max}}{U_1 - U_2} \cdot (U - U_1) + Q_{\max} & U_1 \le U \le U_2 \\ 0 & U_2 < U \le U_3 \\ \dfrac{Q_{\max}}{U_3 - U_4 \cdot (U + U_3)} & U_3 < U \le U_4 \\ -Q_{\max} & U > U_4 \end{cases} \quad (4)$$

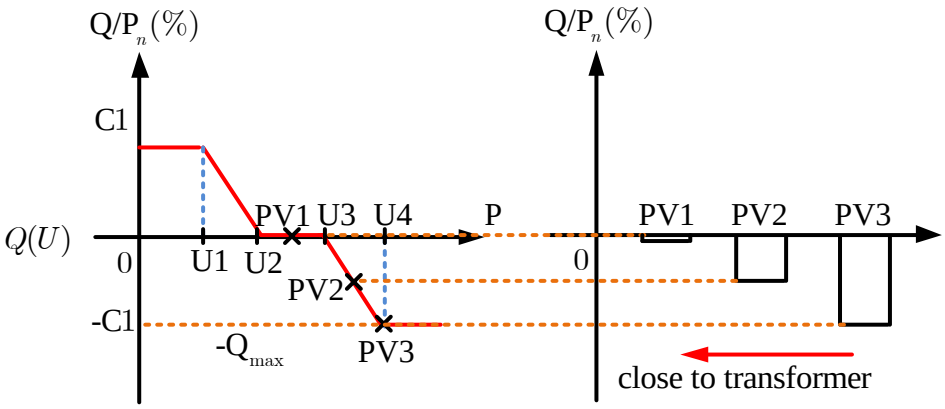

Fig. 7. Reactive power method by using Q(U) method

2.1.2 Active power curtailment

Another effective method to reduce the voltage rise problem is to control the active power injected into the grid. In [19], the limit of injected active power is set to 70% of the total power from MPPT regardless of the grid current. In [6], the active power limitation has been proposed by using a droop controller as shown in Eq. (5). A critical voltage $V_c = 1.06\,pu$ and a maximum voltage $V_{\max} = 1.1\,pu$ are two limits that have been introduced in order to control the injected active power (Eq. (5)). If the bus voltage is between the critical and the maximum voltages, the power will be curtailed to reduce the voltage rise. However, under normal operation, the output of the inverter will be set equal to the power at MPPT. In other cases, the output of inverter will be set to zero.

$$P_{inj} = \begin{cases} P_{\max} & V_{\min} < V_g \le V_c \\ P_{MPPT} - P_{MPPT}\dfrac{(V_g - V_c)}{(V_{\max} - V_c)} & V_c < V_g < V_{\max} \\ 0 & V_{\min} \ge V_g \text{ or } V_g \ge V_{\max} \end{cases} \quad (5)$$

Similarly, in [20] the voltages of the droop have been set to 1.042 *pu* and 1.058 *pu*, which are different from the case in [6]. The voltage set points of the droop controller vary depending on the regulatory of each utility or company.

2.2 Voltage unbalance compensation

Fig. 8 illustrates one technique for unbalanced voltage compensation using Voltage Unbalance Factor (VUF), which is the ratio between the RMS values of the voltages in the negative and positive sequences (V_{rms}^{-}, V_{rms}^{+}), as shown in Eq. (6) [9]. The measured VUF is compared with the reference voltage unbalance factor (VUF*). The error

resulting from the comparison of the two quantities will be used to regulate the DG's output voltage in a way to reduce the unbalanced voltage to zero.

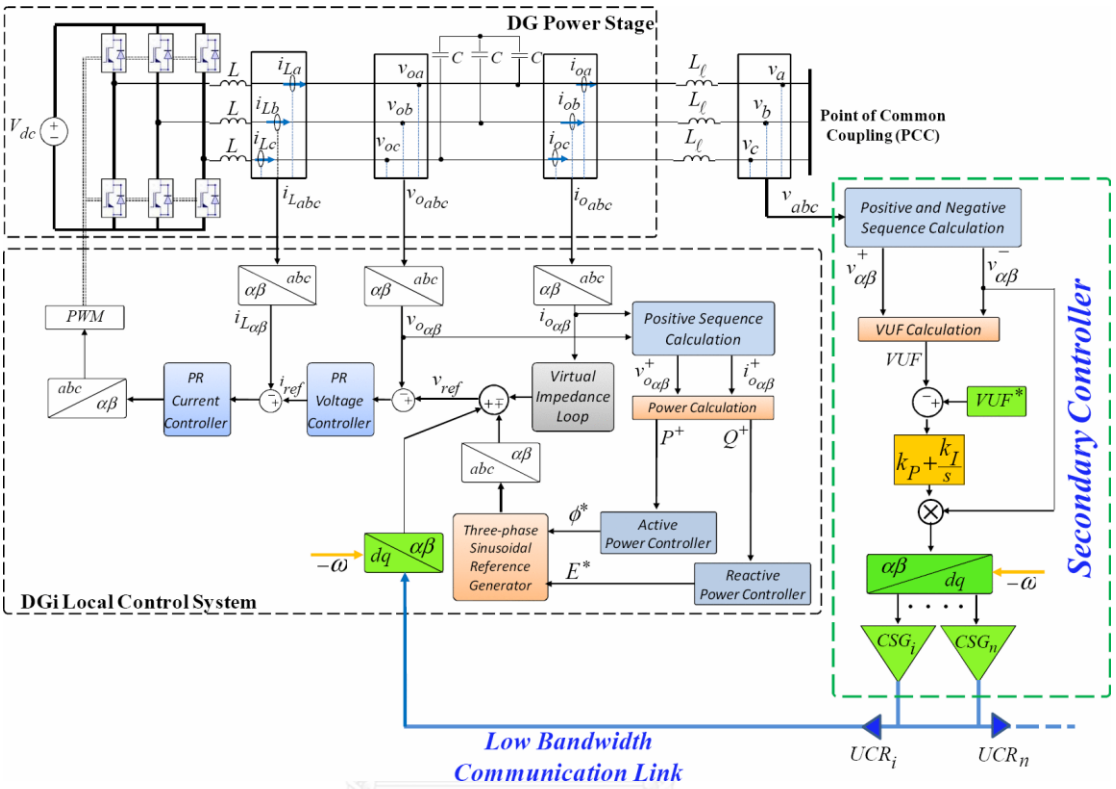

Fig. 8. Unbalanced voltage compensation using VUF [9]

$$VUF = \frac{V^{-}_{rms}}{V^{+}_{rms}} \cdot 100 \tag{6}$$

In [12], a Q-G droop controller as depicted in Fig. 9 was introduced to compensate the unbalanced voltage at the PCC. The proposed method generates a negative-sequence reactive power (Q^{-}) by multiplying the negative sequence current (I^{-}) with positive sequence voltage (E) as expressed in Eq. (7). The negative sequence voltage was neglected due to its small value.

$$Q^{-} = 3EI^{-} \tag{7}$$

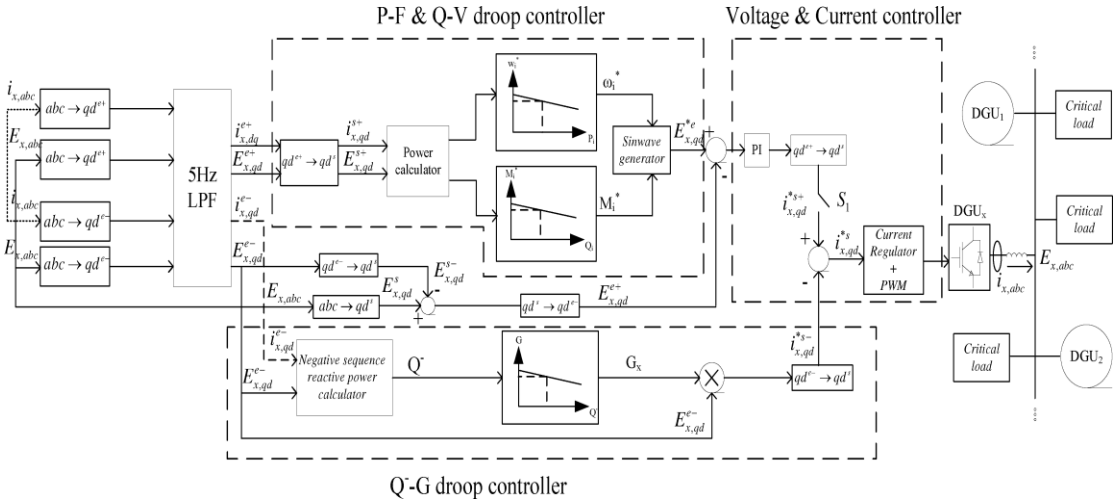

Fig. 9. Block diagram of the Q⁻-G droop control strategy [12]

The proposed droop controller has a correlation between the conductance *G* and the negative-sequence reactive power (Q^-) as shown in Eq. (8).

$$G = G_0 - u\left(Q_o^- - Q^-\right) \tag{8}$$

where G, G_0 are the conductance command and the rated conductance respectively. Q^-, Q_o^- are the negative-sequence reactive power consumption which can be found from Eq. (7) and the rated negative-sequence reactive power. *u* is the droop coefficient. This technique is quite similar to the technique in [9] except that it injects the negative-sequence current instead of voltage. The result shows that the unbalanced voltage at the PCC has been improved and remained only 1.6%.

3 Theoretical relationship between voltage unbalance and voltage rise

The previous chapter reviews the existing techniques to reduce voltage rise by the injection of reactive power and the limitation of active power, and the compensation of unbalanced voltage to improve power quality. However, these two problems are always treated as two unrelated problems. This chapter will reveal that there is a significant quantitative relationship between the unbalanced voltage and the voltage rise. This means that reducing voltage unbalance can help solving the problem of voltage rise simultaneously. The analysis will be done based on the symmetrical components.

3.1 Relationship between unbalanced voltage and maximum line-to-line voltage

In this section, the effect of voltage unbalance on the amplitudes of the line-to-line voltages is analyzed based on the symmetrical component analysis in order to quantify the relationship between the magnitude of the negative-sequence voltage and the maximum line-to-line voltage which defines the voltage rise.

Under unbalanced voltage condition, the line-to-line voltages represented by $\mathbf{V}_{ab}$, $\mathbf{V}_{bc}$ and $\mathbf{V}_{ca}$ may be represented in terms of their symmetrical components as shown in Eq. (9) where $\mathbf{V}^0$, $\mathbf{V}^+$ and $\mathbf{V}^-$ are the line-to-line voltage phasors of zero, positive and negative sequences, respectively. Here $a = e^{j2\pi/3}$.

$$\begin{bmatrix} \mathbf{V}_{ab} \\ \mathbf{V}_{bc} \\ \mathbf{V}_{ca} \end{bmatrix} = \begin{bmatrix} 1 & 1 & 1 \\ 1 & a^2 & a \\ 1 & a & a^2 \end{bmatrix} \begin{bmatrix} \mathbf{V}^0 \\ \mathbf{V}^+ \\ \mathbf{V}^- \end{bmatrix}. \tag{9}$$

For a three-phase three-wire system $\mathbf{V}^0 = 0$, and using the fact that $a^{-1} = a^2$, $|a^2| = |a| = 1$ it can be derived that the magnitudes of the line-to-line voltages V_{ab}, V_{bc} and V_{ca} are given by Eq. (13). The magnitudes of the three voltages therefore depend on the phase angle α between $\mathbf{V}^+$ and $\mathbf{V}^-$.

$$\mathbf{V}_{ab} = \mathbf{V}^+ + \mathbf{V}^- \tag{10}$$

$$\Rightarrow |\mathbf{V}_{ab}| = |\mathbf{V}^+ + \mathbf{V}^-|$$

$$\mathbf{V}_{bc} = a^2\mathbf{V}^+ + a\mathbf{V}^- = a^2(\mathbf{V}^+ + a^{-1}\mathbf{V}^-)$$
$$\Rightarrow |\mathbf{V}_{bc}| = |a^2||\mathbf{V}^+ + a^{-1}\mathbf{V}^-| = |\mathbf{V}^+ + a^{-1}\mathbf{V}^-| = |\mathbf{V}^+ + a^2\mathbf{V}^-| \quad (11)$$

$$\mathbf{V}_{ca} = a\mathbf{V}^+ + a^2\mathbf{V}^- = a(\mathbf{V}^+ + a\mathbf{V}^-)$$
$$\Rightarrow |\mathbf{V}_{ca}| = |a||\mathbf{V}^+ + a\mathbf{V}^-| = |\mathbf{V}^+ + a\mathbf{V}^-| \quad (12)$$

$$\left.\begin{aligned} V_{ab} &= |\mathbf{V}^+ + \mathbf{V}^-| \\ V_{bc} &= |\mathbf{V}^+ + a^2\mathbf{V}^-| \\ V_{ca} &= |\mathbf{V}^+ + a\mathbf{V}^-| \end{aligned}\right\} \quad (13)$$

Fig. 10 (a)-(c) illustrate some examples of the voltage phasor diagram for $0 \le \alpha \le 60°$ during which the maximum line-to-line voltage is V_{ab}. From Fig. 10 we can derive that the maximum line-to-line voltage $V_{\max(LL)}$ satisfies Eq. (14).

$$V_{\max(LL)} \ge V^+ + \cos\alpha \cdot V^- \quad (14)$$

By symmetry, the same can be said for $-60° \le \alpha < 0$. Since normally the ratio between negative-sequence and positive-sequence voltages is very small, Eq. (14) can be approximated by Eq. (15).

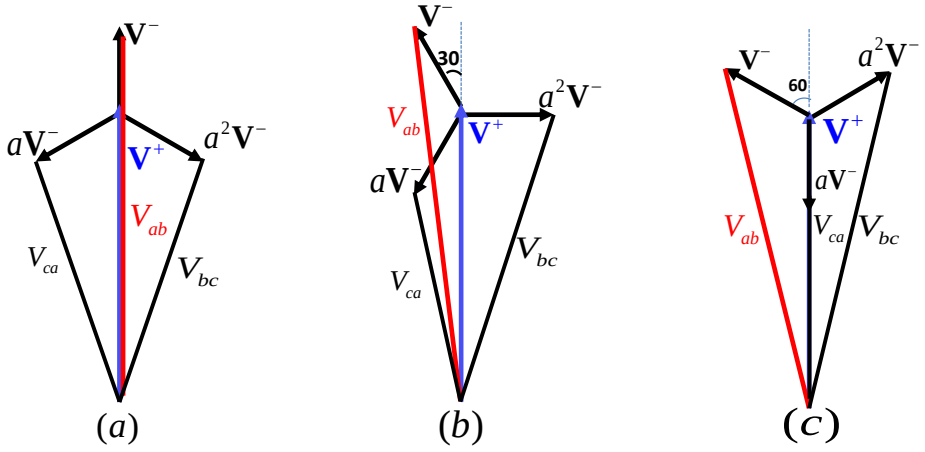

Fig. 10. Phasor diagram showing magnitudes of line-to-line voltages under voltage unbalance for various phase angle α.

When the phase angle α rotates further than 60^0, the maximum line-to-line voltage will change from V_{ab} to be V_{bc} or V_{ca} instead. However, similar relations (14)-(15) are

still valid. From this investigation, it can be concluded that under any unbalanced condition, the maximum line-to-line voltage of the system ($V_{\max(LL)}$) satisfies Eq. (16):

$$V_{\max(LL)} \cong V^{+} + \cos\alpha \cdot V^{-} \tag{15}$$

$$V_{\max(LL)} \geq V^{+} + \frac{1}{2}V^{-} \tag{16}$$

According to Eq. (16) it can be said that the voltage rise is caused by both positive- and negative-sequence voltages. The maximum line-to-line voltage is always increased by the negative-sequence voltage by at least a factor of 0.5. As by the standard, the voltage unbalance in terms of the negative and positive-sequence voltage ratio could reach 2% in the system, and this means that it will cause at least 1% of voltage rise which could not be neglected. Therefore, compensation of voltage unbalance by elimination of the negative-sequence voltage will help reducing overvoltage significantly, especially when the PCC voltage is heavily unbalanced.

3.2 Active and reactive power under voltage unbalance condition

Since injection of negative-sequence currents to compensate voltage unbalance may introduce additional power flow from the PV system and lead to extra charges by the utility, it is thus necessary to clarify this effect and compare with the conventional reactive power injection method.

According to the instantaneous power theory, the instantaneous active and reactive power supplied or consumed by the inverter can be calculated as follows.

3.2.1 Total averaged active power

Let *p(t)* be the total instantaneous power of the three phases. It can be expressed in terms of the positive- and negative-sequence components as follows.

$$p(t) = \sum_{k=a,b,c} v_k(t) \cdot i_k(t) \tag{17}$$

$$v_k(t) = v_k^{+}(t) + v_k^{-}(t) \quad \text{and} \quad i_k(t) = i_k^{+}(t) + i_k^{-}(t) \tag{18}$$

$$\Rightarrow p(t) = \sum_{k=a,b,c} \left[v_k^{+}(t) + v_k^{-}(t) \right] \cdot \left[i_k^{+}(t) + i_k^{-}(t) \right] \tag{19}$$

where $v_k^{+}, v_k^{-}, i_k^{+}$ and i_k^{-} are the instantaneous positive- and negative-sequence voltages and currents of the *abc* phases at the PCC, respectively. The averaged active power ($\overline{P}$) of

the inverter can be computed as shown in Eq. (20) where T is the period of the fundamental frequency.

$$\overline{P} = \frac{1}{T}\int_0^T p(t)dt = \sum_{k=a,b,c}\frac{1}{T}\int_0^T v_k(t)\cdot i_k(t)dt \tag{20}$$

$$= \sum_{k=a,b,c}\frac{1}{T}\int_0^T v_k^+(t)i_k^+(t)dt + \sum_{k=a,b,c}\frac{1}{T}\int_0^T v_k^-(t)i_k^-(t)dt + \sum_{k=a,b,c}\frac{1}{T}\int_0^T v_k^+(t)i_k^-(t)dt + \sum_{k=a,b,c}\frac{1}{T}\int_0^T v_k^-(t)i_k^+(t)dt$$

Since $$\sum_{k=a,b,c}\frac{1}{T}\int_0^T v_k^+(t)i_k^-(t)dt = 0 \quad \text{and} \quad \sum_{k=a,b,c}\frac{1}{T}\int_0^T v_k^-(t)i_k^+(t)dt = 0 \tag{21}$$

$$\Rightarrow \quad \overline{P} = \sum_{k=a,b,c}\frac{1}{T}\int_0^T v_k^+(t)i_k^+(t)dt + \sum_{k=a,b,c}\frac{1}{T}\int_0^T v_k^-(t)i_k^-(t)dt = P^+ + P^- \tag{22}$$

Therefore the total averaged active power is the summation of the active power in the positive sequence (P^+) and the active power in the negative sequence (P^-).

3.2.2 Total reactive power

There are two main methods for calculation of the reactive power, i.e., the *Time Shift* and the *Power Triangle methods*. In this research the *Time Shift* method is adopted because it has been more frequently used in commercial metering [21, 22] . Its principle is similar to active power calculation except that the phase of the voltage waveform is shifted by 90^0 before multiplying with the current waveform as shown in Eq. (23).

Total reactive power $$\overline{Q} = \sum_{k=a,b,c}\frac{1}{T}\int_0^T v_k\left(t+\frac{T}{4}\right)i_k(t)dt \tag{23}$$

$$= \sum_{k=a,b,c}\frac{1}{T}\int_0^T v_k^+\left(t+\frac{T}{4}\right)i_k^+(t)dt + \sum_{k=a,b,c}\frac{1}{T}\int_0^T v_k^-\left(t+\frac{T}{4}\right)i_k^-(t)dt$$
$$+ \sum_{k=a,b,c}\frac{1}{T}\int_0^T v_k^+\left(t+\frac{T}{4}\right)i_k^-(t)dt + \sum_{k=a,b,c}\frac{1}{T}\int_0^T v_k^-\left(t+\frac{T}{4}\right)i_k^+(t)dt$$

If we decompose the voltage and current into positive- and negative-sequence components as shown in Eq. (18), considering Eq. (24) it can be derived that the total reactive power as measured by the power meter will be the summation of the positive- and negative-sequence reactive powers, Q^+ and Q^-, as shown in Eq. (25).

$$\sum_{k=a,b,c}\frac{1}{T}\int_0^T v_k^-\left(t+\frac{T}{4}\right)i_k^+(t)dt = 0 \quad \text{and} \quad \sum_{k=a,b,c}\frac{1}{T}\int_0^T v_k^+\left(t+\frac{T}{4}\right)i_k^-(t)dt = 0 \tag{24}$$

$$\therefore \quad \bar{Q} = \sum_{k=a,b,c} \frac{1}{T}\int_0^T v_k^+\left(t+\frac{T}{4}\right) i_k^+(t)dt + \sum_{k=a,b,c} \frac{1}{T}\int_0^T v_k^-\left(t+\frac{T}{4}\right) i_k^-(t)dt = Q^+ + Q^- \qquad (25)$$

Because the negative-sequence voltage is very small compared to the positive one, considering the same amount of active and reactive currents in the positive and negative sequences, it is concluded that in general $P^+ \gg P^-$ and $Q^+ \gg Q^-$. So, the compensation of the unbalanced voltage not only reduces the voltage rise but also is more economic because the PV owner will be charged less due to the negligible amount of P^- and Q^-.

3.3 Numerical analysis results

In order to verify the correctness of theory described in section 3.1 which identifies the relationship between the amount of unbalanced voltage and the voltage rise (cf. Eq. (16)), the system in Fig. 3 with unbalanced loads will be used for the simulation and calculation of the positive/negative-sequence voltages and the maximum line-to-line voltage. Two cases of simulation will be considered: 1) scenario with no PV injection and 2) with 4-MW PV injection. The load consumptions in each phase are presented in Table 1.

Table 1: The values of single loads, balanced three-phase loads, and PV in Case 1 and Case 2

	Single loads in each phase			Three phases loads, PF=0.85			PV power
	phase a	phase b	phase c	load 1	load 2	load 3	
Case 1	100 kW	300 kW	1000 kW	1 MVA	1 MVA	2 MVA	0 MW
Case 2	100 kW	300 kW	1000 kW	1 MVA	1 MVA	2 MVA	4 MW

3.3.1 Case 1: without PV injection

The simulation result of Case 1 is shown in Table 2. Some important parameters are observed from the simulation: line-to-line voltage, current and angle between the positive and negative sequence voltage (α) at each bus and at the three-phase load bus.

Table 2: Simulation results for Case 1

	Bus				Three-phase load		
line-to-line voltage	B2	B3	B4	B5	Load 1	Load 2	Load 3
Vab [kV]	22.4	22.52	22.22	22.27	22.4	22.52	22.22
Vbc [kV]	22.54	22.85	22.72	22.77	22.54	22.85	22.72
Vca [kV]	22.26	22.29	21.95	21.99	22.26	22.29	21.95
Ia [A]	117.1	83.15	17.43	0	26.46	26.45	52.13
Ib [A]	118	80.09	17.48	0	26.79	27.12	53.98
Ic [A]	128.2	91.5	17.34	0	26.63	26.85	53.33
V^+ab [kV]	22.24	22.55	22.3	22.34	22.24	22.55	22.3
V^+bc [kV]	22.24	22.55	22.3	22.34	22.24	22.55	22.3
V^+ca [kV]	22.24	22.55	22.3	22.34	22.24	22.55	22.3
V^-ab [V]	160.7	324.1	454.9	455.9	160.7	324.1	454.9
V^-bc [V]	160.7	324.1	454.9	455.9	160.7	324.1	454.9
V^-ca [V]	160.7	324.1	454.9	455.9	160.7	324.1	454.9
Angle α	-89.29^0	-96.28^0	-99.54^0	-99.54^0	-89.29^0	-96.28^0	-99.54^0

At bus 2 (B2), the amplitudes of the positive- and negative-sequence voltages are 22.24 kV and 160.7 V, respectively. Substituting these numerical values to Eq. (16) results in Eq. (26)-(27). These results verify the inequality in Eq. (16) since the maximum line-to-line voltage $(V_{\max(LL)})$ which is equal to 22.54 kV is higher than 22.32 kV on the right-hand side of Eq. (27).

$$V_{\max(LL)} \geq 22.24 + \frac{1}{2}(0.1607) \tag{26}$$

$$\Rightarrow V_{\max(LL)} \geq 22.32\ kV \tag{27}$$

In addition, the analysis in the section 3.1 also reveals the relationship between the maximum line-to-line voltage and the phase angle α. The results in Table 2 at the bus B2 show that the phase angle α between V^+ and V^- is -89.29^0 meaning that the

maximum line-to-line voltage will be V_{bc} or V_{ca}. And from the results the maximum line-to-line voltage is V_{bc}.

Similarly, the simulation results at the buses B3, B4, and B5 of the three-phase loads confirm also the correctness of the analysis in section 3.1 based on the results in Table 3 and Table 4.

Table 3: Relationship between $V_{\max(LL)}$ and $V^{+}+\frac{1}{2}V^{-}$.

Bus	$V_{\max(LL)}$	$V^{+}+\frac{1}{2}V^{-}$
B2	22.54 kV	22.32 kV
B3	22.85 kV	22.71 kV
B4	22.72 kV	22.84 kV
B5	22.77 kV	22.57 kV
Load1	22.54 kV	22.32 kV
Load2	22.85 kV	22.71 kV
Load3	22.72 kV	22.84 kV

Table 4: Relationship between $V_{\max(LL)}$ and α

Bus	$V_{\max(LL)}$		α
B2	Vbc	22.54 kV	-89.29^{0}
B3	Vbc	22.85 kV	-96.28^{0}
B4	Vbc	22.72 kV	-99.54^{0}
B5	Vbc	22.77 kV	-99.54^{0}
Load1	Vbc	22.54 kV	-89.29^{0}
Load2	Vbc	22.85 kV	-96.28^{0}
Load3	Vbc	22.72 kV	-99.54^{0}

From the Table 3 and Table 4, it can be confirmed that the maximum line-to-line voltage is always bigger than sum of the positive-sequence voltage and half of the negative-sequence voltage, satisfying the inequality Eq. (16). This means that

compensating the negative-sequence voltage will help to reduce the voltage rise and this is the issue to be discussed further in the next chapter.

Investigating the voltage unbalance in the system, the negative-sequence voltage at the bus B5 is equal to 455.9V, so the voltage unbalance factor (VUF) is around 2% which is in the acceptable range. Moreover, the results in Table 2 also verify the statement discussed in the section3.2. In general, positive-sequence voltage (V^+) is very high compared to the negative-sequence voltage (V^-) as shown in Table 2. Therefore, owing to the difference between V^+ and V^-, a large amount of active and reactive powers will be generated in the positive sequence, and only a small amount of active and reactive powers will occur in the negative sequence and depicts in Fig. 11.

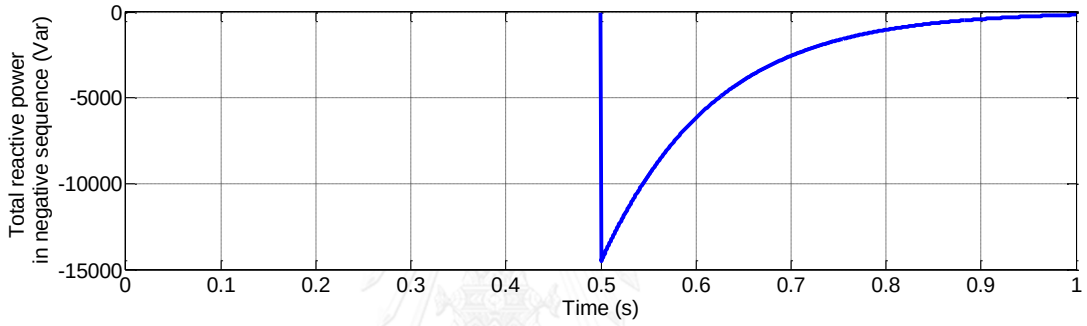

Fig. 11. Total reactive power in negative sequence

3.3.2 Case 2: with 4 MW PV

The results of Case 2 are illustrated in Table 5 showing that the voltage at each bus is increased due to the reverse power from the PV injection and the unbalanced voltage which comes from the unbalanced current in each phase. Fig. 12 shows the variation of voltages before and after the injection active power from the PV generation. The result shows that the injection of 4 MW PV will increase the voltage in the system over the limit.

The current in each phase at the bus B5 increases from 0 A (Table 2) to 92.15A (Table 5) due to the reverse current from the PV inverter. However, the analysis in sections 3.1 and 3.2 are still correct even though the injection of active power from the PV generation produces more voltage rise in the system.

Table 5: Simulation results for Case 2

	Bus				Three-phase load		
line-to-line voltage	B2	B3	B4	B5	Load 1	Load 2	Load 3
Vab [kV]	23.55	24.57	25.02	25.33	23.55	24.57	25.02
Vbc [kV]	23.74	24.97	25.58	25.88	23.74	24.97	25.58
Vca [kV]	23.43	24.35	24.71	25	23.43	24.35	24.71
Ia [A]	63.87	19.54	94.05	92.15	27.82	28.87	56.68
Ib [A]	73.46	32.06	94.28	92.15	28.19	29.61	60.77
Ic [A]	77.87	31.86	93.61	92.15	28.05	29.36	60.04
$V^{+}ab$ [kV]	23.57	24.63	25.1	25.4	23.57	24.63	25.1
$V^{+}bc$ [kV]	23.57	24.63	25.1	25.4	23.57	24.63	25.1
$V^{+}ca$ [kV]	23.57	24.63	25.1	25.4	23.57	24.63	25.1
$V^{-}ab$ [V]	180.9	364.9	512.1	513.2	180.9	364.9	512.1
$V^{-}bc$ [V]	180.9	364.9	512.1	513.2	180.9	364.9	512.1
$V^{-}ca$ [V]	180.9	364.9	512.1	513.2	180.9	364.9	512.1
Angle α	$^{-}97.37^{0}$	-99.89^{0}	-99.52^{0}	-98.32^{0}	$^{-}97.37^{0}$	-99.89^{0}	-99.52^{0}

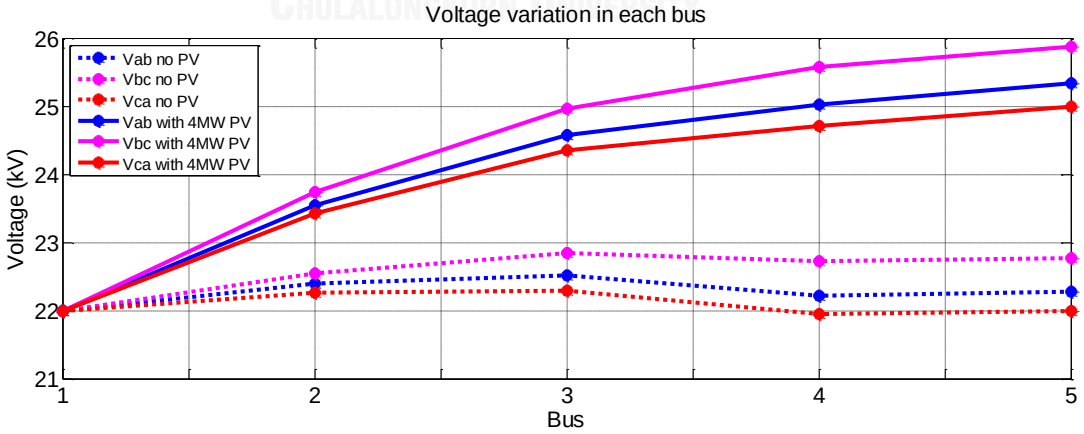

Fig. 12. The voltage variation at each bus before and after PV penetration

Table 6 and Table 7 compare the numerical values from the simulation with the analytical results of sections 3.1 and 3.2. The results show that the maximum line-to-line voltages are bigger than the sum of positive-sequence voltage and half of the

negative-sequence voltage. Moreover, the phase angles α at each bus are in the range from -97^0 to -99^0, so the maximum line-to-line voltage will always be the line voltage Vbc as shown in Table 7. This fact can be confirmed also from Fig. 12 wherein the purple lines are always the maximum line-to-line voltages.

Table 6: Relationship between $V_{\max(LL)}$ and $V^+ + \frac{1}{2}V^-$.

Bus	$V_{\max(LL)}$	$V^+ + \frac{1}{2}V^-$
B2	23.74 kV	22.32 kV
B3	24.97 kV	22.71 kV
B4	25.58 kV	22.84 kV
B5	25.88 kV	22.57 kV
Load1	23.74 kV	22.32 kV
Load2	24.97 kV	22.71 kV
Load3	25.58 kV	22.84 kV

Table 7: Relationship between $V_{\max(LL)}$ and α

Bus	$V_{\max(LL)}$		α
B2	Vbc	23.74 kV	-97.37^0
B3	Vbc	24.97 kV	-99.89^0
B4	Vbc	25.58 kV	-99.52^0
B5	Vbc	25.88 kV	-98.32^0
Load1	Vbc	23.74 kV	-97.37^0
Load2	Vbc	24.97 kV	-99.89^0
Load3	Vbc	22.72 kV	-99.52^0

With the injection of 4 MW PV generation, it is seen that the increasing of voltage is extremely high especially at the bus 5 which is the point of connection. Since the voltages cannot be over the limit defined by the Grid code, in Chapter 4 a strategy to suppress the voltage rise and bring the voltages back into the acceptable range will be discussed.

4 Voltage rise mitigation by unbalanced voltage compensation

Typically, the PV plant is connected to the power system through a current-controlled inverter. In this research this PV inverter will be exploited to mitigate the voltage rise by a control strategy proposed in Fig. 13. The proposed controller's structure can be decomposed into three main parts: (1) unbalanced voltage compensation by negative-sequence current injection, (2) reactive power injection, and (3) power curtailment. In Fig. 13, v_{PCC} is the instantaneous voltage at the point of common coupling, $i^{-}, i_q^{+}, i_{PV}^{+}$ are the injected negative-sequence current, the reactive current and the active current from the PV inverter, respectively, while i_{inj} is the total injected current.

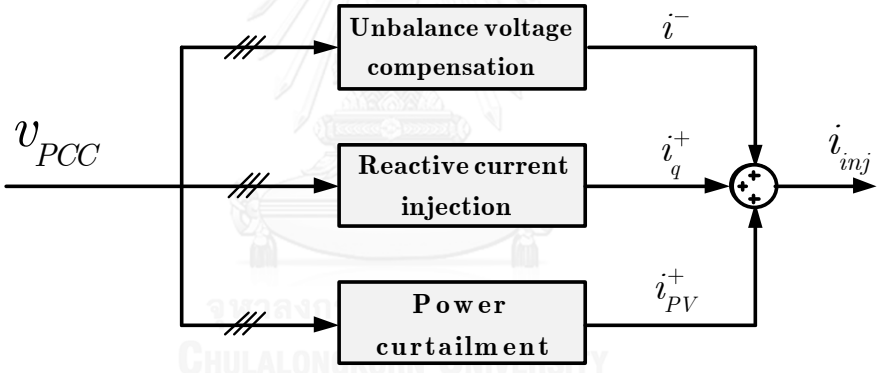

Fig. 13. Proposed structure of the controller for voltage rise mitigation.

The three controllers in Fig. 13 operate in parallel depending on the PCC voltage level. If the negative-sequence current injection fails to mitigate the voltage rise, the reactive power injection will be activated to assist the negative-sequence current injection. And if the injection of both the negative-sequence current and the reactive current is unsuccessful, then the power curtailment will be lastly executed. All operations of these controllers are carried out under the constraint of the inverter's current capacity.

The unbalanced voltage compensation will be described first in this Chapter. Then, time and phasor simulation using MATLAB/SIMULINK will be carried out to examine the dynamic and steady-state performances of the proposed unbalanced voltage compensator.

4.1 Unbalanced voltage compensation

The PV inverter as shown in Fig. 14 feeds the power from the PV panels to the network by injection of the positive-sequence active current according to the maximum-power-point-tracking (MPPT) algorithm (cf. appendix A.1). It compensates the voltage unbalance by injection of the negative-sequence current in addition to the MPPT current. The unbalanced voltage compensator consists of two main parts: (1) the negative-sequence voltage extraction and (2) negative-sequence current injection.

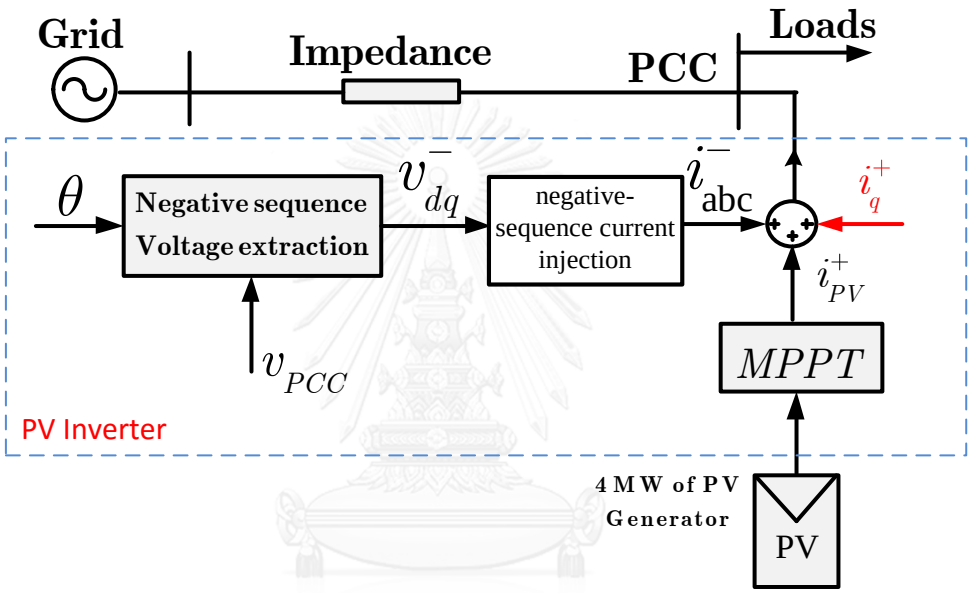

Fig. 14. Schematic diagram of the PV system with the unbalanced voltage compensator.

4.1.1 Negative-sequence voltage extraction

The block diagram of negative-sequence voltage extraction using a phase-locked loop (PLL) technique is given in Fig. 15.

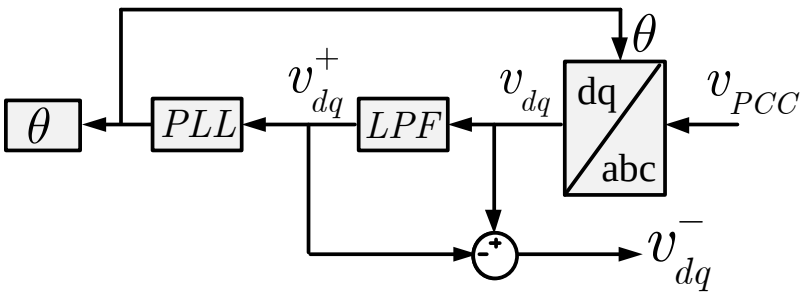

Fig. 15. Negative-sequence voltage extraction.

The following notations are applied to Fig. 15.

- v_{dq}: the d-q axis components of v_{PCC},
- v_{dq}^{+}: the positive-sequence component of v_{PCC} on d-q axis of the positive sequence,
- v_{dq}^{-}: the negative-sequence component of v_{PCC} on d-q axis of the positive sequence,
- i_d^-, i_q^-: the d-q axis components of the injected negative-sequence current,
- i_{abc}^-: the negative-sequence current injected into the three phases *a*,*b*, and *c*
- θ: the phase angle of the positive-sequence voltage v^+,
- superscripts $+,-$ denote the positive and negative sequences,
- subscripts α,β denote the $\alpha-\beta$ axis components,
- subscripts d,q denote the *d*-*q* axis components,
- subscripts a,b,c denote the three-phase quantities.

Detail explanation of the PLL is given in the appendix A.4. The three-phase voltages are transformed into the instantaneous voltages in the $d-q$ reference frame (v_{dq}) by the transformation stated in Eq. (A.10), and Eq. (A.11) in the appendix A.4.

Referred to the $d-q$ reference frame rotating at the fundamental frequency of the positive sequence, the positive-sequence voltage contained in v_{dq} will become a dc component, while the negative-sequence voltage will oscillate at the double frequency of 2ω as shown in Eq. (28) where $\theta=\omega t$ is the phase angle on the stationary $\alpha-\beta$ plane, and ω is the power frequency of the system. The positive-sequence voltage v_{dq}^{+} is extracted by using a low-pass filter (LFP), and then the negative-sequence voltage v_{dq}^{-} can be extracted as shown in Eq. (29).

$$v_{dq}=\begin{bmatrix} v_d \\ v_q \end{bmatrix}=v_{dq}^{+}+v_{dq}^{-}=\mathbf{V}^{+}\begin{bmatrix}1\\0\end{bmatrix}+\mathbf{V}^{-}\begin{bmatrix}\cos(-2\omega t)\\ \sin(-2\omega t)\end{bmatrix} \tag{28}$$

$$v_{dq}^{-}=\mathbf{V}^{-}\begin{bmatrix}\cos(-2\omega t)\\ \sin(-2\omega t)\end{bmatrix}=v_{dq}-v_{dq}^{+} \tag{29}$$

where $\mathbf{V}^{+},\mathbf{V}^{-}$ are the phasors of the positive- and negative-sequence voltages, respectively.

4.1.2 Negative-sequence current injection for unbalanced voltage compensation

4.1.2.1 Block diagram of the compensator

The block diagram of negative-sequence voltage compensation is given in Fig. 16.

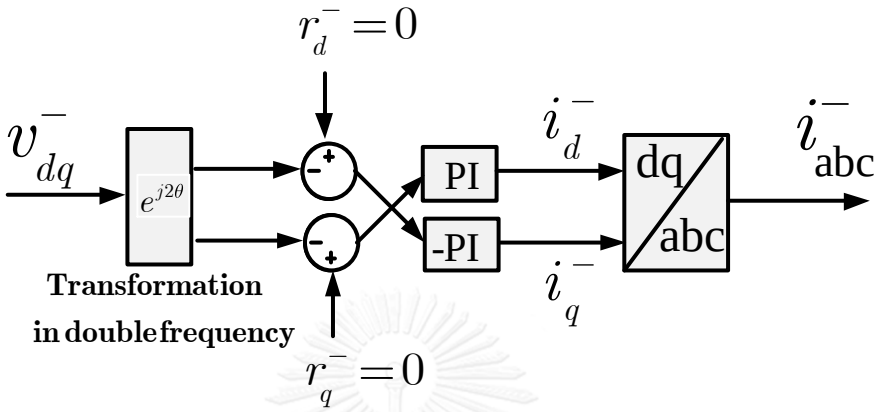

Fig. 16. Negative-sequence current injection for unbalanced voltage compensation.

In Fig. 16, the negative-sequence voltage in $d-q$ frame v_{dq}^- which rotates at the double frequency of 2ω in clockwise direction is transformed into dc components in the $d^- - q^-$ rotating frame using the transformation in Eq. (30).

$$\begin{bmatrix} d^- \\ q^- \end{bmatrix} = \begin{bmatrix} \cos 2\theta & -\sin 2\theta \\ \sin 2\theta & \cos 2\theta \end{bmatrix} \begin{bmatrix} d \\ q \end{bmatrix} \tag{30}$$

Using the extracted negative-sequence voltages, the commanded negative-sequence currents i_d^-, i_q^- are computed using the PI controllers. Subsequently, the $d^- - q^-$ components of the commanded currents are transformed into $\alpha - \beta$ components and then to the *abc* components using the transformations shown in Eq. (31) and Eq. (32).

$$\begin{bmatrix} \alpha \\ \beta \end{bmatrix} = \begin{bmatrix} \cos\theta & \sin\theta \\ -\sin\theta & \cos\theta \end{bmatrix} \begin{bmatrix} d^- \\ q^- \end{bmatrix} \tag{31}$$

$$\begin{bmatrix} a \\ b \\ c \end{bmatrix} = \sqrt{\frac{2}{3}} \begin{bmatrix} 1 & 0 \\ -1/2 & \sqrt{3}/2 \\ -1/2 & -\sqrt{3}/2 \end{bmatrix} \begin{bmatrix} \alpha \\ \beta \end{bmatrix} \tag{32}$$

4.1.2.2 Controller design

The design of unbalanced voltage compensation is based on the simplified system model as depicted in Fig. 17, in which v_s is the generator voltage, R, L are the resistance and inductance of the network system, i_s is the source current of the system, i_L is the load current, and i_{inj} is the current injected from the PV inverter. From Fig. 17, the mathematical equations of the system model can be written as shown in Eq. (33). The mathematical model on the $\alpha-\beta$ frame is shown in Eq. (34). Since the design is focused on the negative-sequence compensation, therefore the voltage at the generator and the active current from MPPT which are the positive sequences will be neglected in the following analysis.

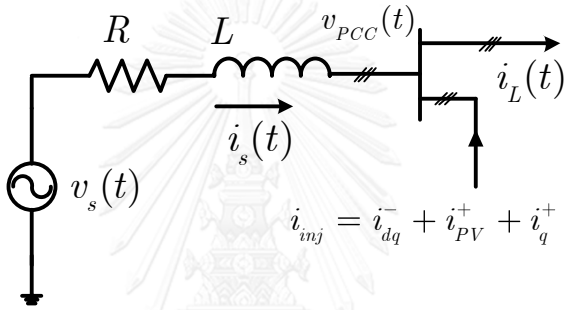

Fig. 17. Simplified system model for design of the unbalanced voltage compensation.

$$v_{PCC} = v_s - Ri_s - L\frac{di_s}{dt} \tag{33}$$

$$\begin{bmatrix} v_{PCC,\alpha} \\ v_{PCC,\beta} \end{bmatrix} = \begin{bmatrix} v_{S,\alpha} \\ v_{S,\beta} \end{bmatrix} - R\begin{bmatrix} i_{L\alpha} - i_{inj,\alpha} \\ i_{L\beta} - i_{inj,\beta} \end{bmatrix} - L\frac{d}{dt}\begin{bmatrix} i_{L\alpha} - i_{inj,\alpha} \\ i_{L\beta} - i_{inj,\beta} \end{bmatrix} \tag{34}$$

Considering only the negative-sequence components, Eq. (34) can be transformed onto the rotating $d^- - q^-$ frame as shown in Eq. (35). It should be noted that there are coupling terms between the $d^- - q^-$ axes. Eq. (35) can be written as a block diagram as in Fig. 18.

$$\begin{bmatrix} v_{PCC,d}^- \\ v_{PCC,q}^- \end{bmatrix} = -\left\{ R\begin{bmatrix} i_{Ld}^- - i_d^- \\ i_{Lq}^- - i_q^- \end{bmatrix} + L\frac{d}{dt}\begin{bmatrix} i_{Ld}^- - i_d^- \\ i_{Lq}^- - i_q^- \end{bmatrix} + \begin{bmatrix} +\omega L(i_{Lq}^- - i_q^-) \\ -\omega L(i_{Ld}^- - i_d^-) \end{bmatrix} \right\} \tag{35}$$

According to Fig. 18, the relevant transfer functions as shown in Eq. (B.1) can be computed. For example, $G_{11}(s)$ can be derived as shown in Eq. (B.6) (detailed derivation is given in the appendix B).

$$\begin{bmatrix} e_d \\ e_q \end{bmatrix} = \begin{bmatrix} G_{11} & G_{12} \\ G_{21} & G_{22} \end{bmatrix} \cdot \begin{bmatrix} r_d \\ r_q \end{bmatrix} \tag{B.1}$$

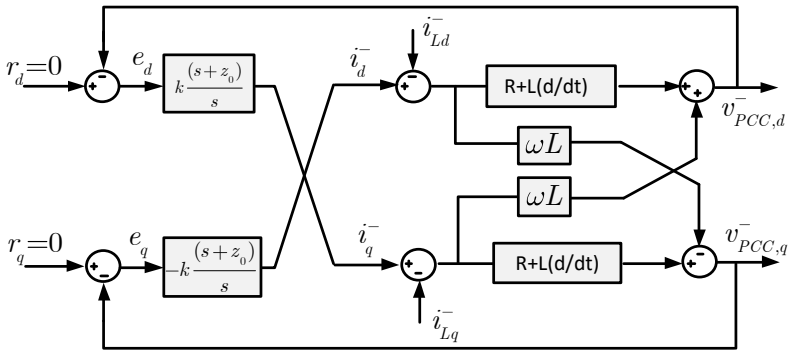

Fig. 18. Block diagram of the unbalanced voltage compensation by injection of negative-sequence current.

$$G_{11}(s) = \frac{s^2 + k\omega L s^2 + k\omega L z_0 s}{\left[\begin{array}{l} k^2L^2s^4\left(2RLk^2 + 2z_0k^2L^2\right)s^3 + \left(1 + k^2R^2 + 4RLz_0k^2 + k^2z_0^2L^2 + k^2\omega^2L^2\right)s^2 \\ \left(2k^2R^2z_0 + 2RLz_0^2k^2 + 2k^2z_0\omega^2L^2\right)s + \left(k^2z_0^2R^2 + k^2z_0^2\omega^2L^2\right) \end{array}\right]} \tag{B.6}$$

where

$$k_p = k \quad \text{and} \quad z_0 = \frac{k_I}{k_p} \tag{36}$$

k_P, k_I are the gains of the PI controllers. From the denominator $D(s)$ of $G_{11}(s)$ shown in Eq. (37), we can find the poles of the closed-loop system which determine response of the system.

$$\begin{aligned} D(s) = {} & k^2L^2s^4 + \left(2RLk^2 + 2z_0k^2L^2\right)s^3 + \left(1 + k^2R^2 + 4RLz_0k^2 + k^2\omega^2L^2\right)s^2 \\ & + \left(2k^2R^2z_0 + 2RLz_0^2k^2 + 2k^2z_0\omega^2L^2\right)s + \left(k^2z_0^2R^2 + k^2z_0^2\omega^2L^2\right) \end{aligned} \tag{37}$$

The following values of the parameters have been used in the design.

$$\omega = -2\pi f = -100\pi \quad \textit{in negative sequence}$$

$$L = \frac{X}{\omega} = \frac{0.33}{2\pi f}/km = \frac{0.33 \times 100}{100\pi} = \frac{0.33}{\pi}/100km$$

$$R = 16\Omega/100km$$

$$z_0 = 5\,\text{rad/s}$$

Fig. 19 shows the result when $k = k_p = 0.2$ and $k_I = 1$. All the closed-loop poles lie in the left-half s-plane, meaning that the system is stable with the selected PI gains.

However, we may need more analysis on the closed-loop pole location if the performance of the compensator is to be optimized.

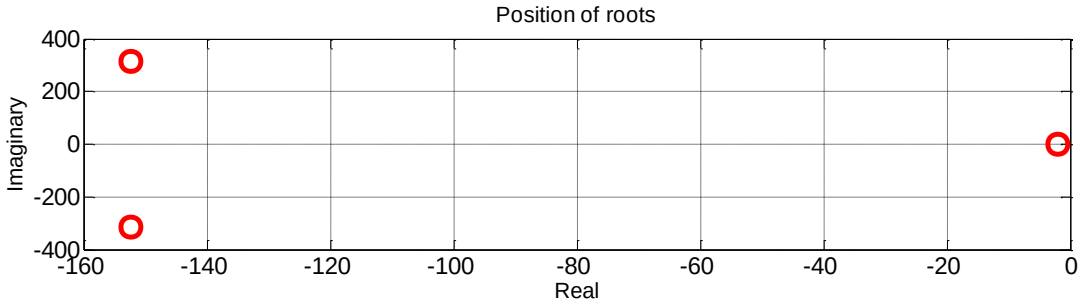

Fig. 19. Position of the closed-loop poles of the unbalanced voltage compensation.

4.2 Time simulation of unbalanced voltage compensation

The parameters listed in Table 8 are used for simulation purpose. The bus of interest is number 5, where the PV generation is connected to the grid (cf. Fig. 3). Time simulation is done in the following to confirm the operation of the unbalanced voltage compensator.

Table 8: Parameters of the system components

System components	Paramaters
Line = 100 km	Impedance= $0.16 + j0.33\Omega / km$
AVR 1	Rated = 16MVA (400A)
AVR 2	Rated = 12MVA (300A)
Load 1	1 MVA, PF = 0.85 lagging
Load 2	1 MVA, PF = 0.85 lagging
Load 3	2 MVA, PF = 0.85 lagging
Load 4, a phase	100 kW
Load 4, b phase	300 kW
Load 4, c phase	1000 kW
PV power plant	0
LPF cut-off frequency (PLL)	10 Hz
PLL PI gain	kp = 0.01, ki = 0.0628

4.2.1 Time simulation of negative-sequence voltage extraction

Fig. 20 depicts the voltage values extracted at the bus 5. Fig. 20(a) shows that the three-phase voltages are unbalanced with $V_{ab} = 22.27kV, V_{bc} = 22.77kV, V_{ca} = 21.99kV$. Note that there is a step change of voltage at the starting because of the charateristic of the RMS calculation block which outputs the specified initial value (22 kV) for the first cycle (20ms) of the simulation. From the positive- and negative-sequence voltages extraction, it is found that the positive-sequence voltages at PCC are $V_{ab}^{+} = 22.37\,kV, V_{bc}^{+} = 22.33\,kV, V_{ca}^{+} = 22.33\,kV$, and the negative-sequence voltages are $V_{ab}^{-} = V_{bc}^{-} = V_{ca}^{-} = 455V$ as depicted in Fig. 20(b) and Fig. 20(c), respectively.

The values of the three-phase positive-sequence voltages are not perfectly equal because the LPF used in the PLL cannot eliminate all the negative-sequence voltage. The filtered q-axis voltage still contains some high frequency term which oscillates in the steady state, so the positive-sequence voltages extracted still contain some negative-sequence voltages. However, the ripple is small and causes no problem to the operation of the compensator. From Fig. 21, the dynamic response of the PLL is quite fast with the q-axis positive-sequence voltage converges to zero in around 0.2 s.

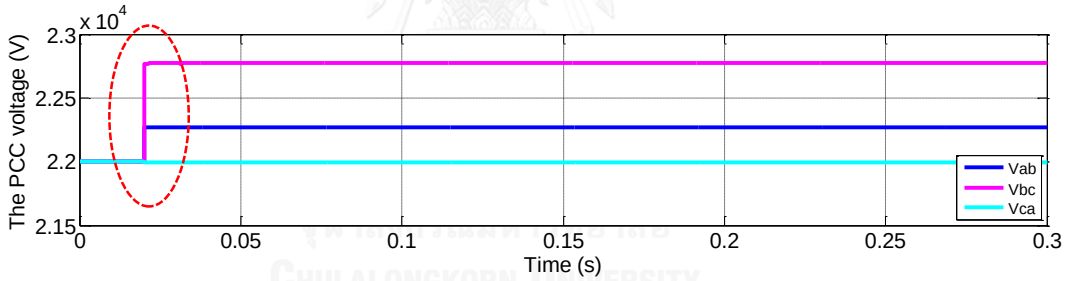

(a)

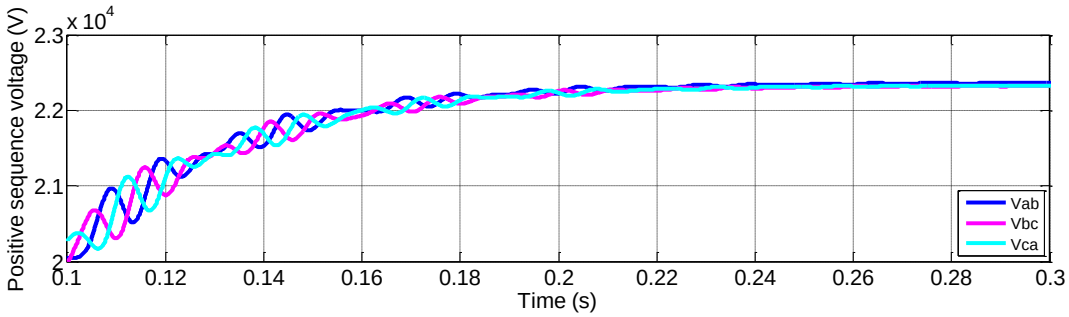

(b)

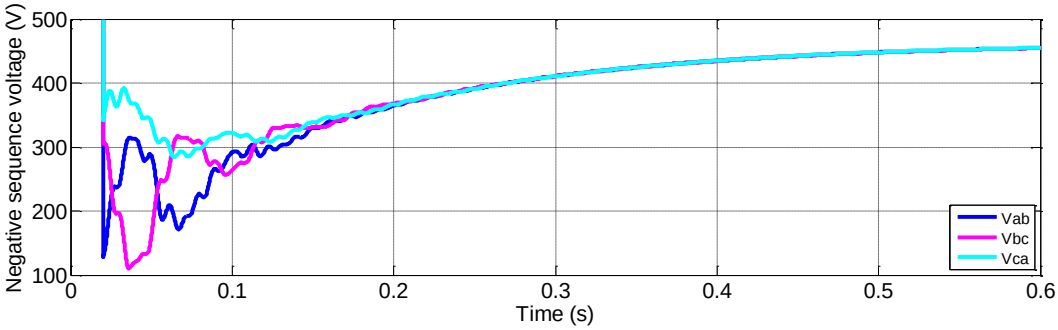

(c)

Fig. 20. The voltage extraction. (a) The PCC voltage. (b) The positive-sequence voltage. (c) The negative-sequence voltage.

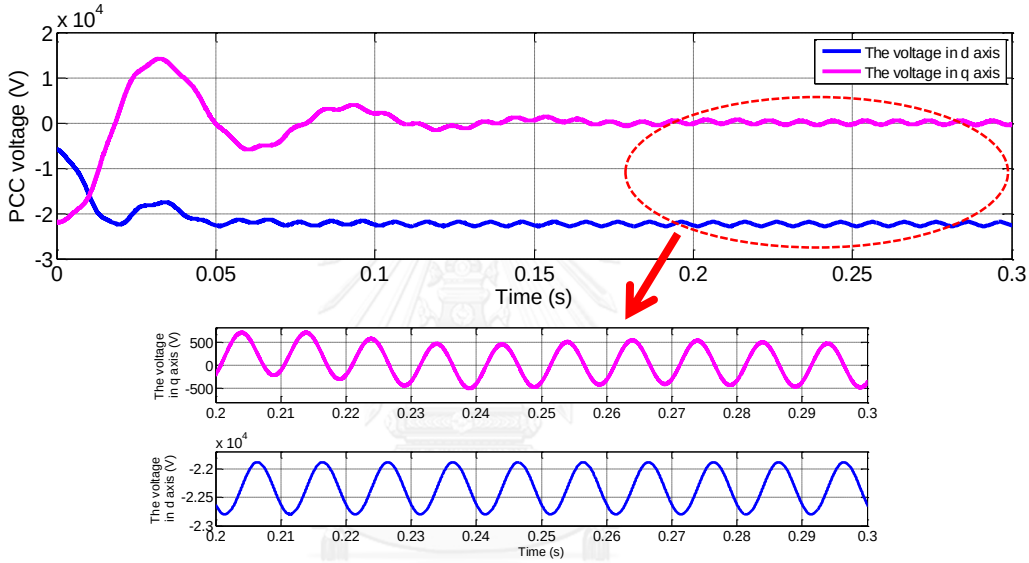

Fig. 21. d-q axis components of the PCC voltage from the PLL.

4.2.2 The result of unbalanced voltage compensation

The controller designed in the subsection 4.1.2.2 is applied first to the simplified system in order to investigate the feasibility of the controller. Later on, the same controller will be used in the real system of Fig. 24.

4.2.2.1 Compensation results with the simplified system

The result in Fig. 22 shows that before the injection of negative-sequence current at the instant of 0.5s, the negative-sequence voltages V_d^- and V_q^- are -341V and -122V, respectively. After the injection of the negative-sequence current, the negative-sequence voltages in both axes become zero at around 0.6 s, and From Fig. 23 the injected negative-sequence currents are equal to $I_d^- = -3.12A$ and $I_q^- = -11.18A$, respectively. Therefore, the controller takes only 0.1s to compensate the negative-

sequence voltages. It can be concluded that the controller works well with the designed PI gains for the simplified system.

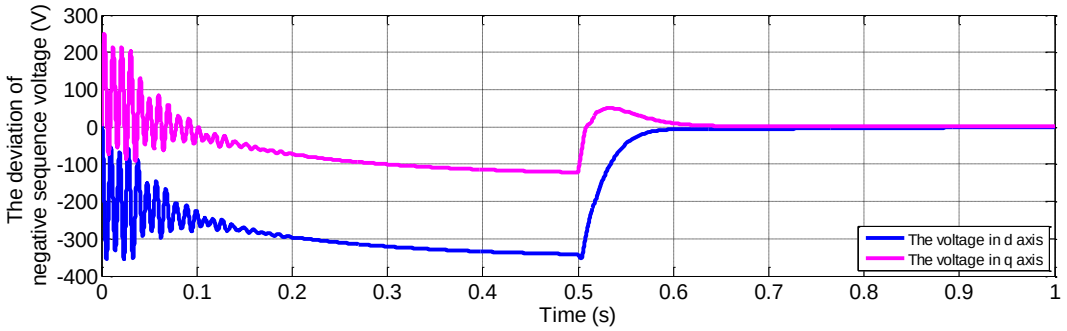

Fig. 22. The deviation of negative-sequence voltages before and after compensation.

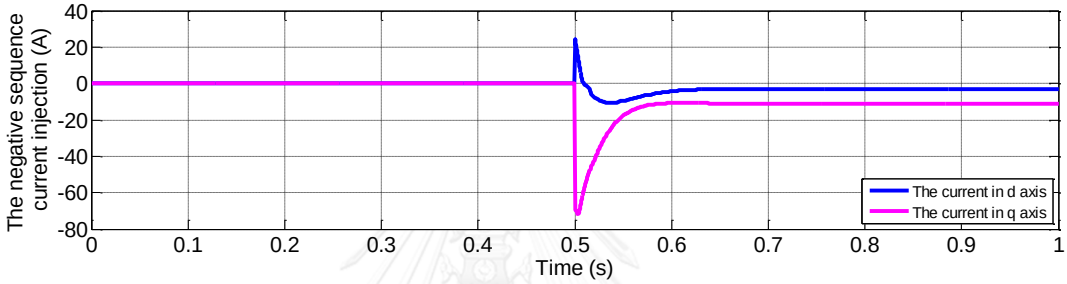

Fig. 23. The injected negative-sequence currents before and after compensation.

4.2.2.2 Compensation results with the real system

The aforementioned PI gains are applied to the real system in Fig. 24.

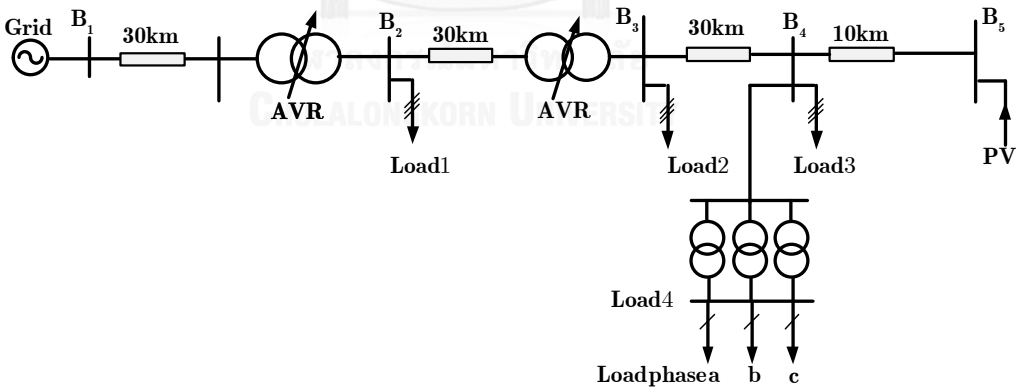

Fig. 24. System diagram of a distribution feeder in Mae Hong Son area.

Fig. 25 illustrates the negative-sequence voltage deviation (error) before and after the injection of the negative-sequence current (at 0.5 s). Before compensation, the d- and q-axis negative-sequence voltages are $V_d^- = -430V$ and $V_q^- = -130V$. After the compensation is activated, the two voltages are reduced to almost zero at 0.6s, and as depicted in Fig. 26 the injected negative-sequence currents are $I_d^- = -2.9A$ and

$I_q^- = -11A$, respectively. The voltages and currents in Fig. 25 and Fig. 26 are similar to Fig. 22 and Fig. 23, respectively. Therefore, the designed PI gain from the simplified method in the subsection 4.2.2.1 is still acceptable in the real system model, even though the system configuration and impedances are different.

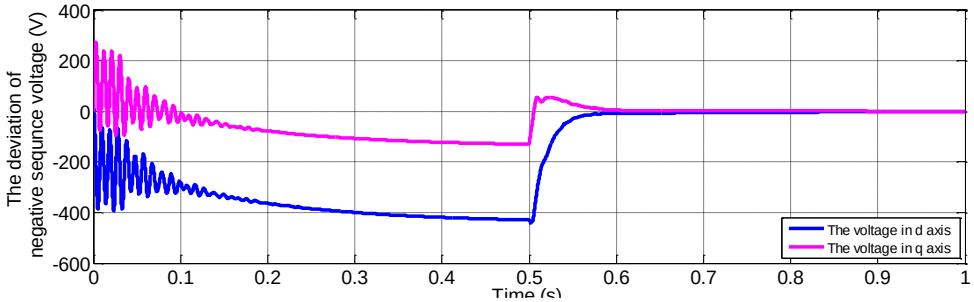

Fig. 25.The deviation of negative-sequence voltages before and after compensation.

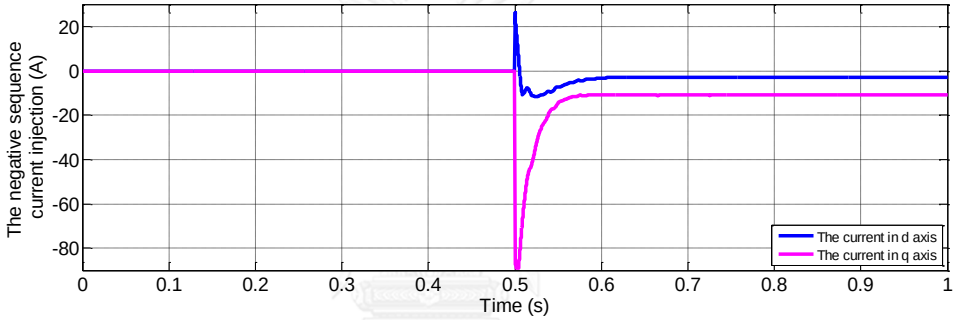

Fig. 26.The injected negative-sequence currents before and after compensation.

Four simulation cases shown in Table 9 are used to investigate the dynamic responses of the system in order to confirm the robustness of the unbalanced voltage controller with the variation of PV power injection.

Table 9: Four simulation cases at various PV power.

	Single loads in each phase			Three phases loads, PF=0.85			PV power
	phase a	phase b	phase c	load 1	load 2	load 3	
Case 1	100 kW	300 kW	1000 kW	1 MVA	1 MVA	2 MVA	0 MW
Case 2	100 kW	300 kW	1000 kW	1 MVA	1 MVA	2 MVA	600 W
Case 3	100 kW	300 kW	1000 kW	1 MVA	1 MVA	2 MVA	2 MW
Case 4	100 kW	300 kW	1000 kW	1 MVA	1 MVA	2 MVA	4 MW

4.2.2.2.1 Dynamic response against various PV powers

Fig. 27(a)-(d) illustrate the results of compensation of negative-sequence voltages in d-q axis of the Case1-4, respectively. The results show that at starting the transient of the system and also of the PLL exhibit more oscillation when the injected power of PV increased. The PLL works well even with the high injection of power from PV. In fact, the change of the transients among the four cases is due to the variation of the bus voltages in the system. When the injected power of PV is increased, the voltages at the PCC also increase which create more transient in the response.

However, as depicted in Fig. 28 the injection of negative-sequence currents started at the instant of 0.5 s for Case1-Case 3 and at 1s for Case 4 does not create any oscillation at all. The negative-sequence voltages are reduced to almost zero at the instant of 0.6 s for Case 1-Case 3 and at around 1.1 s for Case 4. Therefore, the controller needs around 0.1 s to compensate the unbalanced voltages in the system. Consequently, it can be concluded that the controller with the designed PI gains is robust enough to the changing of PV power in the system.

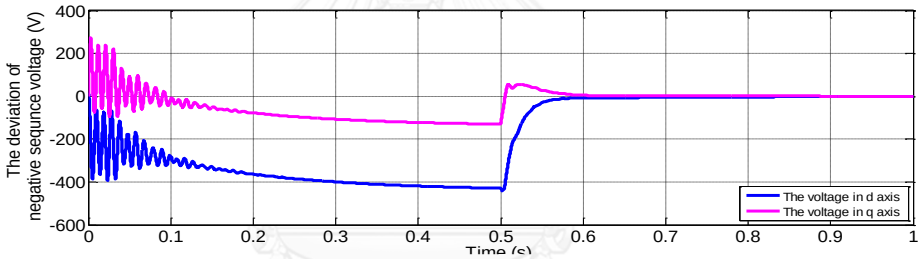

(a)

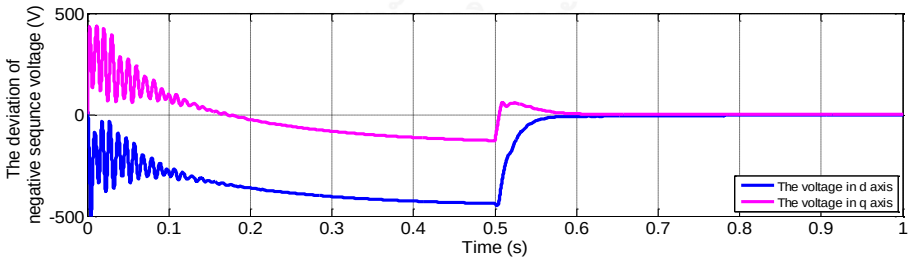

(b)

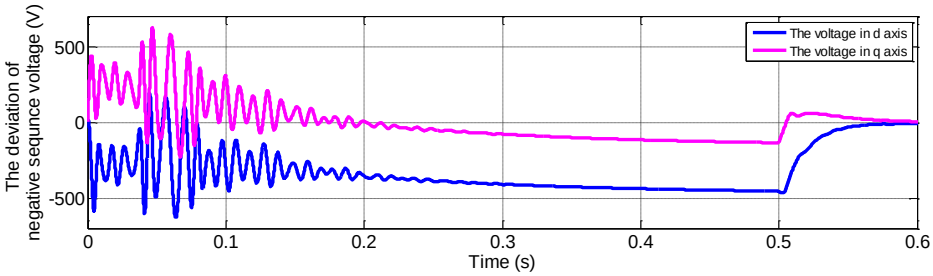

(c)

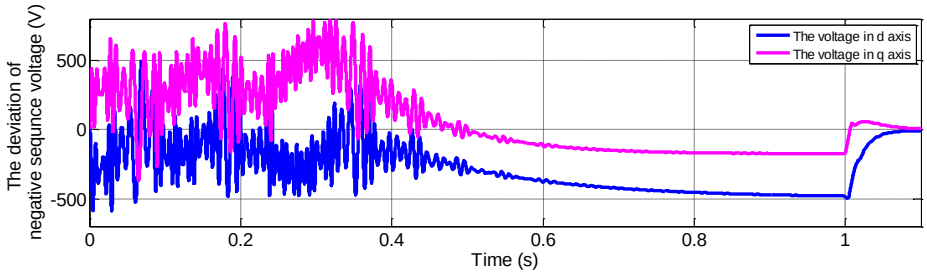

(d)

Fig. 27.The deviation of negative-sequence voltages before and after compensation. (a)without the PV power.(b) with 600kW PV. (c) with 2MW PV. (d) with 4MW PV

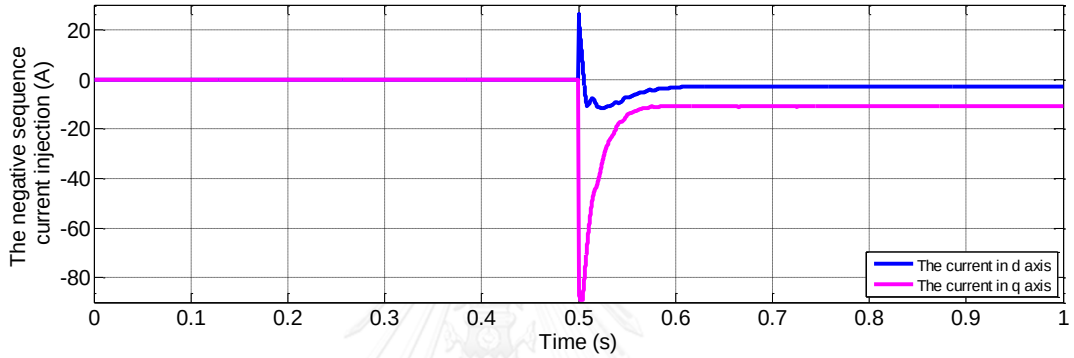

(a)

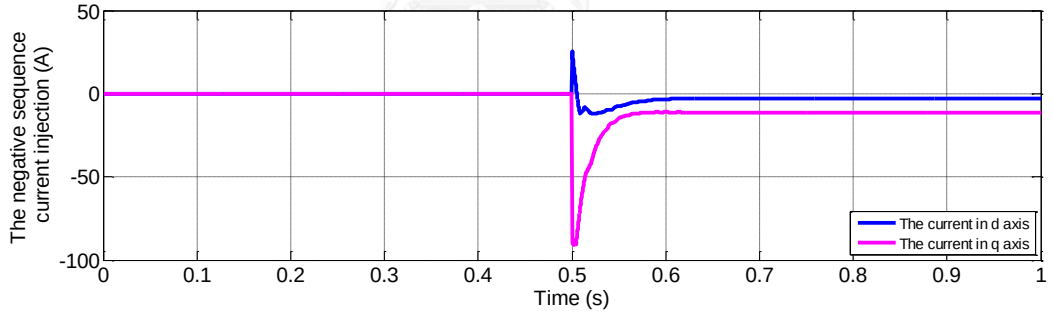

(b)

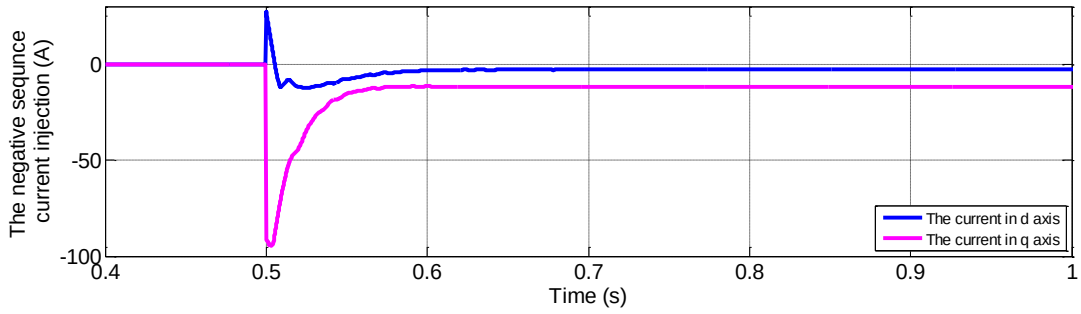

(c)

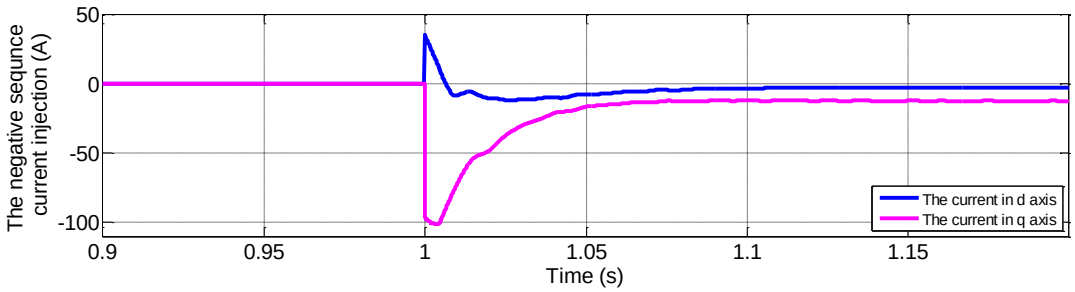

(d)

Fig. 28.The injected negative-sequence currents before and after compensation. (a) without PV injection. (b) with 600 kW PV. (c) with 2MW of PV. (d) with 4MW of PV

Fig. 29(a) illustrates the PCC voltages and currents without PV. There is a step change at the beginning of the simulation which is due to the response of the RMS calculation block. The RMS value is held at the specified initial value for the first cycle. Before the injection of negative-sequence currents, the inverter current is zero because there is no current from both the PV generation and the negative-sequence current controller. After the injection of negative-sequence currents at the instant of 0.5 s, the PCC voltages become balanced and the inverter currents are equal to the currents from negative-sequence current controller.

Fig. 29(b)-(d) illustrate the changing of the PCC voltages when the corresponding PV power is injected into the system. The transient at the beginning is caused by the PV injection, and it can be seen that the PCC voltages are increased when the injected PV power increased. However, the system still stays stable even though the injection of PV is very high. Besides, the negative-sequence current controller can compensate the unbalanced voltages within a short time period.

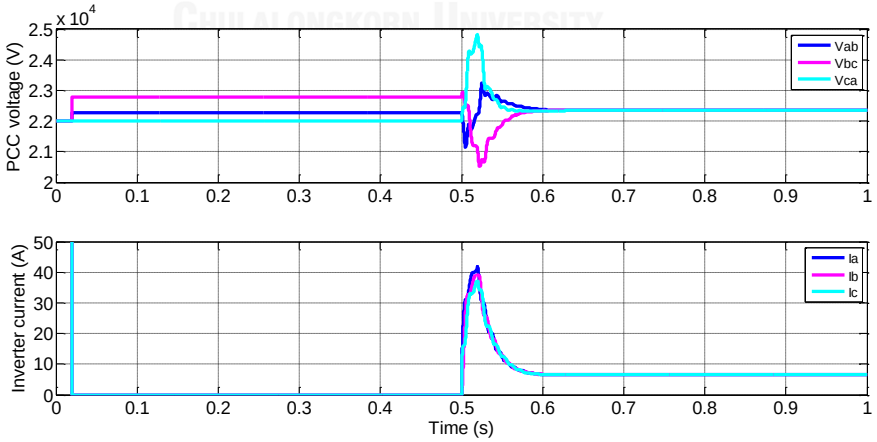

(a)

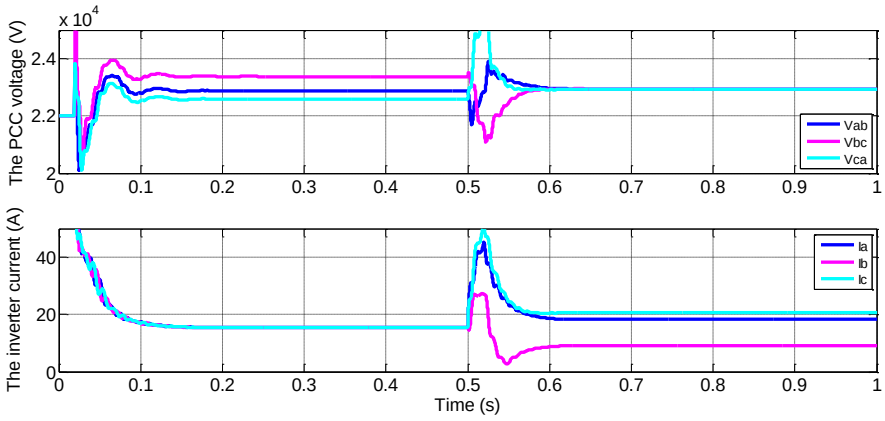

(b)

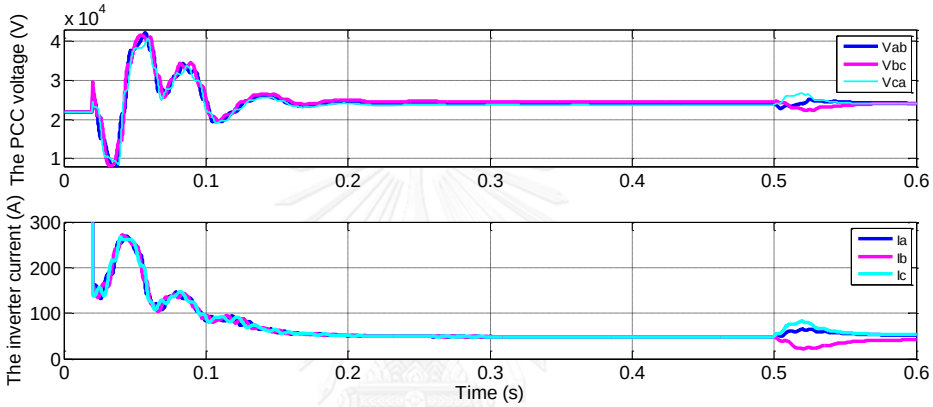

(c)

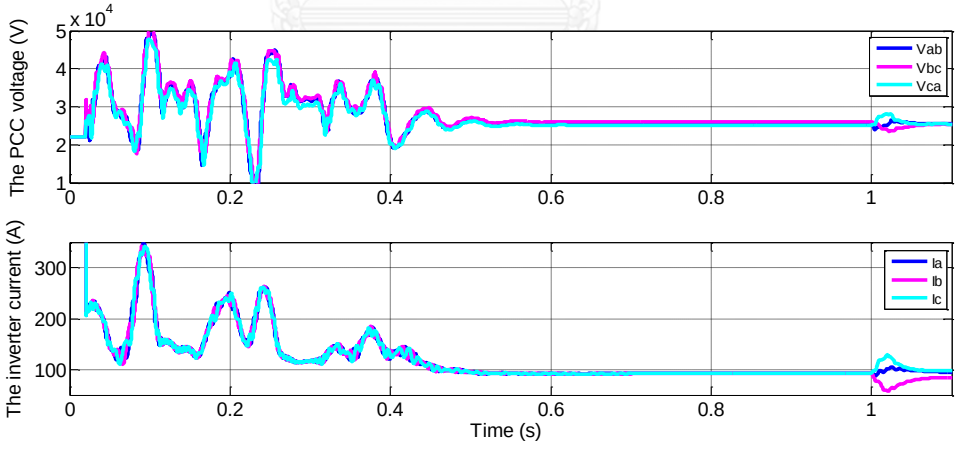

(d)

Fig. 29. The PCC voltages and inverter currents before and after compensation. (a)without PV injection. (b) with 600 kW PV. (c) with 2 MW PV. (d) with 4MW PV.

4.2.2.2.2 Steady-state response against various PV powers

Table 10-Table 12 summarize all the numerical results of Case 1, and Tables 13-16 are those of Case 2. The results of Case 3 and 4 are given in the appendix C.

The voltages and currents are unbalanced without the injection PV and without compensation as depicted in Table 10. The bus 1 is the swing bus so the generator generates a constant voltage, while the buses 2-5 are load buses so the voltages are changed depending on the loads. The balanced three-phase loads are connected at the buses 2 and 3, and the single-phase loads which produce the negative-sequence currents in the system exist only at the bus 4. Therefore, the unbalanced voltages can be observed at all buses except the bus 1. The voltages at the buses 2 and 3 are not heavily unbalanced as compared to those of the buses 4 and 5 because they are far away from the unbalanced loads and are located next to the AVR.

Table 11 shows the results after the injection of negative-sequence currents at the instant of 0.5 s. The voltages at PCC become balanced and the maximum line-to-line voltage is reduced with the injection of 6.597A of negative-sequence current in each phase. The unbalanced voltage compensation at the bus 5 also helps to balance the voltages at other buses. The voltages and currents at the bus 2 and 3 are almost balanced. The bus 4 which is connected to the unbalanced loads also has nearly balanced voltages even though the current in each phase is still unbalanced.

Table 10: Voltages and currents at each bus with 0 MW PV and without negative-sequence current injection.

	Bus					Three-phase loads			Single-phase loads
	B1	B2	B3	B4	B5	load 1	load2	load3	load4
Vab [kV]	22	22.4	22.52	22.22	22.27	22.4	22.52	22.22	22.22
Vbc[kV]	22	22.54	22.85	22.72	22.77	22.54	22.85	22.72	22.72
Vca [kV]	22	22.26	22.29	21.94	21.99	22.26	22.29	21.94	21.94
Ia [A]	142.2	117.2	83.16	16.84	0	26.47	26.46	52.14	16.18
Ib [A]	147.2	118	80.11	17.44	0	26.8	27.12	53.99	5.852
Ic [A]	154.2	128.3	91.52	17.23	0	26.63	26.85	53.34	18.19

Table 11: Voltages and currents at each bus with 0 MW PV and negative- sequence current injection at 0.5 s.

	Bus					Three-phase loads			Single-phase loads
	B1	B2	B3	B4	B5	load 1	load2	load3	load4
Vab [kV]	22	22.4	22.54	22.28	22.34	22.4	22.54	22.28	22.28
Vbc[kV]	22	22.41	22.58	22.34	22.34	22.41	22.58	22.34	22.34
Vca [kV]	22	22.39	22.53	22.27	22.34	22.39	22.53	22.27	22.27
Ia [A]	147.6	120.9	84.84	23.59	6.597	26.62	26.78	53.05	16.45
Ib [A]	147.9	120.8	84.38	16.71	6.597	26.65	26.84	53.22	5.745
Ic [A]	148.8	121.8	85.5	13.37	6.597	26.64	26.82	53.19	18.33

Table 12 shows the positive- and negative-sequence voltages of the bus 5 before and after compensation. It is clear that after the compensation the PCC voltages are reduced and become equal to the positive-sequence voltages because the negative-sequence voltages are almost zero.

Therefore, the injection of negative-sequence currents not only helps to balance the voltage at the PCC bus, but it also helps to balance the voltage at other buses. As a result, the maximum line-to-line voltages at each bus are reduced too.

Table 12: PCC voltages and inverter currents before and after the injection of negative-sequence current.

Bus 5 (B 5) before compensation							
Vab [kV]	22.27	V^+ab [kV]	22.37	V^-ab [V]	447	Ia [A]	0
Vbc [kV]	22.77	V^+bc [kV]	22.33	V^-bc [V]	447	Ib [A]	0
Vca [kV]	21.99	V^+ca [kV]	22.33	V^-ca [V]	447	Ic [A]	0
Bus 5 (B 5) after compensation							
Vab [kV]	22.34	V^+ab [kV]	22.34	V^-ab [V]	1.34	Ia [A]	6.597
Vbc [kV]	22.34	V^+bc [kV]	22.34	V^-bc [V]	1.35	Ib [A]	6.597
Vca [kV]	22.34	V^+ca [kV]	22.34	V^-ca [V]	1.36	Ic [A]	6.597

Similar simulation is done when a 600 kW PV is integrated into the system and the results are shown in Table 13. The voltages at each bus are increased compared to those of Table 10 with 0 MW PV. The maximum line-to-line voltages of the buses 3, 4 and 5 are increased over the limit and the voltages are unbalanced. The currents at the buses 2, 3 and 4 are somewhat unbalanced, while the currents at the bus 5 are balanced without the negative-sequence current injection. Table 14 shows the results after the injection of negative-sequence currents at the instant of 0.5 s. The PCC voltages (bus 5) now become balanced, and the PV inverter's currents are the sum of PV active current and the negative-sequence current from the unbalanced voltage compensator. The voltages and currents at other buses are almost balanced too. The maximum line-to-line voltages of all buses are reduced and stay within the limit. Therefore, it is necessary to compensate the unbalanced voltage because it helps to solve the voltage rise problem. Table 15 shows in more details the voltages at the bus 5. It contains only positive-sequence voltages because the negative-sequence voltages are suppressed to zero by the unbalanced voltage compensation.

Table 13: Voltages and currents at each bus with 600kW PV and without the injection of negative-sequence current.

	Bus					Three-phase loads			Single-phase loads
	B1	B2	B3	B4	B5	load 1	load2	load3	load4
Vab [kV]	22	22.64	22.94	22.78	22.87	22.64	22.94	22.78	22.78
Vbc[kV]	22	22.78	23.28	23.28	23.38	22.78	23.28	23.28	23.28
Vca [kV]	22	22.5	22.71	22.49	22.58	22.5	22.71	22.49	22.49
Ia [A]	136.2	106.9	70.38	23.21	15.33	26.75	26.95	53.43	16.58
Ib [A]	142.2	108.7	68.05	23.73	15.32	27.08	27.63	55.33	5.997
Ic [A]	149.3	118.7	79.43	23.18	15.32	26.92	27.36	54.66	18.64

Table 14: Voltages and currents at each bus with 600kW PV and with the injection of negative-sequence current at 0.5 s.

	Bus					Three-phase loads			Single-phase loads
	B1	B2	B3	B4	B5	load 1	load2	load3	load4
Vab [kV]	22	22.64	22.96	22.84	22.94	22.64	22.96	22.84	22.84
Vbc[kV]	22	22.65	23	22.89	22.94	22.65	23	22.89	22.89
Vca [kV]	22	22.63	22.95	22.82	22.94	22.63	22.95	22.82	22.82
Ia [A]	142.1	111.1	72.45	72.45	18.26	26.9	27.28	54.37	16.86
Ib [A]	142.4	111.1	72.06	72.06	8.971	26.93	27.34	54.54	5.888
Ic [A]	143.2	112.1	73.19	73.19	20.68	26.92	27.32	54.51	18.79

Table 15: PCC voltages and inverter currents with 600 kW PV before and after the injection of negative-sequence current.

Bus 5 (B 5) before compensation							
Vab [kV]	22.87	V^+ab [kV]	22.97	V^-ab [V]	455	Ia [A]	15.33
Vbc [kV]	23.38	V^+bc [kV]	22.93	V^-bc [V]	455	Ib [A]	15.32
Vca [kV]	22.58	V^+ca [kV]	22.93	V^-ca [V]	455	Ic [A]	15.32
Bus 5 (B 5) after compensation							
Vab [kV]	22.94	V^+ab [kV]	22.94	V^-ab [V]	0	Ia [A]	18.26
Vbc [kV]	22.94	V^+bc [kV]	22.94	V^-bc [V]	0	Ib [A]	8.971
Vca [kV]	22.94	V^+ca [kV]	22.94	V^-ca [V]	0	Ic [A]	20.68

The results of the Case 3 and Case 4 are shown in the appendix C. The resultant PCC voltages for the four Cases are summarized in Fig. 30 below. The dashed and solid lines are the results with and without the unbalanced voltage compensation, respectively.

Fig. 30 shows that the maximum line-to-line voltages are increased when the injection of PV is increased. The blue line is the maximum line-to-line voltage without the injection of PV. The voltages with 0 MW PV are in the acceptable range. However, when the PV power is increased to 600kW, without unbalanced voltage compensation the voltage is over the limit as shown by the solid red line. However, after the injection of negative-sequence current, the voltages becomes balanced and reduced to the

acceptable range again as shown by the dashed red line. Therefore, the negative-sequence current injection alone is enough to solve the voltage rise problem in this case. However when the PV injection is increased to 2MW and 4MW, the unbalanced voltage compensation alone cannot successfully suppress the voltage rise. Therefore, additional controllers are needed to reduce the voltage rise in this case which will described in the next chapter.

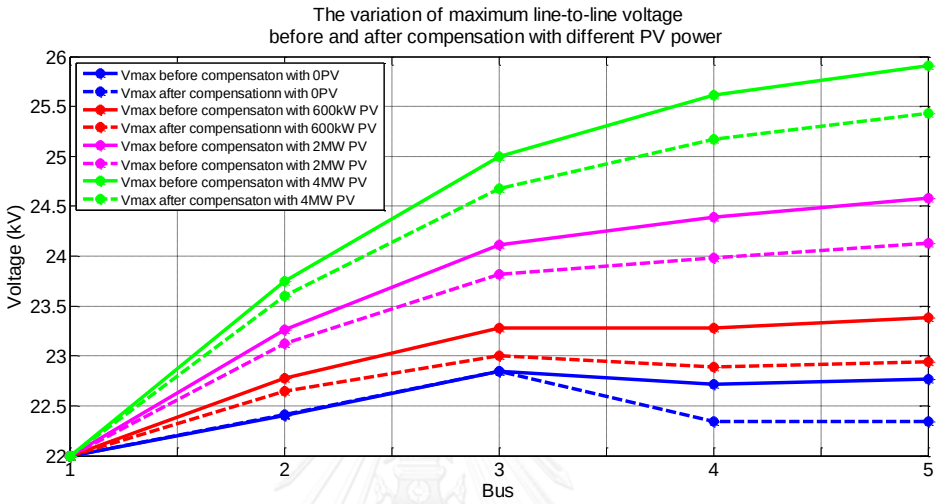

Fig. 30. Variation of maximum line-to-line voltages before and after unbalanced voltage compensation for various PV powers.

4.3 Phasor simulation of unbalanced voltage compensation

4.3.1 Negative-sequence current controller for phasor simulation

The positive- and negative-sequence voltage phasors denoted by $\mathbf{V}^{+}$ and $\mathbf{V}^{-}$ can be found from the PCC voltage phasor as depicted in Fig. 31 and explained in the appendix A.2.

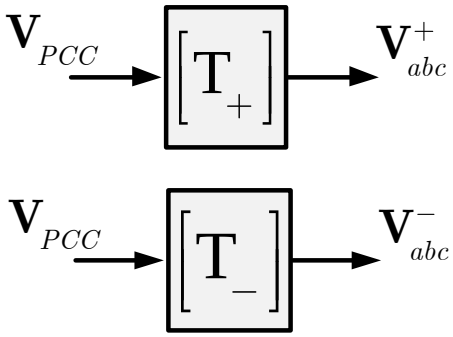

Fig. 31. The positive- and negative- sequence extraction in phasor simulation

Table 16 shows the relationship between space-vector calculation and the corresponding complex variables in the unbalanced voltage compensation scheme. The

space vector of the instantaneous three-phase voltage can be represented as a complex variable. For the negative-sequence voltage, the corresponding space vector on the stationery frame will be a rotating vector at the frequency ω in the clockwise direction $v_\alpha + jv_\beta = \mathbf{V}_a^{-*} e^{-j\omega t}$. Note here that the coefficient of the space vector is just the conjugated voltage phasor $\mathbf{V}_a^{-*}$. This space vector becomes $v_d + jv_q = \mathbf{V}_a^{-*} e^{-j2\omega t}$ on the d-q reference frame. Therefore, the after using the transformation $\left(\times e^{j2\omega t}\right)$ the resultant space vector is $v_d^- + jv_q^- = \mathbf{V}_a^{-*}$ (which corresponds to the calculation of the negative-sequence voltage space vector on the $d^- - q^-$ reference frame; $v_{dq}^- e^{j2\omega t}$). In summary, the calculation of the negative-sequence voltage space vector in the unbalanced voltage compensation is equivalent to the calculation of the conjugated negative-sequence voltage phasor. The same conclusion can be deduced for the negative-sequence current space vector as well, i.e., $i_d^- + ji_q^- = \mathbf{I}_a^{-*}$. Since the phasor is represented by a complex value, the real part and imagination part of the complex variables are related to the d-q axis components directly. The block diagram of the unbalanced voltage compensation can be drawn as shown in the last row of Table 16. The same PI controllers appear in both the time and phasor calculation diagram.

Fig. 32 shows the phasor simulation blocks of the unbalanced voltage compensation for *a* and *b* phases, respectively. The block diagram for *c* phase is unnecessary because in the simulation the current in *c* phase will be automatically calculated from the information of the *a* and *b* phases.

Table 16: The relationship between space-vector calculation and complex variables in the negative-sequence current injection

Space vector	Complex quality
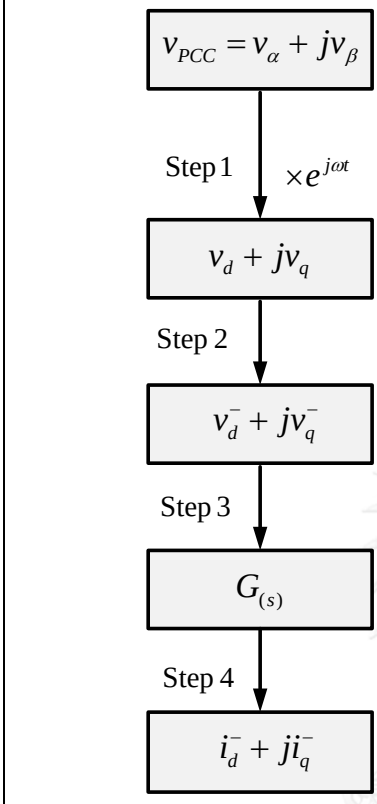	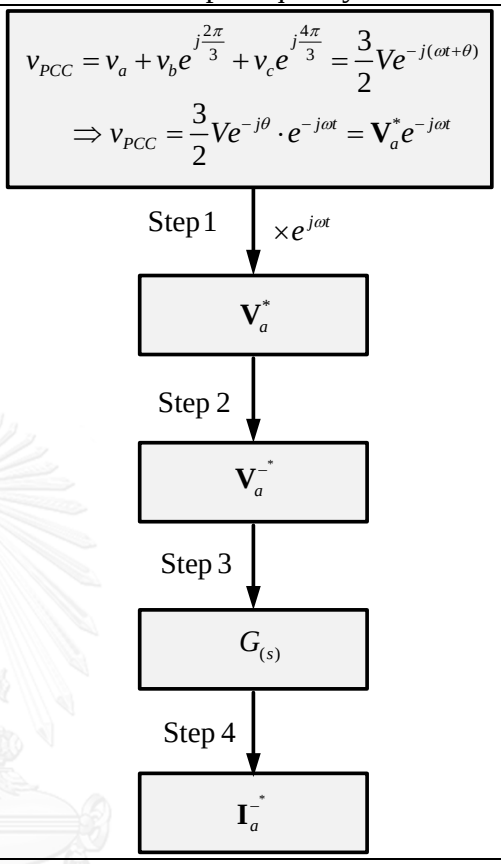
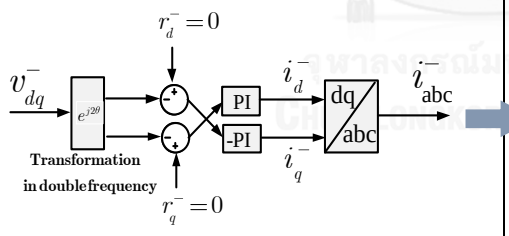	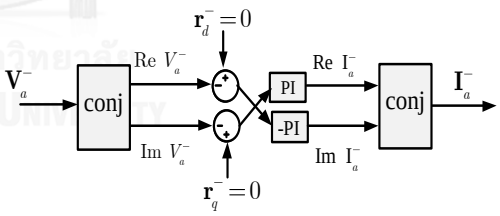
(a)	(b)

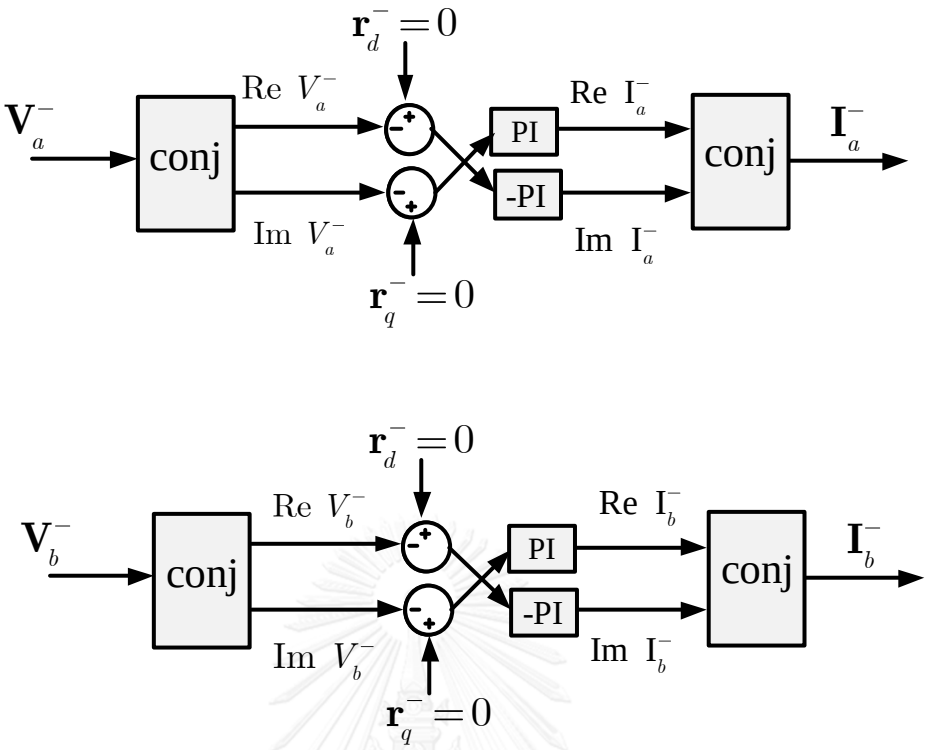

- $\mathbf{V}_{PCC}$: the voltage phasor at the PCC
- $[\mathrm{T}_+], [\mathrm{T}_-]$: the positive- and negative- sequence transformations, respectively.
- $\mathbf{V}_{abc}^+, \mathbf{V}_{abc}^-$: the voltage phasors of *a*, *b*, and *c* phases in the positive and negative sequences, respectively.
- $\mathbf{V}_a^-, \mathbf{I}_a^-$: the phasors of the negative-sequence voltage and current in *a* phase.
- $\mathrm{Re}(V_a^-), \mathrm{Re}(V_b^-)$: the real parts of the negative-sequence voltage phasors of *a*, *b* phases.
- $\mathrm{Im}(V_a^-), \mathrm{Im}(V_b^-)$: the imaginary parts of the negative-sequence voltage phasors of *a*, *b* phases.
- $\mathrm{Re}(I_a^-), \mathrm{Re}(I_b^-)$: the real parts of the negative-sequence current phasors of *a*, *b* phases.
- $\mathrm{Im}(I_a^-), \mathrm{Im}(I_b^-)$: the imaginary parts of the negative-sequence current phasors of *a*, *b* phases.

Fig. 32. Unbalanced voltage compensation in phasor simulation.

4.3.2 Phasor simulation results of the unbalanced voltage compensation for the simplified system

In the following, the phasor simulation will be used to investigate long-term steady-state behaviors of the system when the single-phase loads are varied according to Table 17. The negative-sequence voltage extraction and the unbalanced voltage compensation are carried out using the aforementioned equations and block diagrams for phasor simulation.

Table 17: The variation of single-phase loads

time (s)	Single-phase loads			Three-phase loads, PF=0.85		
	phase a	phase b	phase c	load 1	load 2	load 3
t=[0,0.7]&[1.2,2]	100 kW	300 kW	1000 kW	1 MVA	1 MVA	2 MVA
t=[0.7, 1.2]	0 kW	300 kW	1000 kW	1 MVA	1 MVA	2 MVA

Fig. 33 and Fig. 34 show that during $t \in [0,0.2]$ (s) the negative-sequence voltages in d-q axis are 233V and 190V, respectively. When the negative-sequence current I^- is injected into the system at the instant of 0.2 s as depicted in Fig. 34, the negative-sequence voltages reduce to zero. Consequently, the PCC voltages become balanced with the injection of negative-sequence current as shown in Fig. 35. However, at the instant of 0.7s, the single-phase load of *a* phase changes and is equal to zero immediately. The voltages thus become unbalanced again, and the unbalanced voltage controller reacts by generating new negative-sequence currents in order to compensate the new unbalanced voltages. And finally the negative-sequence voltages are suppressed to zero again, so the PCC voltages become balanced. Next, at the instant of 1.2s the single-phase loads of *a* phase were reconnected to the system making the unbalanced voltage compensator to start to compensate the unbalanced voltage again. The three-phase load currents and the single-phase load currents are illustrated in Fig. 36(a)-(b). It is confirmed then that the designed unbalanced voltage compensator works fast enough to suppress the unbalanced voltages even when the loads are changed.

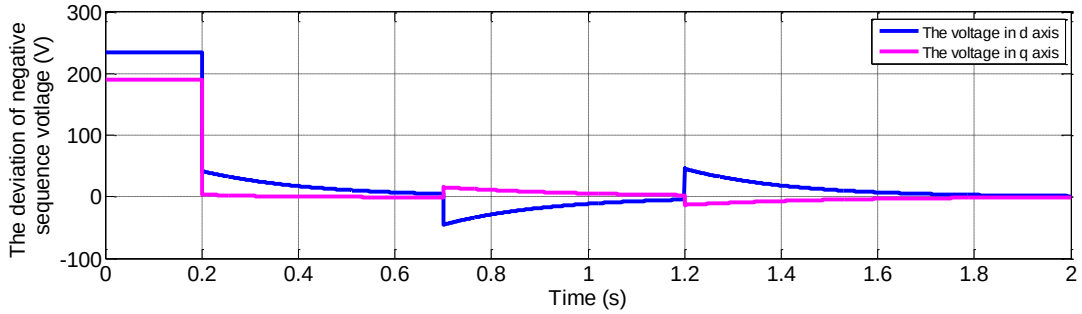

Fig. 33. The deviation of negative-sequence voltages in phasor simulation with the simplified system.

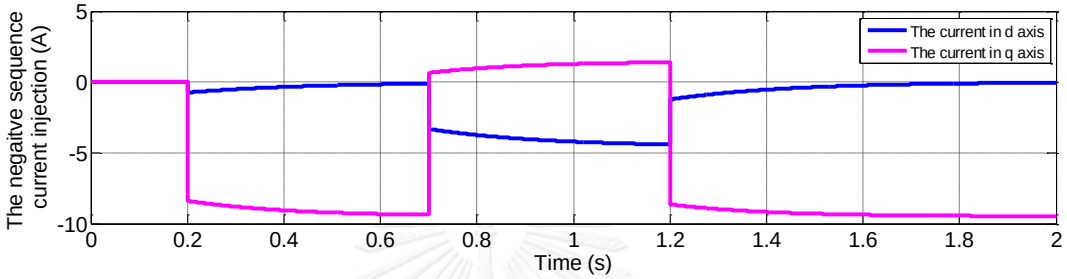

Fig. 34. The injected negative-sequence currents in phasor simulation with the simplified system.

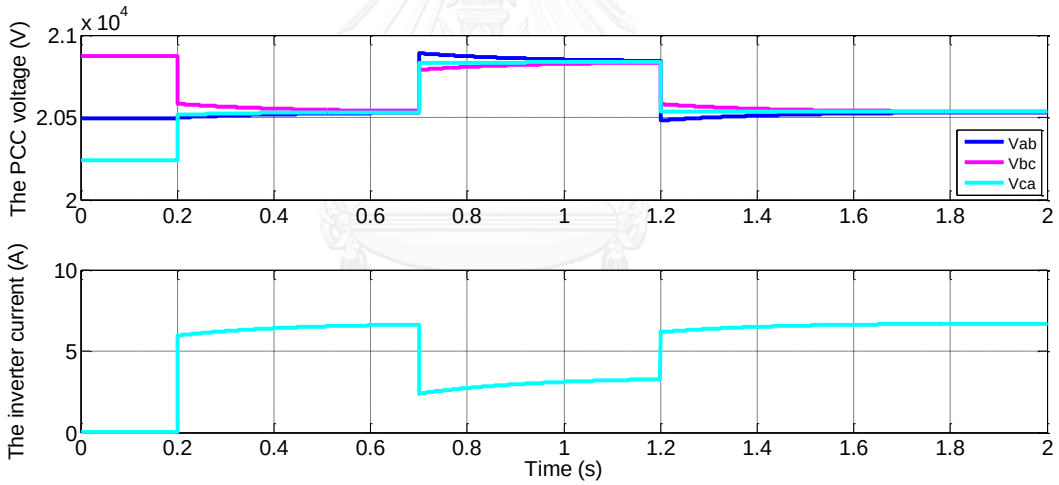

Fig. 35. The PCC voltages and inverter currents in phasor simulation with the simplified system.

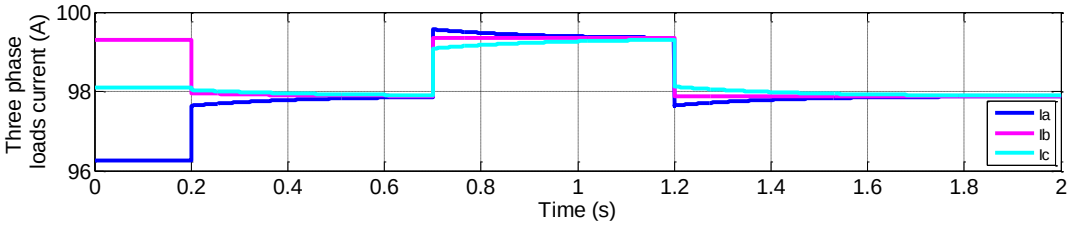

(a)

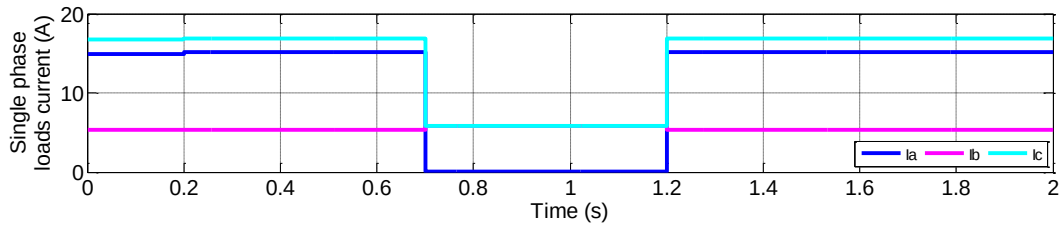

(b)

Fig. 36. Load currents in phasor simulation with the simplified system. (a)Three-phase load currents. (b) Single-phase load currents.

4.3.3 Phasor simulation result of the unbalanced voltage compensation for the real system

Phasor simulation is now done with the real system in order to confirm the effectiveness of the controller to compensate the unbalanced voltage in the system. The same load variations shown in Table 17 are applied to the real system. Fig. 37 illustrates the variation of the PCC voltages and the inverter currents similar to those of Fig. 35. There are some differences due to the differences in system configuration and line impedances. The designed unbalanced voltage compensator works well both with the simplified and the real systems.

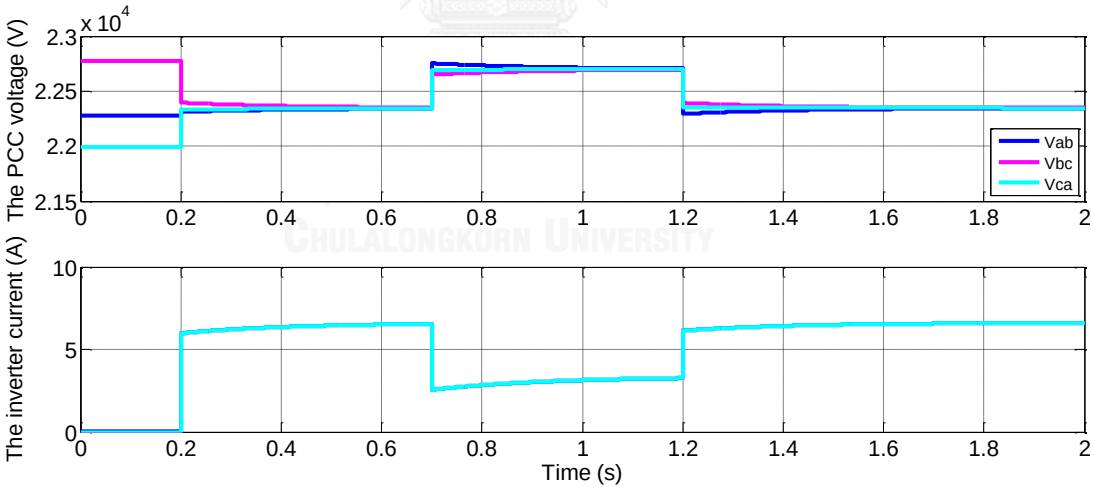

Fig. 37. The variation of the PCC voltages and the inverter currents in phasor simulation with the real system.

Fig. 38 is the phasor simulation results showing the bus voltages at different PV powers. The phasor simulation results in Fig. 38 are similar to those of time simulation shown in Fig. 30. Therefore, it is confirmed that both time and phasor simulation can be used to study the system behavior in a short- and long-time scale.

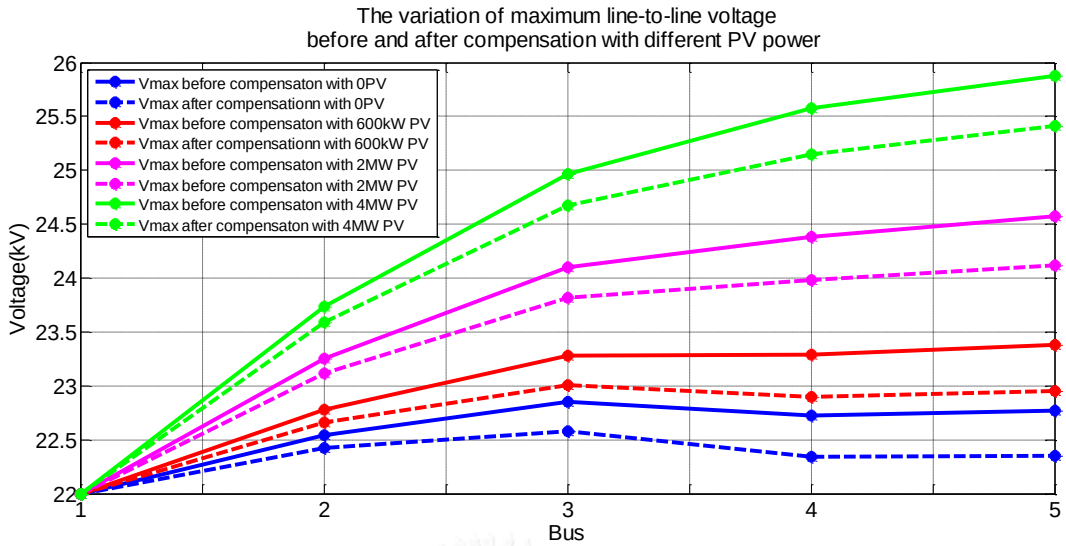

Fig. 38. Phasor simulation results showing variation of maximum line-to-line voltages before and after unbalanced voltage compensation for various injected PV powers.

4.4 Comparison between time and phasor simulation for the real system

The voltages at the PCC of the time and phasor simulations will be compared to show the correctness of the two simulation methods. Fig. 39 shows the differences of the PCC voltages for the investigated four cases as explained in Table 9. Figures in the left-hand and the right-hand columns are the PCC voltages before and after unbalanced voltage compensation, respectively. The PCC voltages calculated from the time simulation are shown in bar graphs along with the values calculated from the phasor simulation on the right. It can be concluded then that both time and phasor simulations give almost exactly the same numerical values, except for some negligible small discrepancies which may be due to the modeling of the PLL part.

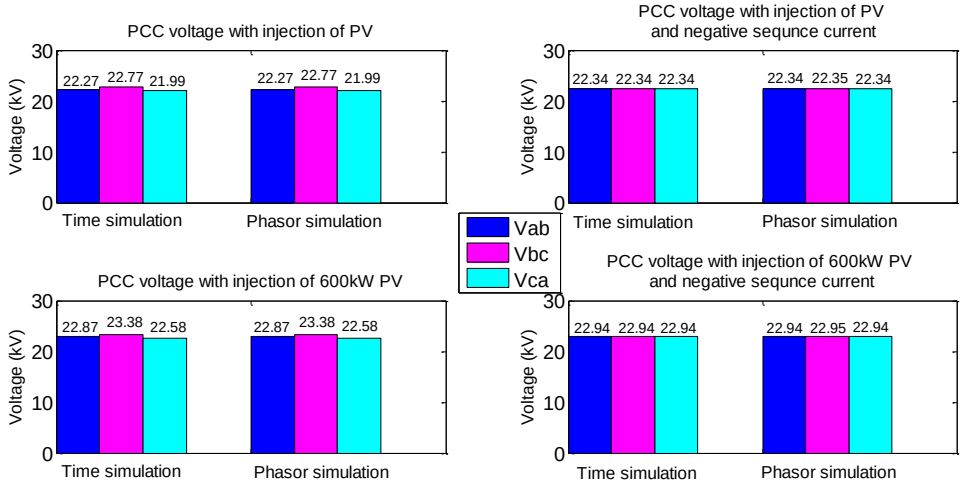

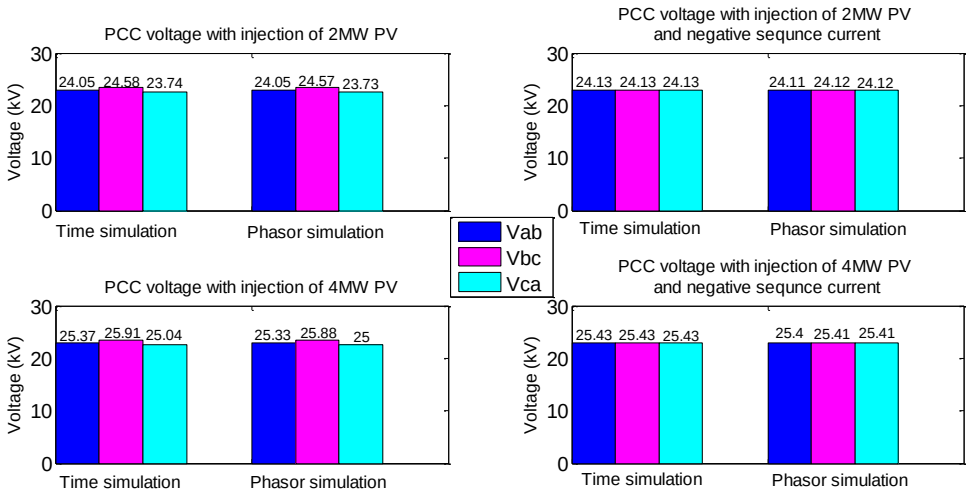

Fig. 39. Comparison of the PCC voltages calculated from time and phasor simulations for four cases.

5 Voltage rise mitigation by reactive current injection

Previous chapter demonstrates how the unbalanced voltage compensation automatically helps to solve the voltage rise problem by using the negative-sequence current injection. However, in several cases the unbalanced voltage compensation alone is incapable to bring the voltages back into the limit. This chapter will introduce additional reactive current injection which operates in parallel with the unbalanced voltage compensator to suppress the voltage rise.

5.1 Reactive current injection

The reactive current in the positive sequence denoted by i_q^+ is injected along with the negative-sequence current. If the inverter has some margin for additional current injection, the reactive current injection will be determined by the droop controller depicted in Fig. 40(a). The maximum reactive current that can be injected depends on the capacity inverter, whose value can be calculated from Eqs. (38)-(41). If the inverter does not have enough capacity, the reactive current injection may not be able to successfully suppress the voltage rise.

5.1.1 Sizing and rated current of the PV inverter

Usually, the inverter is sized at 10% higher than the connected PV capacity. In this study the maximum power of PV generation is 4 MW. Therefore, the rated power of inverter is assumed to be 4.4 MVA, and the rated current in each phase is calculated from Eqs. (38)-(40). The numerical result in Eq. (41) shows that the rated current of each phase is equal to 163.3 A.

$$P = \frac{P_{total}}{3} = \frac{V_{rms}}{\sqrt{3}} \cdot I_{rms} \tag{38}$$

$$\Rightarrow I_{rms} = \frac{P\sqrt{3}}{3V_{rms}} \tag{39}$$

$$\Rightarrow I = \sqrt{2} I_{rms} \tag{40}$$

$$I_{\max} = \sqrt{2} \cdot \sqrt{3} \cdot \frac{4.4 \times 10^6}{3 \times 22 \times 10^3} = 163.3\,A \tag{41}$$

5.1.2 Calculation of the maximum reactive current in the positive sequence

After knowing the rated current of the PV inverter, the maximum reactive current (in positive sequence) can be found as shown in Eqs. (42)-(45).

$$i_d = i_{PV}^{+} + i_d^{-} \tag{42}$$

$$i_q = i_q^{+} + i_q^{-} \tag{43}$$

$$i_q \le \sqrt{I_{\max}^2 - i_d^2} \tag{44}$$

$$\Rightarrow i_q^{+} \le i_{q\_\max}^{+} = \sqrt{I_{\max}^2 - i_d^2} - i_q^{-} \tag{45}$$

where

- i_d, i_q : the total active and reactive currents of the PV inverter, respectively,
- i_{PV}^{+} : the active current determined by MPPT or power curtailment algorithm,
- i_d^{-} : the active current in the negative sequence injected by the unbalanced voltage compensation,
- i_q^{+}, i_q^{-} : the reactive currents in positive and negative sequences,
- $i_{q\_\max}^{+}$: the maximum reactive current that can be injected into the system, and
- $I_{\max}$: the rated current of the PV inverter.

5.1.3 The characteristic of droop controller

The injected reactive current is determined according to the algorithm shown in Fig. 40(b)-(c). m_q is the droop coefficient and is calculated from Eq. (46).

$$m_q = \frac{i_{q\_\max}^{+}}{V_{cri} - V_{\lim}} \tag{46}$$

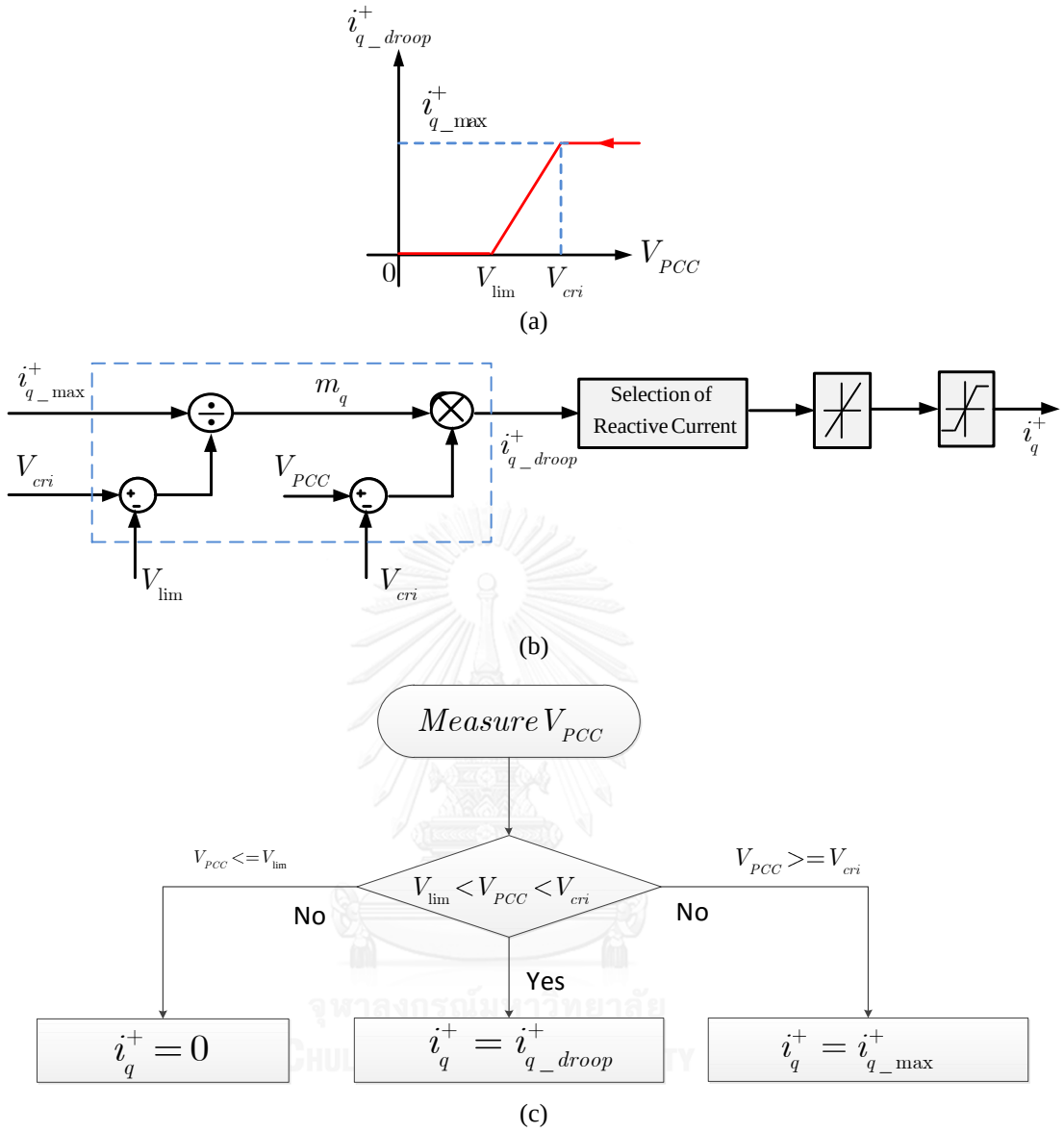

Fig. 40. Droop controller for reactive current injection. (a) Droop characteristic. (b) Schematic of droop controller. (c) Selection algorithm of reactive current.

According to Thailand's Grid code, the values of the nominal voltage (V_n) and the critical voltage (V_{cri}) are set at 1 pu and 1.05 pu, respectively. Although the aim of this research is to reduce the voltage rise to be within the acceptable limit, it is preferable that the reactive current injection is activated only when necessary. From this reason, the threshold voltage (V_{lim}) which determines the starting of the reactive current injection is set closed to the critical voltage to be 1.04 pu. Consequently, the droop controller will work when the voltage is in the range from 22.9kV to 23.1kV. Some additional elements, i.e., the rate limiter and the saturation are also needed. The rate limiter is used to limit the rate of change of the reactive current to prevent the droop controller from fluctuation between 0 and $i^+_{q\_\max}$. The saturation is used to limit the

minimum current to be zero to assure a non-negative value of the reactive current because the controller is designed only for the voltage rise suppression. All the parameters of the reactive current injection are listed in Table 18.

Table 18: Parameters of the reactive current injection.

Parameters	Value
Rated current of the PV inverter	163.3 A
Threshol voltage of the droop controller (V_{lim})	1.04 pu
Critical voltage of the droop controller (V_{cri})	1.05 pu
Rising slew rate of the rate limiter	350
Falling slew rate of the rate limiter	-1
Saturation (upper limit/lower limit)	none/0

The reactive current controller is integrated with the negative-sequence current injection in order to reduce voltage rise. Both time and phasor simulation will be carried out in order to investigate the behavior during transients and steady states.

5.2 Simulation results with constant loads

The data of three-phase loads and single-phase loads in Table 9 are applied again. However, the simulation is done based on three different situations as depicted in Table 19.

Table 19: Simulation conditions for constant load operation.

time	2MW PV injection	I^{-} injection	I_q^{+} injection
at 0s	✓		
at 0.3s	✓	✓	
at 0.5s	✓	✓	✓

5.2.1 Time simulation results

Fig. 41 depicts the maximum reactive current in the positive sequence $(i_{q\_\max}^{+})$ that can be injected by the PV inverter. The maximum current of the inverter in time

simulation (expressed as a space vector quantity) is 1.5 times the amplitude of the rated current in phasor simulation $\left(\frac{3}{2}I_{\max}\right)$, so it is 245A. In the simulation, the PV generation is connected to the grid at the instant of 0 s. Consequently, the maximum line-to-line voltage and the inverter current are increased extremely high during transient as depicted in Fig. 43(a). Therefore, $i^{+}_{q\_\max}$ will be zero when inverter current hits the rated capacity. The negative-sequence current is injected into the system at the instant of 0.3 s in order to compensate the unbalanced voltage and to reduce the voltage rise. The injection of i^{-} produces some transient; however, it disappears after a short-time. When the negative-sequence current i^{-} is injected into the system, $i^{+}_{q\_\max}$ is reduced a little bit. By the unbalanced voltage compensation, the PCC voltages are decreased and become balanced. However, the PCC voltages still stay around 24 kV and are over the limit. Therefore, the reactive current in positive sequence (i^{+}_{q}) is injected into the system at the instant of 0.5 s as shown in Fig. 42. After the injection of the reactive current i^{+}_{q} as depicted in Fig. 43, the PCC voltages are reduced to around 23 kV and are now within the limit.

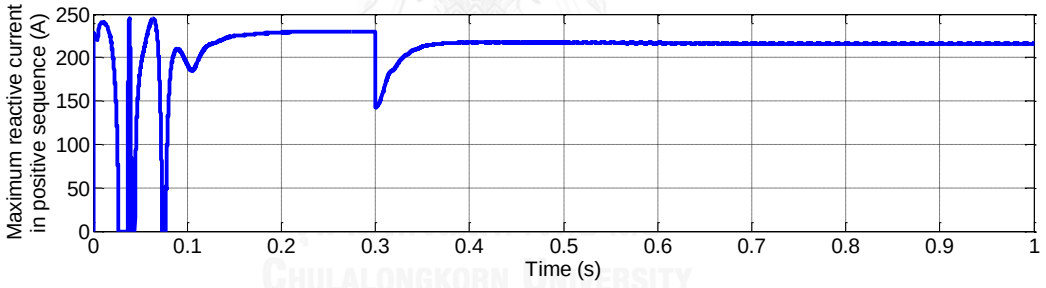

Fig. 41. The maximum limit for the reactive current injection from time simulation.

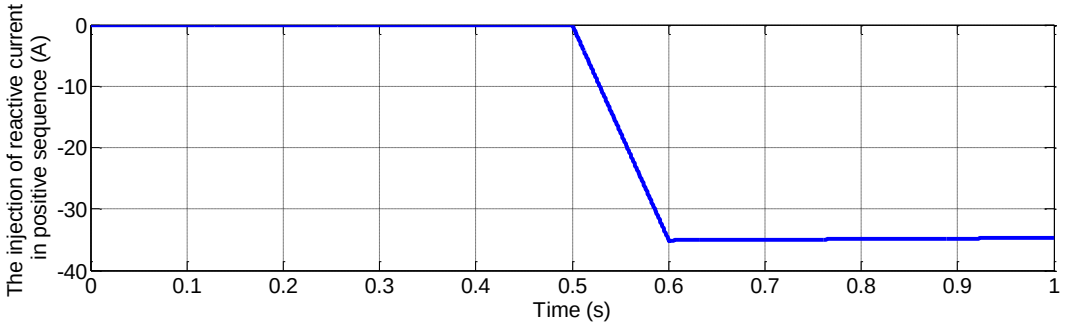

Fig. 42. The injected reactive current from time simulation.

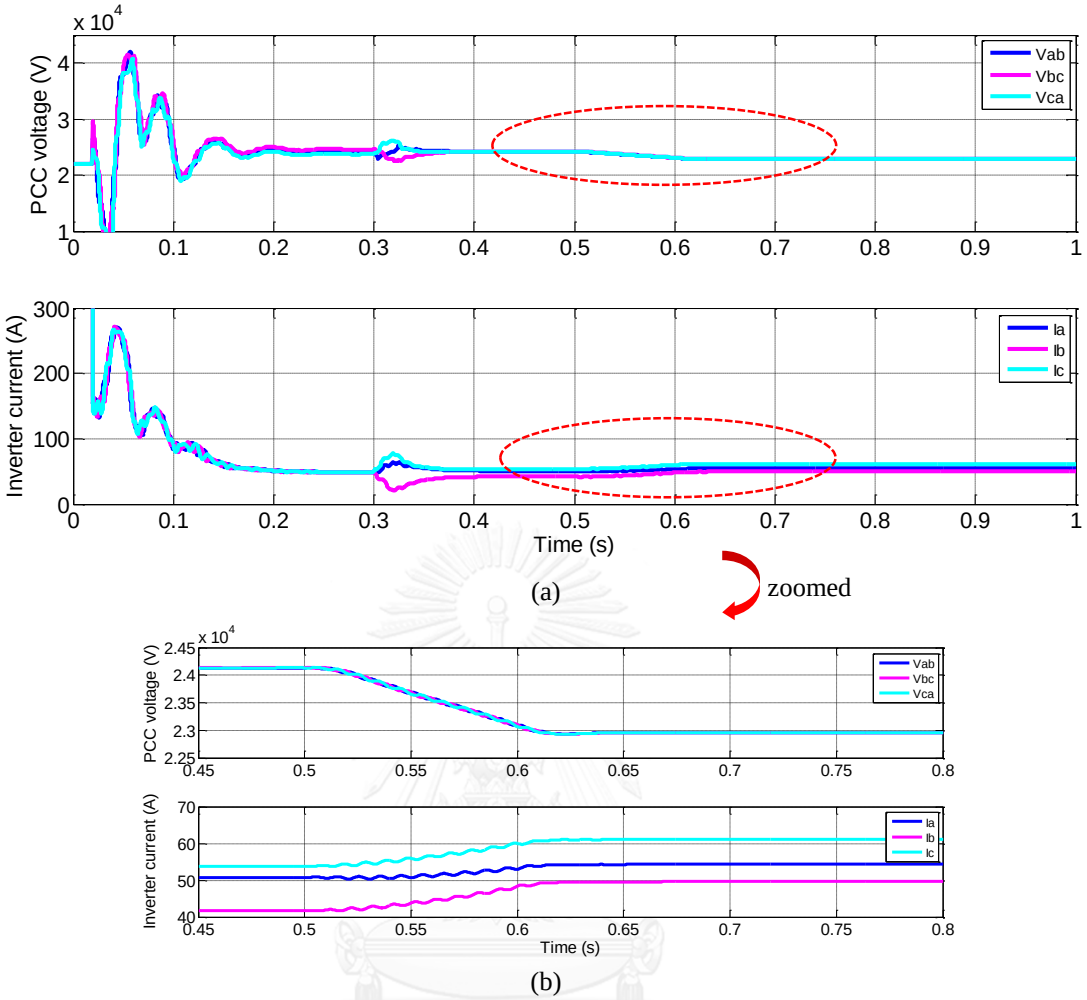

Fig. 43. The PCC voltages and the inverter currents from time simulation.

5.2.2 Phasor simulation results

Similar to Fig. 41, the maximum reactive current in positive sequence $(I^{+}_{q\_\max})$ that can be injected by the inverter is shown in Fig. 44. The PV generation is connected to the grid at the instant of 0 s. The maximum line-to-line voltage is increased over 24.5 kV, and the inverter current is around 50 A as observed in Fig. 46. The negative-sequence current is injected into the system at the instant of 0.3s in order to reduce the voltage rise. After the injection of the negative-sequence current I^{-}, the maximum reactive current in Fig. 44 drops, and the PCC voltages are reduced to 24 kV and become balanced. Furthermore, the reactive current in the positive sequence (I^{+}_{q}) is injected into the system at the instant of 0.5 s as shown in Fig. 45. After the injection of the reactive current I^{+}_{q}, the PCC voltages are reduced to around 23.1 kV as depicted in Fig. 46.

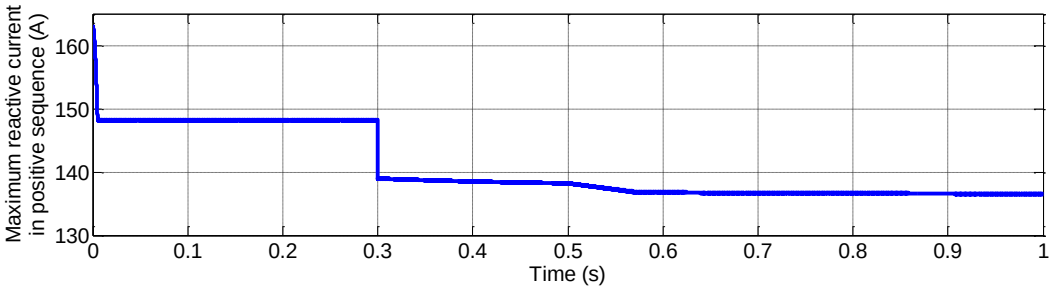

Fig. 44. The maximum limit of the reactive current in phasor simulation.

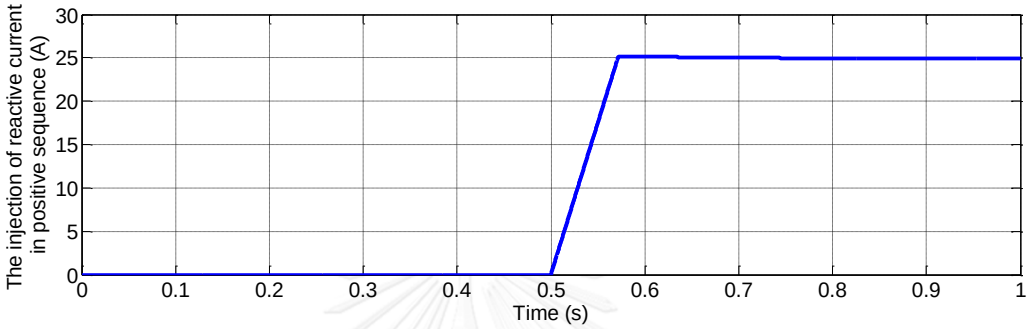

Fig. 45. The injected reactive current in the positive sequence in phasor simulation.

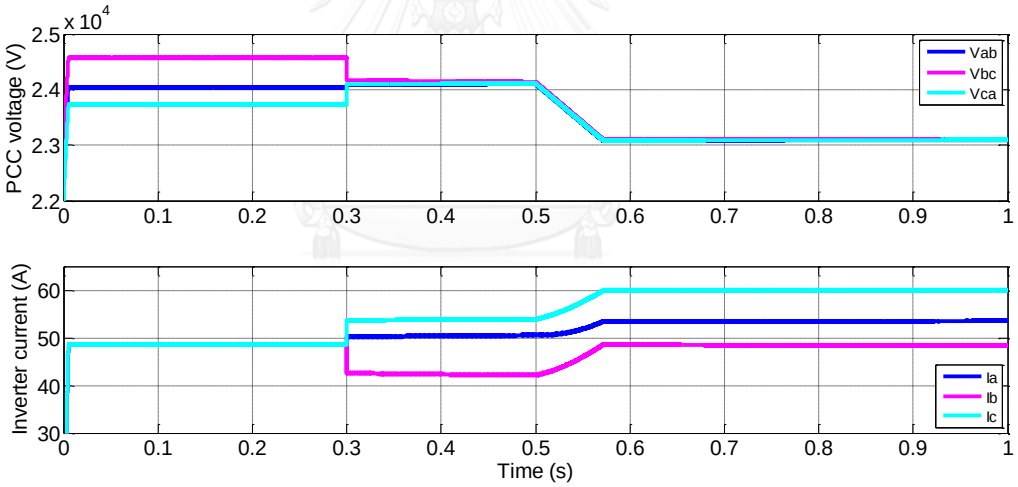

Fig. 46. The PCC voltages and the inverter currents in phasor simulation.

Table 20 compares the numerical values from time and phasor simulations of the PCC voltages and inverter currents in the steady state after the injection of reactive current. It can be seen that time and phasor simulations give almost exactly the same results.

Table 20: PCC voltages and currents after reactive current injection in time and phasor simulation.

	time simulation	phasor simulation
Vab [kV]	22.97	23.1
Vbc [kV]	22.97	23.1
Vca [kV]	22.97	23.1
Ia [A]	54.35A	53.58
Ib [A]	49.55A	48.39
Ic [A]	61.08 A	60.02

6 Voltage rise mitigation by power curtailment

Two previous chapters describe the voltage rise mitigation techniques by using the unbalanced voltage compensation (negative-sequence current injection) and the reactive current injection. However, in some situations these two techniques are still not adequate to suppress the voltage rise, e.g. in the case of high penetration of PV generation. In order to bring the voltages back within the allowable limit, in this chapter power curtailment control will be lastly introduced. As a result, the unbalanced voltage compensation, the reactive current injection, and the power curtailment will finally be combined and operate together to solve the voltage rise problem.

6.1 Power curtailment controller

The power curtailment controller is decomposed into two parts, i.e., the power controller and the droop controller, as shown in Fig. 47. The power controller will curtail the PV power if the PCC voltage is greater than the critical value (1.05 pu). The droop controller will further limit the output power of the power controller part if the voltages remain over the acceptable range.

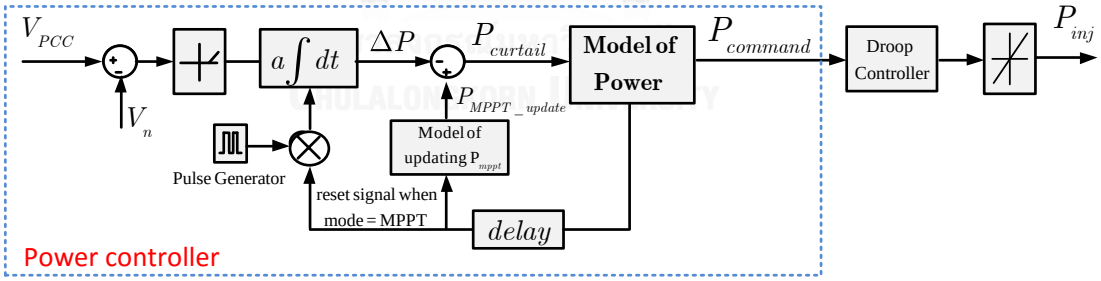

Fig. 47. Schematic for power curtailment controller.

6.1.1 Design of the power controller

The power controller in Fig. 47 is designed to work only when the PCC voltage (V_{PCC}) exceeds the critical voltage (V_{cri}),which is equal to 23.1 kV. This is to avoid unnecessary power curtailment when the voltage is in the acceptable range between 22 kV and 23.1kV.

Based on trial and error, the adjusting factor a of the integrator is set to 4000 so as not to cause any instability. The integrator will be reset according to the signal of the

pulse generator and the reset signal from the MPPT algorithm as illustrated in the flow chart of Fig. 48(a). The action of the integrator helps to decrease the commanded power ($P_{command}$) to be generated from the PV inverter until the PCC voltage comes back to the acceptable range. Normally, during power curtailment $P_{command}$ will be lower than the MPPT power P_{MPPT} . However, when the requested $P_{command}$ becomes higher than the MPPT power P_{MPPT} , the inverter will switch to operate in the MPPT mode and will also acknowledge and update the new value of P_{MPPT} (denoted by P_{MPPT_update} in Fig. 47) as shown in Fig. 49. At this moment, the integrator will also be reset because there is no need to curtail power anymore. The overall operation of MPPT with power curtailment is explained in Fig. 50(a)-(b). The output of the MPPT block as defined by $P_{command}$ will be sent to the droop controller, by which the final output power from the PV inverter denoted by P_{inj} , will be determined according to the power-voltage droop characteristic shown in Fig. 51.

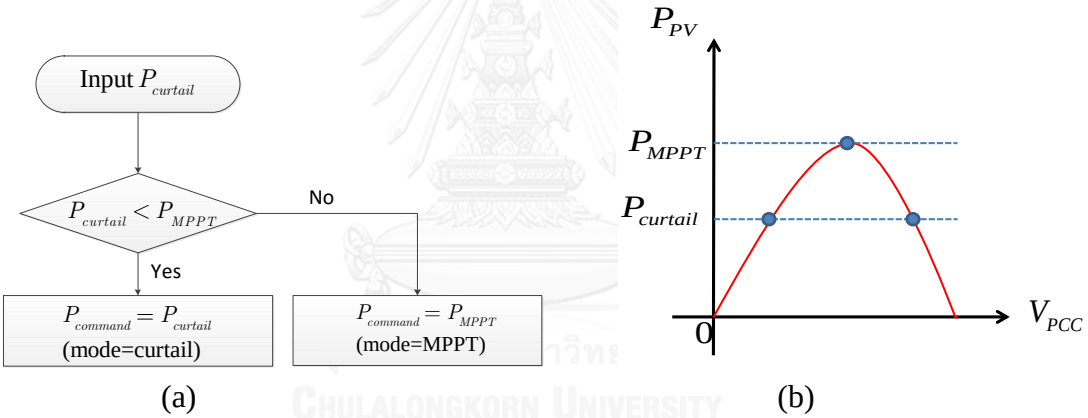

Fig. 48. MPPT with power curtailment. (a) Mode of operation and output power. (b) Operating point on PV curve.

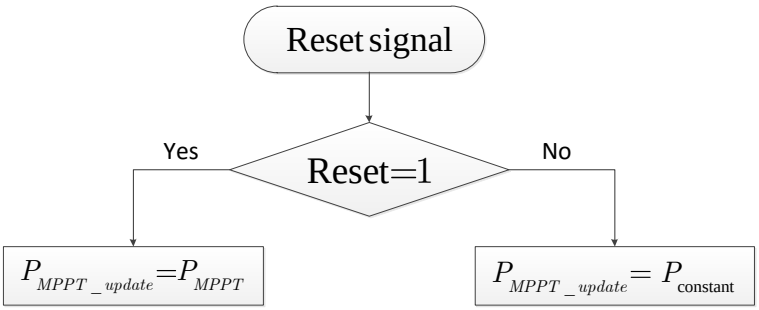

Fig. 49. The flow chart for updating the MPPT power.

6.1.2 Design of the droop controller

Fig. 50(a) shows the details inside the droop controller. This droop controller will help to further reduce the power from PV during transient. The droop will reduce the power injection when the PCC voltage is between 1.05 pu and 1.1 pu according to the slop m_2 defined in Eq. (47). The injected power (P_{inj}) will become zero when the voltage is larger than 1.1 pu as depicted in Fig. 50(b). Therefore, the power injected into the system is determined by the flow chart in Fig. 51.

$$m_2 = \frac{P_{command}}{V_{\max} - V_{cri}} \tag{47}$$

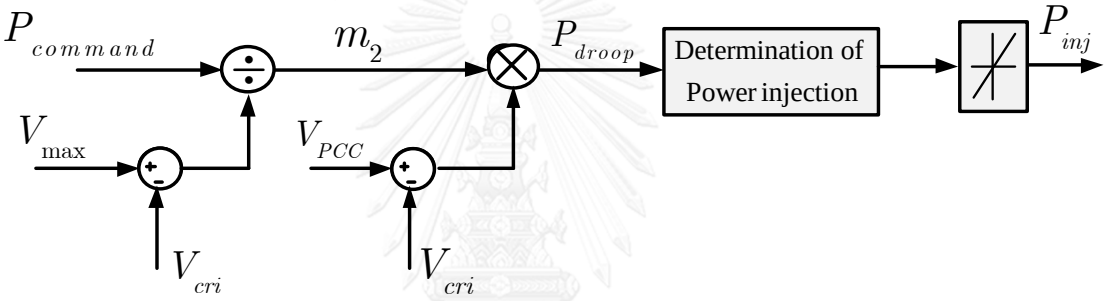

(a)

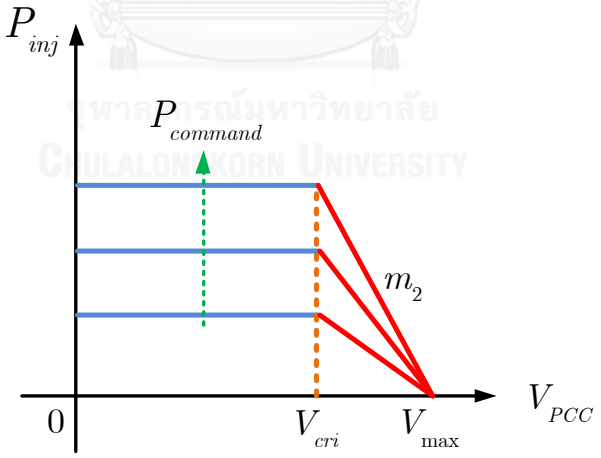

(b)

Fig. 50. Details of the droop controller. (a) Schematic of droop controller. (b) power-voltage droop characteristic.

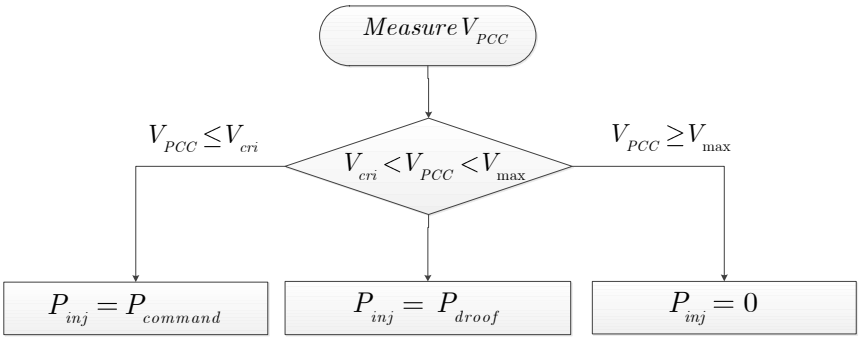

Fig. 51. Algorithm for determination of power injection.

6.2 Phasor simulation of power curtailment

All the parameters used in the simulation of power curtailment are listed in Table 21. The simulation will be carried out for two different scenarios in order to examine the feasibility of the controller.

- Scenario 1: the power from PV is maintained constant and is equal to 4 MW.
- Scenario 2: the power from PV is varied.

Table 21: Parameters of the power curtailment controller.

Parameters	Value
Nominal voltage (V_n)	1 pu
Voltage limit for droop controller (V_{lim})	1.04 pu
Critical voltage (V_{cri})	1.05 pu
Maximum voltage $(V_{\max})$	1.1 pu
$P_{constant}$	5 MW
Dead zone (start/end of dead zone)	0/1100V
Pulse generator (Period/pulse width)	1.5s/0.1%
Rising slew rate	4×10^{6} MW/s
Falling slew rate	-4×10^{6} MW/s

6.2.1 Scenario 1: Constant PV power

The load variation listed in Table 22 is applied to the system with 4 MW PV generation. This PV power is kept constant along the total simulation time of 10

seconds. It should also be noted that three-phase loads are also present with Load 1= Load 2 = 1 MVA and Load 3 = 2 MVA.

Table 22: The variation of single loads in the power curtailment simulation.

	phase	Single-phase loads	time (s)										
			0	1	2	3	4	5	6	7	8	9	10
Load [kW]	a	100											
	b	300											
	c	1000											
Load [kW]	a	700											
	b	300											
	c	100											
Load [kW]	a	500											
	b	300											
	c	400											
Load [kW]	a	100											
	b	200											
	c	300											

Fig. 52 shows the generated power from the PV without and with power curtailment. In the former case, the power from PV is constant and equal to 4 MW. On the other hand, there is a serious over voltage at PCC as can be seen from Fig. 53. With power curtailment control, the power injected by the PV is decreased to be the purple line in Fig. 52. As a consequence, the voltages at the PCC stay almost always within the allowable limit. There are some intervals where the PCC voltages are suppressed but not fast enough to become lower than the limit. This may be because the adjust factor of the integrator used is too small or the rate limiter is too strict. So, besides stability, the dynamic response of the power curtailment control should also be considered in the design. The instantaneous voltage changes are also seen, and it is due to the sudden change of loads connected to the system.

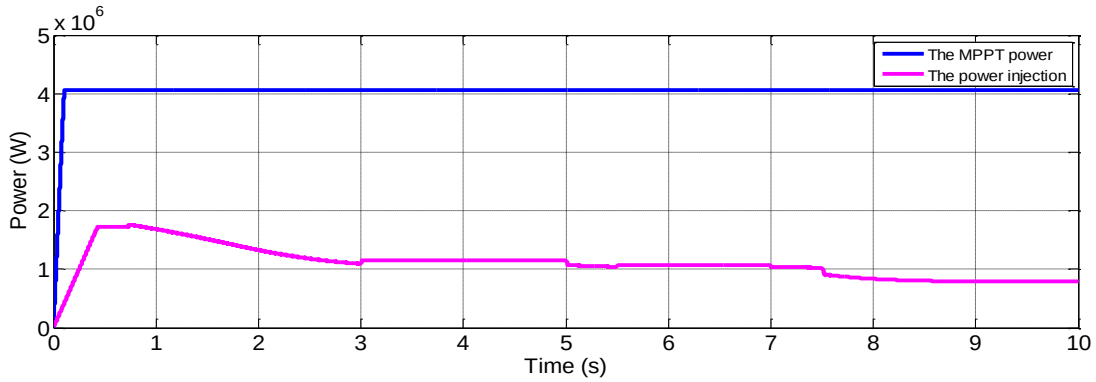

Fig. 52. The generated PV power before and after curtailment.

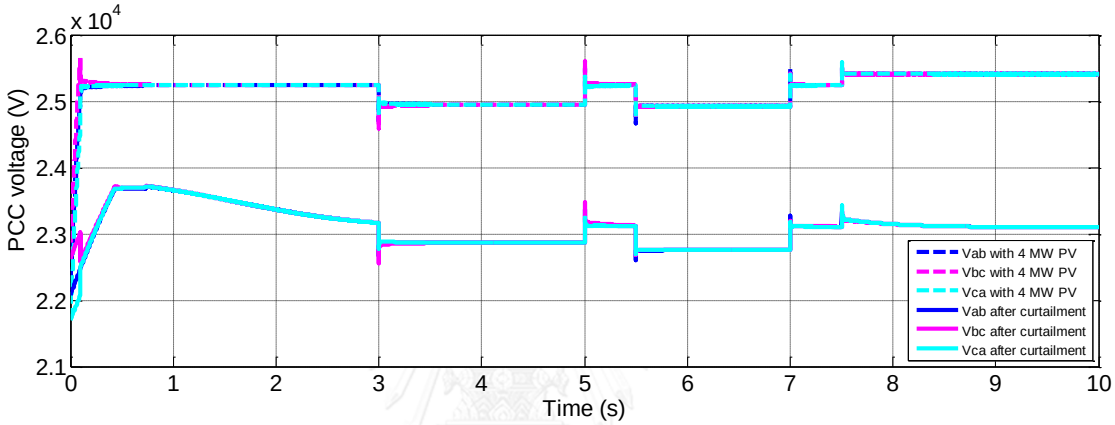

Fig. 53. PCC voltages and inverter currents with power curtailment.

Fig. 54 illustrates the detailed signals of the power curtailment controller. The injected power is lower than both the commanded power and that of the droop controller at the starting point due to the action of the rate limiter. The injected power and the power from the droop controller become equal between 0.4-3 s. This is indeed caused by the fact that the PCC voltage lies in the range from 1.05 pu to 1.1 pu, as depicted in Fig. 55. During 3-10 s, the voltages at PCC lie below 1.05 pu (cf, Fig. 55). Hence, the injected power is equal to the commanded power.

The simulation results thus verify the effectiveness of the power curtailment control in reducing the PCC voltage even with the varying loads.

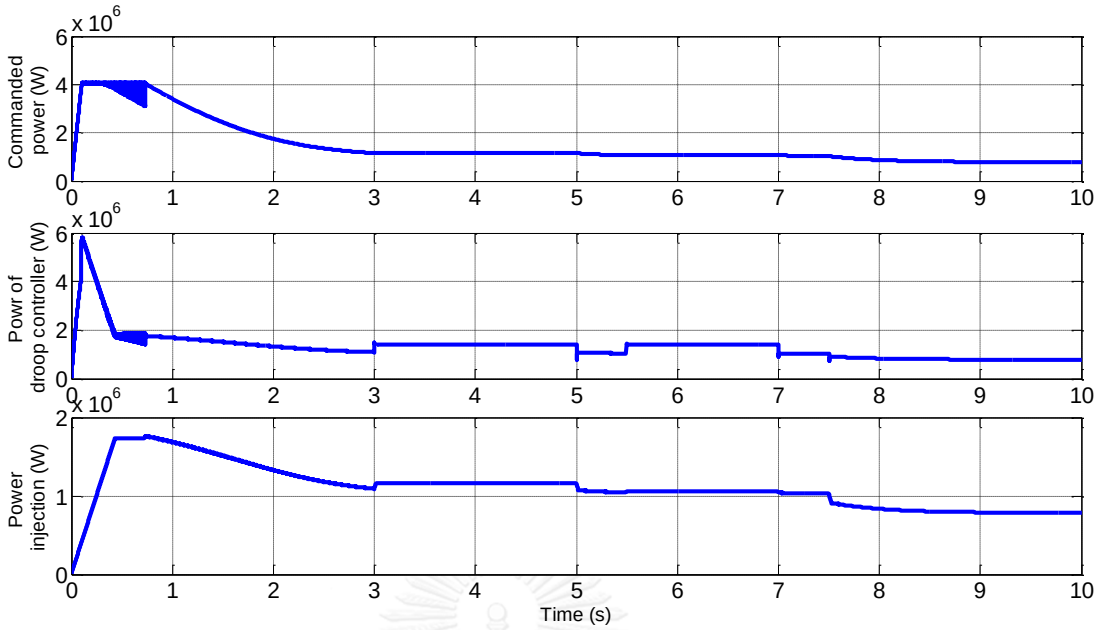

Fig. 54. Variation of the power signals of the power curtailment controller.

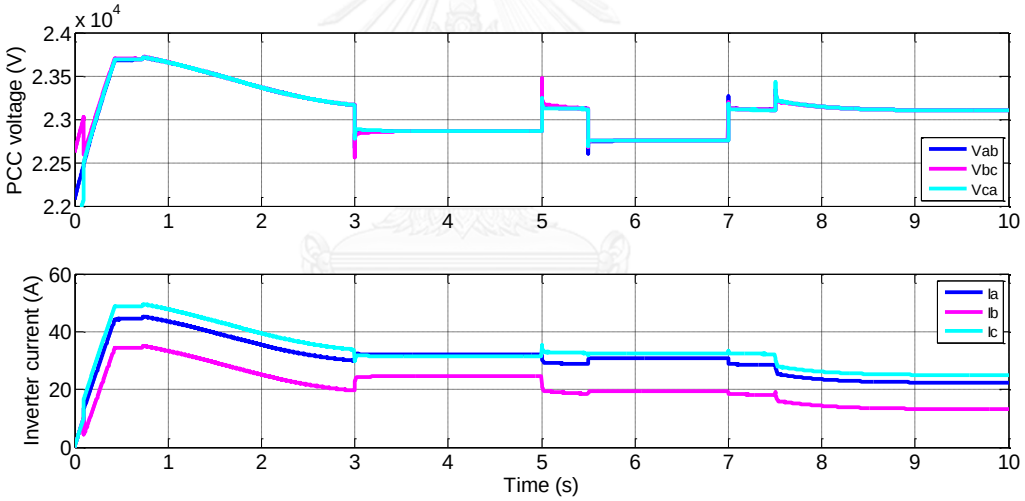

Fig. 55. The PCC voltages and inverter currents after power curtailment.

6.2.2 Scenario 2: Varying PV power

In real situation, the output power from the PV is not constant. It varies according to the weather condition. In this scenario, the MPPT power of the PV is varied according to Fig. 56(a). With the proposed power curtailment control, the real injected power is lowered as depicted in Fig. 56(b), and the corresponding PCC voltages and the inverter currents are illustrated in Fig. 56(c).

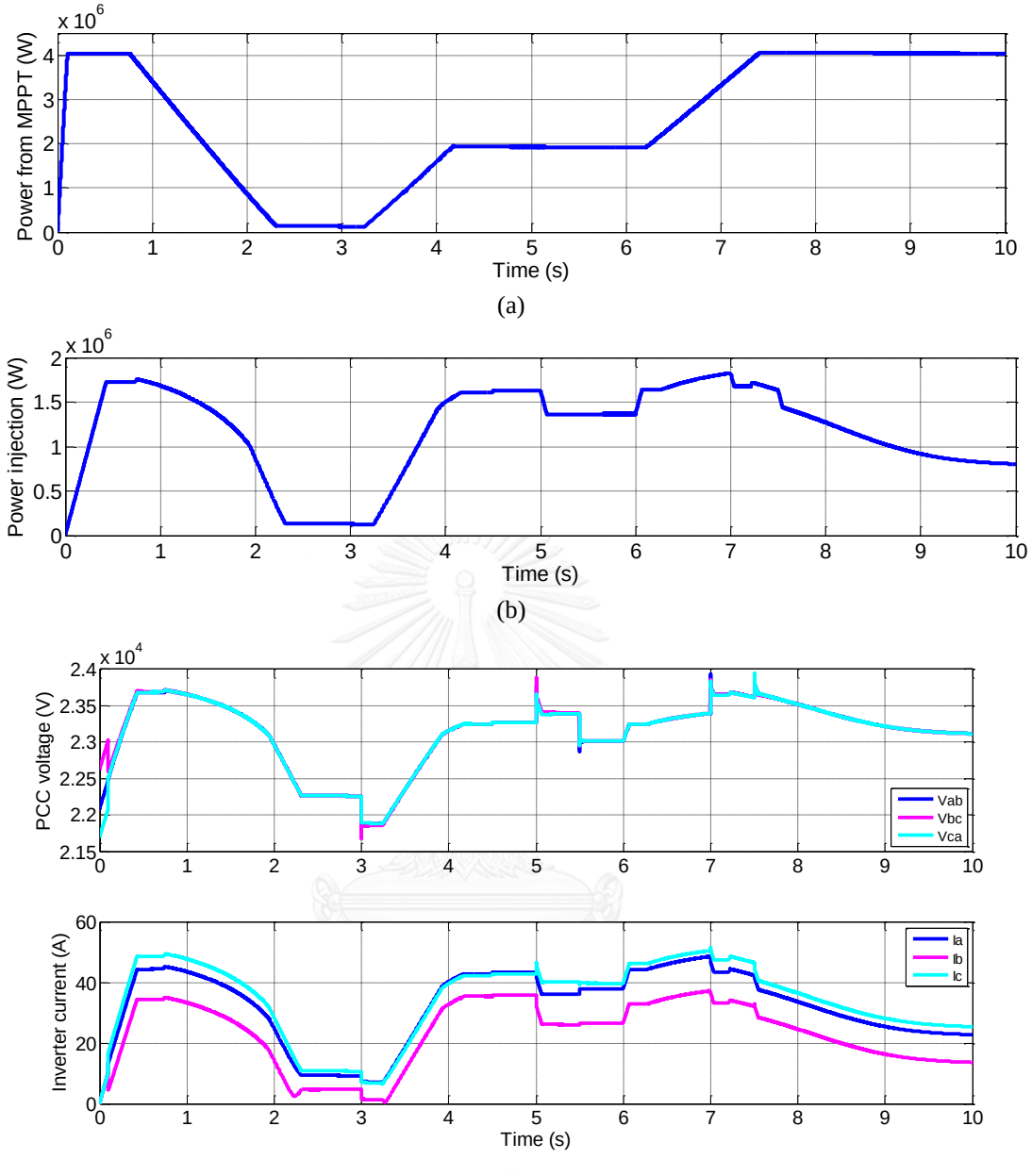

Fig. 56. Simulation results with varying PV generation. (a) The MPPT power . (b)The injected power by the PV inverter. (c) PCC voltages and inverter currents.

According to Fig. 56(c), the PCC voltages start decreasing because of the reduction of the output power from the PV. At around 2s, the generated PV power P_{inj} is decreased to be lower than 1MW, which results in the drop of the PCC voltages below 23 kV. The voltages continue to drop below 22 kV at 3 s as the consequence of the connection of loads to the system (see Table 23).

When the irradiation becomes high and the MPPT power of the PV P_{mppt} increases to 2 MW at the instant 4.2 s, the generated PV power P_{inj} is regulated to 1.6 MW in

order to keep the PCC voltages around 23.1 kV. At the instant of 5s, a single-phase load is disconnected, and the PCC voltage is increased again. At the instant of 5.5s, another single-phase load is connected to the system. Hence, the PCC voltages are reduced to 23 kV. As a result, the PV still injects the same amount of power into the system.

From the instant 6s to 7s, the generated PV power is increased by a small amount due to the rise of PV MPPT power up to 4MW. However, the voltages become a little higher than the acceptable range. Hence, the power curtailment stays around the same level as that at the instant of 5s. At instant 7s and 7.5s, two single-phase loads are disconnected, and the PCC voltages are increased to 23.6 kV. The power curtailment starts to regulate slowly the generated PV power in order to bring the voltage down to the allowable limit. As a result, the generated PV power reaches roughly 0.7 kW at the instant 10s.

6.3 Parallel operation of the three controllers

In this section, the power curtailment will be integrated with the unbalanced voltage compensator and the reactive current injection. So, the three controllers will hereafter work in parallel. Three simulation cases will be done to investigate the performances of the proposed voltage rise mitigation strategy. The MPPT power (P_{MPPT}) is varied as depicted in Fig. 57, and the loads in the simulation are the combination of three-phase loads, Load1 = 1 MVA, Load 2 = 1 MVA, Load 3 = 2MVA, and single-phase loads from Table 22. All the parameters of the three controllers are shown again in Table 23. For Case 1, the three-phase loads will be kept the same as mentioned above. Load3 of the three-phase loads will change from 2MVA to 0.5MVA in Case 2. The rated current of the PV inverter will be changed to 94 A in order to investigate the operation of the inverter controllers in Case 3.

Table 23: Parameters of the overall system.

Parameters	Value
System	
Line = 100 km	Impedance= $0.16 + j0.33\Omega / km$
AVR 1	Rated = 16 MVA (400A)
AVR 2	Rated = 12 MVA (300A)
LPF cut of frequency (PLL)	10 Hz
PI gain (PLL)	kp = 0.01, ki = 0.0628
Controller 1 (Negative-sequence current injection)	
LPF	$1/10\pi$ rad/s
kp	0.2
ki	1
Controller 2 (Reactive current injection)	

Rated current of the PV inverter	163.3 A
Threshol voltage of the droop controller ($V_{\lim}$)	1.04 pu
Critical voltage of the droop controller (V_{cri})	1.05 pu
Rising slew rate of the rate limiter	350
Falling slew rate of the rate limiter	-1
Saturation (upper limit/lower limit)	none/0
Controller 3 (Power curtailment controller)	
Nominal voltage (V_n)	1 pu
Voltage limit for droop controller ($V_{\lim}$)	1.04 pu
Critical voltage (V_{cri})	1.05 pu
Maximum voltage ($V_{\max}$)	1.1 pu
$P_{constant}$	5 MW
Dead zone (start/end of dead zone)	0/1100V
Pulse generator (Period/pulse width)	1.5s/0.1%
Rising slew rate	4×10^6 MW/s
Falling slew rate	-4×10^6 MW/s

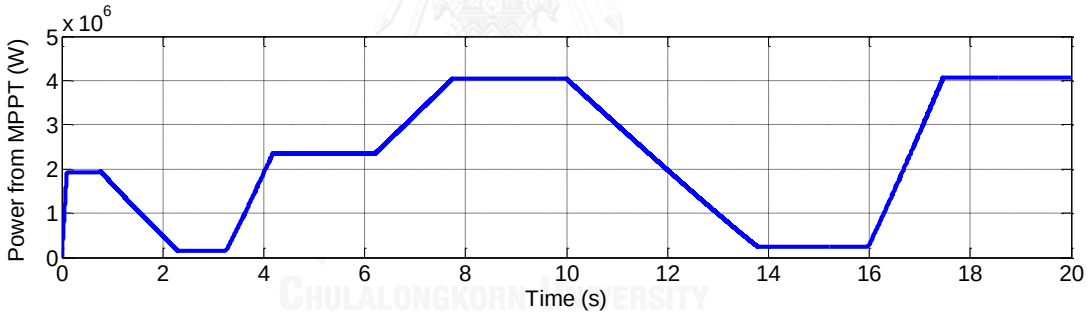

Fig. 57. The MPPT power variation for testing of the parallel operation of the three controllers.

6.3.1 Scenario 1

Fig. 58 shows the maximum reactive current ($I^+_{q\_\max}$) that can be injected into the system. The injected reactive current (I^+_q) illustrated in Fig. 59 is mostly less than the maximum possible reactive current ($I^+_{q\_\max}$) depending on the voltage levels at the PCC.

During 0-8 s, the MPPT power available from the PV (P_{MPPT}) is not high (see Fig. 60), and the increase of the PCC voltages is only at a certain low level (see Fig. 61). To bring this voltage back to the allowable limit, a small amount of reactive current (I^+_q) is needed. On the other hand, from instant 8s to 10s and from 17.5s to 20s, the active power injected by the PV into the system is very high (4 MW). As a result, the PCC

voltages increase considerably. To bring back these voltages to the allowable limit, a considerably high amount of reactive current (I_q^+) is needed. In this situation, the injected reactive current (I_q^+) goes up nearly to the maximum possible reactive current $(I_{q\_\max}^+)$. So long as there is enough reactive current to be injected into the system, the PCC voltages can always be kept at the expected level.

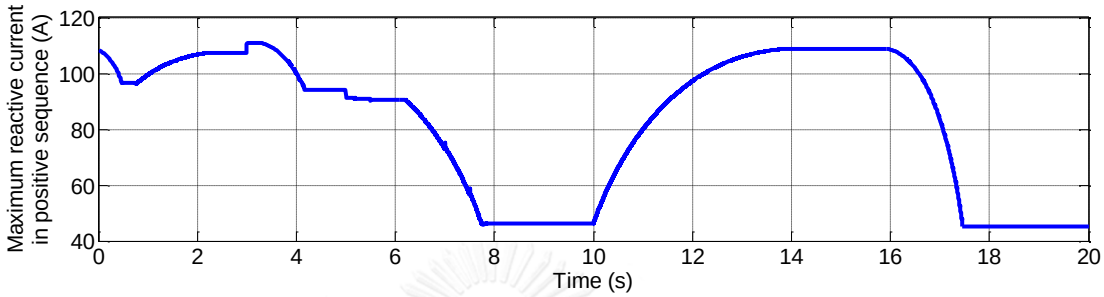

Fig. 58. The maximum limit of the reactive current in Scenario 1.

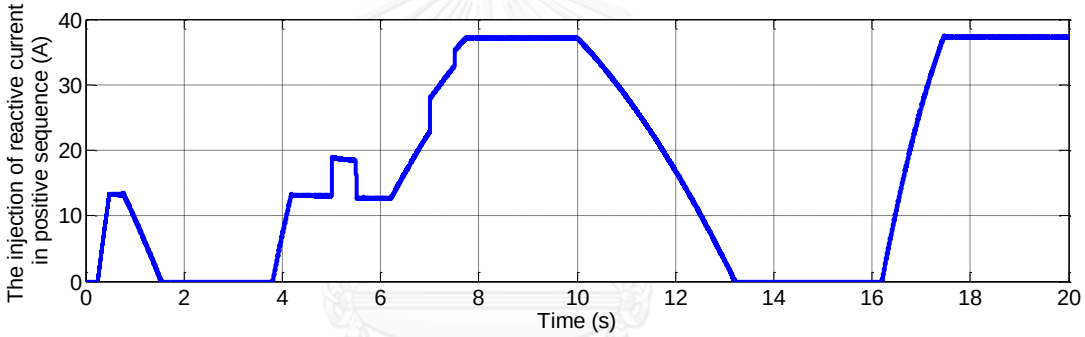

Fig. 59. The injected reactive current in Scenario 1.

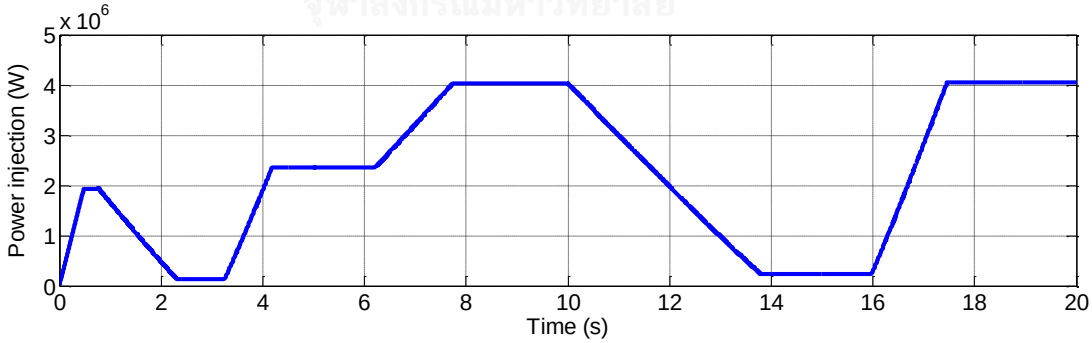

Fig. 60. PV power generated in Scenario 1.

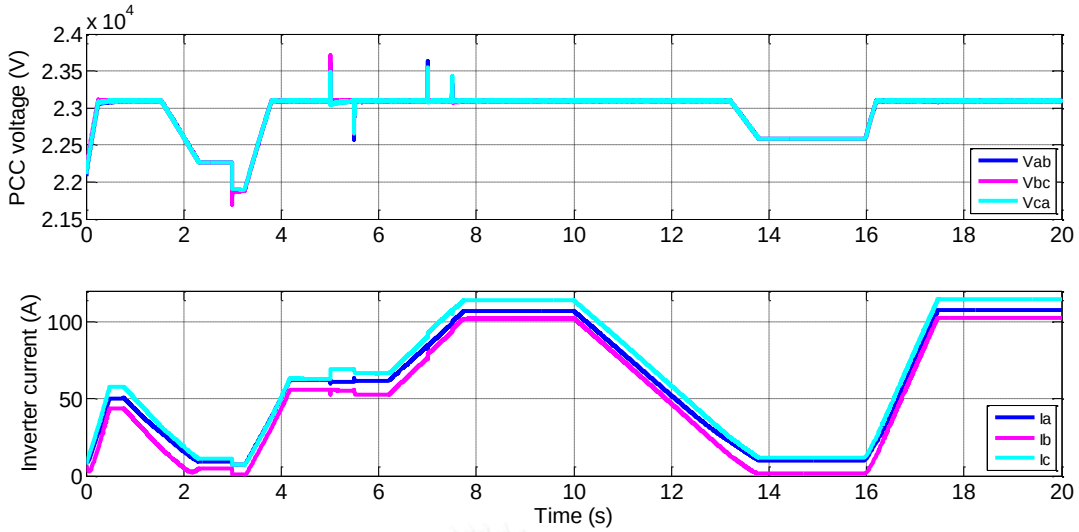

Fig. 61. PCC voltages and inverter currents in Scenario 1.

6.3.2 Scenario 2

In the previous scenario, the injection of reactive current alone can solve the problem of voltage rise. In the next scenario, one of the three-phase loads (Load 3), connected to the system is decreased dramatically from 2MVA to 0.5MAV in order to simulate severe voltage rise.

Fig. 62, Fig. 63 and Fig. 64 depict, respectively, the maximum reactive current available for injection into the grid ($I^{+}_{q\_\max}$), the actual injected reactive current (I^{+}_{q}) and the actual power injected by the PV to the grid. When the load is changed to 0.5 MVA, the PCC voltages increase significantly. The active power curtailment controller is then activated and reduces the injected active power whenever the voltage is over the limit.

At the instant of 8 s, the power generated from the PV reaches its maximum value, which is equal to 4MW in this case. Hence, the maximum reactive current available for injection ($I^{+}_{q\_\max}$) becomes very small. The reactive power controller tries to inject all the available reactive current in order to bring down the voltages back to the limit, but does not success. This behavior can be observed during 8-10 s of Fig. 62 and Fig. 63. Further action by curtailing active power is then executed. As a consequence, the active power injected into the grid does not reach the available MPPT value and is equal to only 3.5 MW in this situation.

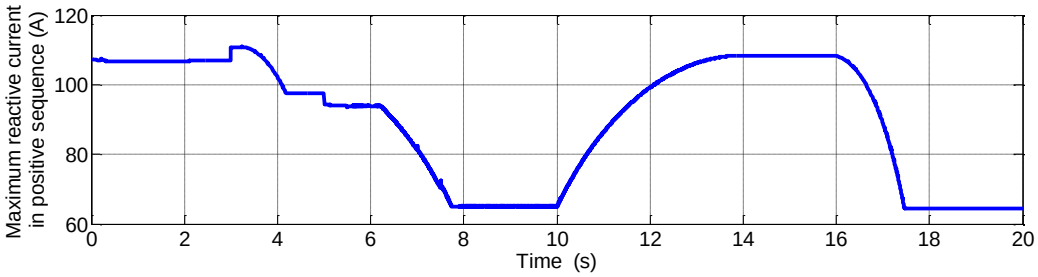

Fig. 62. The maximum limit of the reactive current in Scenario 2.

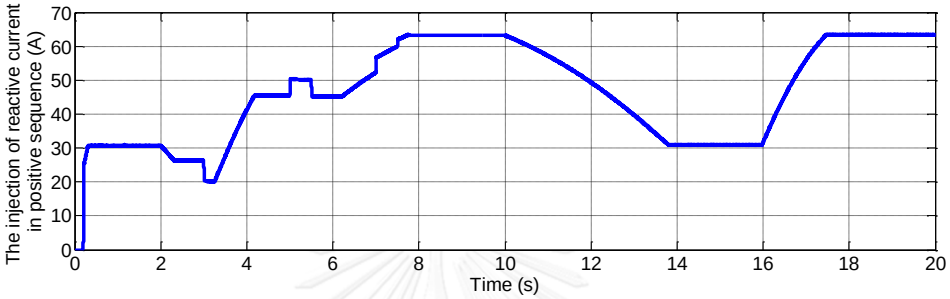

Fig. 63. The injected reactive current in Scenario 2.

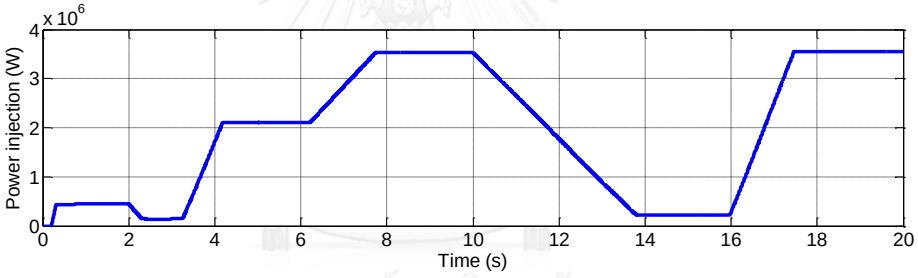

Fig. 64. PV power generated in Scenario 2.

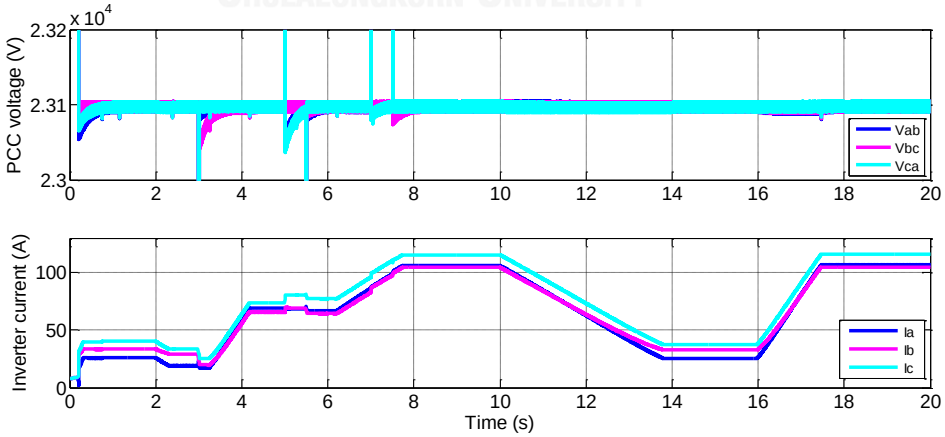

Fig. 65. PCC voltages and inverter currents in Scenario 2.

6.3.3 Scenario 3

Fig. 66 shows the maximum reactive current that can be injected into the system. $I^{+}_{q\_\max}$ is very high during the first part of operation when P_{MPPT} is very low because the remaining current capacity of inverter is increased. The PCC voltages do not exceed the limitation as can be seen from Fig. 69, when P_{MPPT} is very low. Therefore, the injection of reactive current (I^{+}_{q}) is zero for that interval (see Fig. 67). In the following period, the PCC voltages stay at 23.1 kV when P_{MPPT} increases to 2.4 MW. During this period, there is no power curtailment because enough reactive current I^{+}_{q} can be injected to reduce the voltage rise. However, when P_{MPPT} continues to increase at the instant of 6.1s, the remaining capacity inverter is reduced and it could not provide enough current capacity to generate the required I^{+}_{q} for voltage rise suppression. As a result, the active PV power has to be curtailed to maintain the voltages in the acceptable range. The PCC voltages become equal to 23.1 kV again at the instant of 10 s while P_{MPPT} is equal to 4 MW. The spikes in the voltages are noticed when the loads are changed. However, it does not provoke any problems in the system. For the subsequent period, the PCC voltages reduce below 23.1 kV when P_{MPPT} drops significantly. The capacity for $I^{+}_{q\_\max}$ is almost equal to the rated current of the inverter. However, the injection of I^{+}_{q} is zero because the controller is designed to function only for reduction of voltage rise not voltage dip.

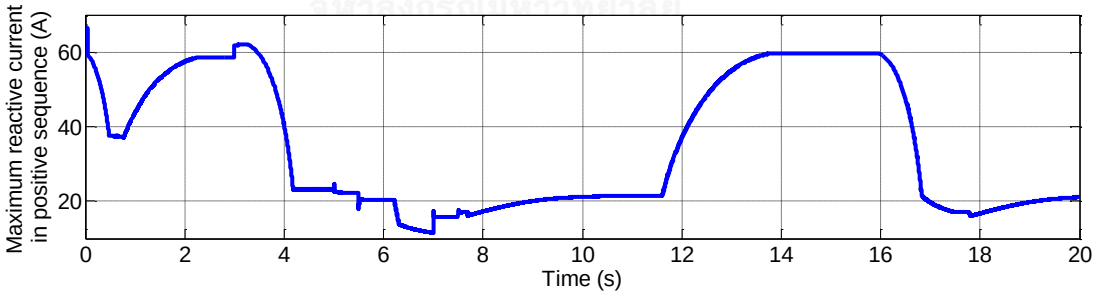

Fig. 66. The maximum limit of the reactive current in Scenario 3.

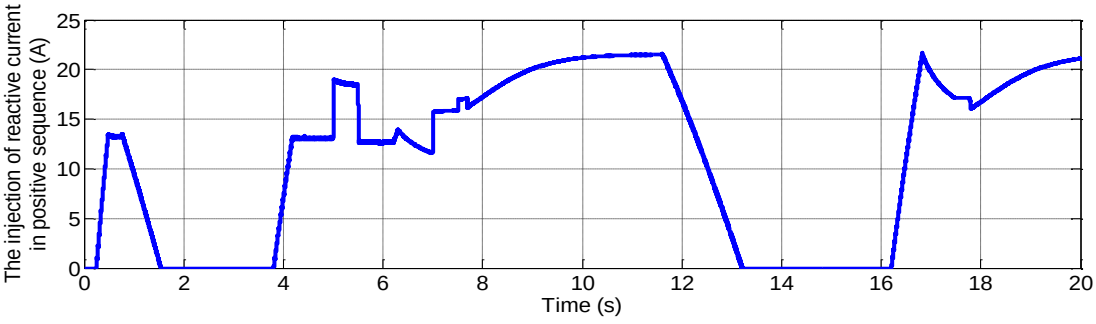

Fig. 67. The injected reactive current in Scenario 3.

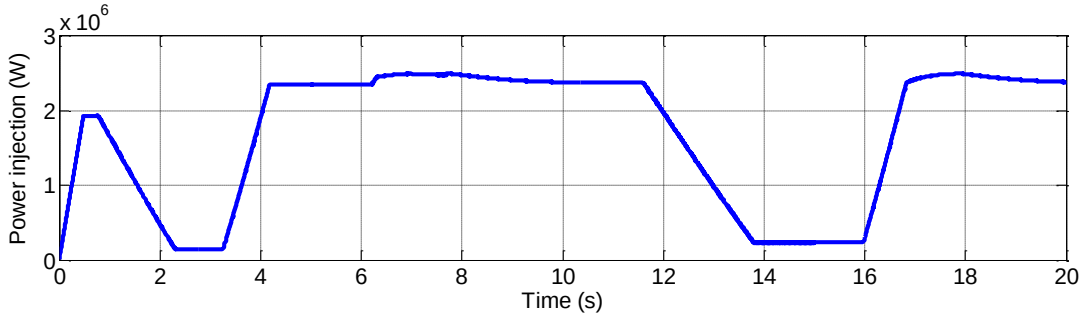

Fig. 68. PV power generated in Scenario 3.

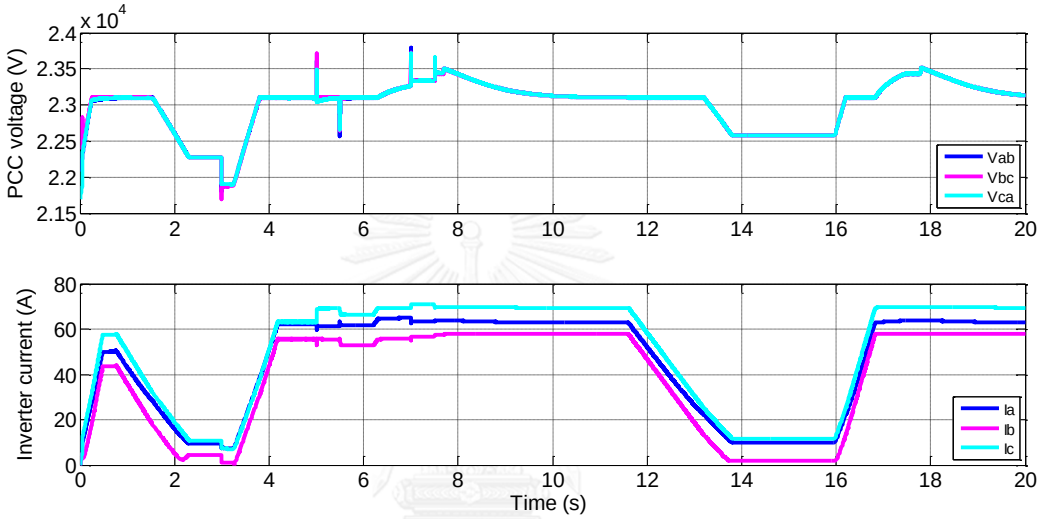

Fig. 69. PCC voltages and inverter currents in Scenario 3.

Fig. 70 illustrates the effectiveness of each controller in suppression of the voltage rise. Fig. 70(a) compares the PCC voltages for the case when none of the three controllers are applied (the three red lines) with those when the unbalanced voltage compensation is applied (the green lines). The plotted results show that the PCC voltages become balanced and the amplitudes are reduced by roughly 500 V. However, the PCC voltages are still over the acceptable range. After the application of both the negative-sequence current and the reactive current injections (I^- and I_q^+) the PCC voltages become the purple lines shown in Fig. 70(b). Parts of the PCC voltages can be kept within 23.1 kV when the current capacity of inverter is adequate. However, for the time interval (e.g. from around 6-11 s) when the PV power is high, the allowable reactive current I_q^+ is too small to suppress the voltage rise. Fig. 70(c) illustrates the PCC voltages (the blue lines) when all the three controllers are working in parallel. With the additional power curtailment, the PCC voltages now are further reduced and become mainly within the limit.

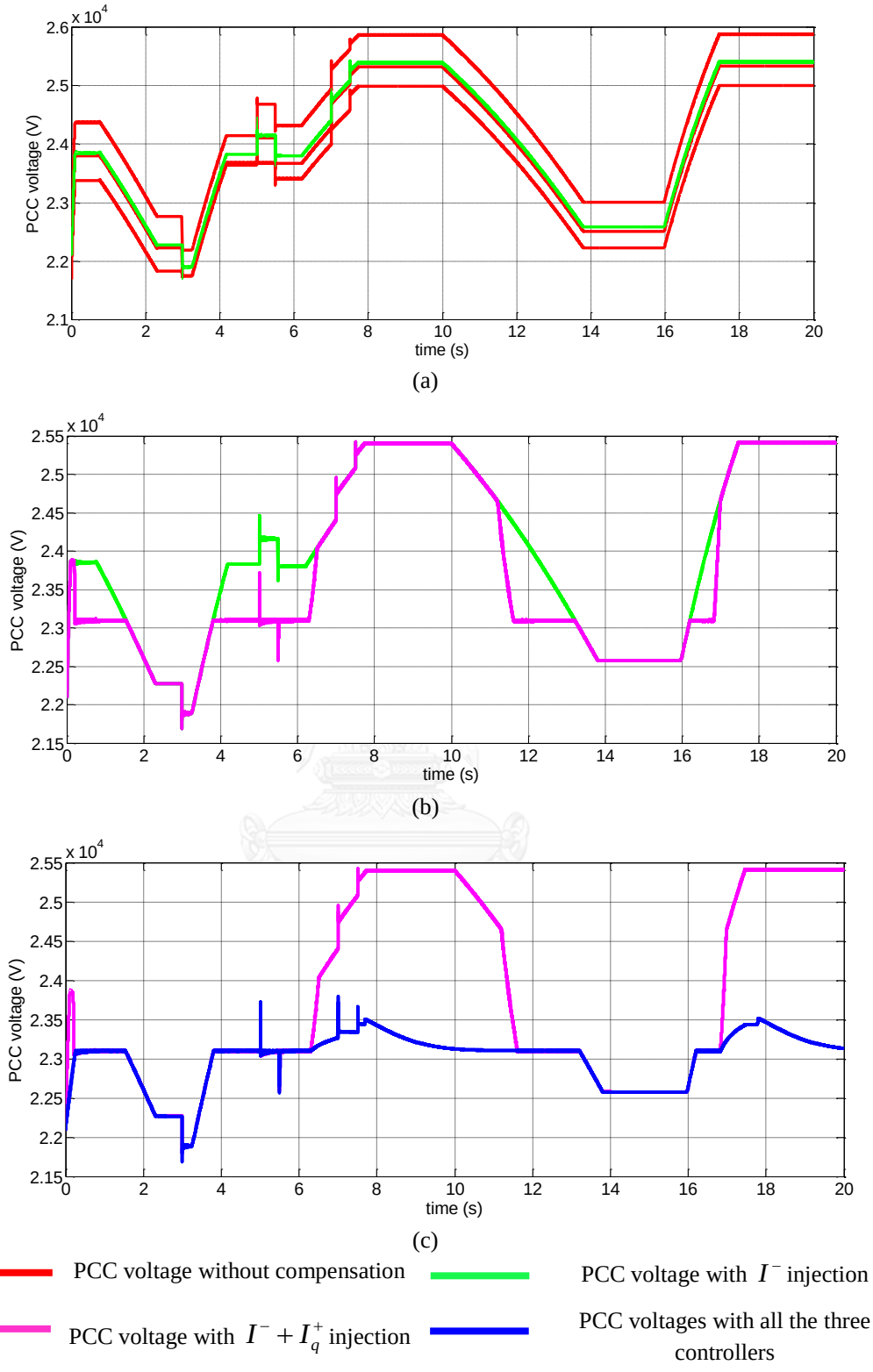

Fig. 70. Comparison of PCC voltages (a) no compensation against I^- injection. (b) I^- injection against $I^- + I_q^+$ injection. (c) $I^- + I_q^+$ injection with and without power curtailment.

7 Conclusions

The objective of this research is to reveal how unbalanced voltages can worsen the voltage rise problem and to propose a strategy to mitigate the voltage rise due to high penetration of PV generation in the unbalanced distribution network. Three controllers have been proposed: (1) unbalanced voltage compensator, (2) reactive current injection, and (3) active power curtailment.

By the first controller (1) proposed, the negative-sequence currents are injected to compensate the voltage unbalance aiming mainly to reduce the voltage rise rather than to improve the power quality. The unbalanced voltages are analyzed based on the symmetrical components. And a quantitative relationship between the voltage rise and the negative-sequence voltage is identified.

For the situations under which the voltage rise could not be totally suppressed by the unbalanced voltage compensation, the reactive current injection and the power curtailment have been proposed to provide further reduction of the voltage. Reactive current injection could help to reduce the voltage rise with some limitation depending on the inverter capacity. If there is enough remaining capacity of the PV inverter, the reactive current injection will successfully mitigate the voltage rise. Otherwise, the power curtailment will start to decrease the PV power and to bring the voltages back within the limit.

Time and phase simulations are used to confirm the correctness of the analytical results and to verify the feasibility of the proposed strategy to mitigate the voltage rise. More investigation is needed to optimize the performances of the three controllers, and it will be left as the future works.

REFERENCES

1. Quanwei, L., et al., *Voltage unbalance and harmonics compensation for islanded microgrid inverters.* IET Power Electronics, 2014. **7**(5): p. 1055-1063.
2. Demirok, E., *"Control of Grid Interactive PV Inverters for High Penetration in Low Voltage Distribution Networks"*. 2012.
3. Tonkoski, R., L.A.C. Lopes, and T.H.M. El-Fouly, *Coordinated Active Power Curtailment of Grid Connected PV Inverters for Overvoltage Prevention.* IEEE Transactions on Sustainable Energy, 2011. **2**(2): p. 139-147.
4. Bhattarai, B.P., et al. *Overvoltage mitigation using coordinated control of demand response and grid-tied photovoltaics*. in *Technologies for Sustainability (SusTech), 2015 IEEE Conference on*. 2015.
5. Marti, P., et al. *Distributed reactive power control methods to avoid voltage rise in grid-connected photovoltaic power generation systems*. in *Industrial Electronics (ISIE), 2013 IEEE International Symposium on*. 2013.
6. Ali, M.M.V.M., et al., *Fair power curtailment of distributed renewable energy sources to mitigate overvoltages in low-voltage networks*, in *PowerTech, 2015 IEEE Eindhoven*. 2015. p. 1-5.
7. Hong-Tzer, Y., et al. *Over-voltage mitigation control strategies for distribution system with high PV penetration*. in *Intelligent System Application to Power Systems (ISAP), 2015 18th International Conference on*. 2015.
8. Moawwad, A., V. Khadkikar, and J.L. Kirtley. *Interline photovoltaic (I-PV) power plants for voltage unbalance compensation*. in *IECON 2012 - 38th Annual Conference on IEEE Industrial Electronics Society*. 2012.
9. Savaghebi, M., et al. *Secondary control for voltage unbalance compensation in an islanded microgrid*. in *Smart Grid Communications (SmartGridComm), 2011 IEEE International Conference on*. 2011.
10. Yun Wei, L., D.M. Vilathgamuwa, and L. Poh Chiang, *A grid-interfacing power quality compensator for three-phase three-wire microgrid applications.* IEEE Transactions on Power Electronics, 2006. **21**(4): p. 1021-1031.
11. Yunwei, L., D.M. Vilathgamuwa, and L. Poh Chiang, *Microgrid power quality enhancement using a three-phase four-wire grid-interfacing compensator.* IEEE Transactions on Industry Applications, 2005. **41**(6): p. 1707-1719.
12. Cheng, P.T., et al., *A Cooperative Imbalance Compensation Method for Distributed-Generation Interface Converters.* IEEE Transactions on Industry Applications, 2009. **45**(2): p. 805-815.
13. Kulmala, A., *"Active Voltage Control in Distribution Networks Including Distributed Energy Resources"*. Tampere University of Technology, May 2014.
14. Hoffmann, A.G.a.V.U., *"Photovoltaic solar energy generation"*. vol. 112: Springer Science & Business Media, 2005.
15. Eth, O., *"Reactive power control of inverter for reducing voltage deviation due to solar PV generation "*. Chulalongkorn University, 2014.
16. M. Braun, T.S., T. Reimann, B. Valov, and G. Arnold, *"Optimal reactive power supply in distribution networks – Technological and economic assessment for PV systems"*. 24th European Photovoltaic Solar Energy Conference, Hamburg, September 2009: p. 1-10.
17. J. Backes, C.S., and H. Basse, *"Cost-efficient integration of dispersed generation using voltage dependent reactive power control"*. CIRED Workshop, Lyon, France, 2010: p. 1-5.
18. Demirok, E., *"Control of Grid Interactive PV Inverters for High Penetration in Low Voltage Distribution Networks"*. Department of Energy Technology, Aalborg University, 2012.
19. Stetz, T., F. Marten, and M. Braun, *Improved Low Voltage Grid-Integration of Photovoltaic Systems in Germany.* IEEE Transactions on Sustainable Energy, 2013. **4**(2): p. 534-542.
20. Wang, Y., et al., *Online Overvoltage Prevention Control of Photovoltaic Generators in Microgrids.* IEEE Transactions on Smart Grid, 2012. **3**(4): p. 2071-2078.
21. U. Stephen, C.V.a.K.V., *Implementation of a Three-Phase Electronic Watt-Hour Meter Using the MSP430F471xx.* 2009.
22. *EPM 6100 Multi-Function Power Metering System.* 2011.

23. Reginatto, R. and R. Bainy. *Induction generators phasor simulation in dq coordinates with unbalanced operating conditions*. in *2014 IEEE PES General Meeting | Conference & Exposition*. 2014.
24. Ferrero, A. and G. Superti-Furga, *A new approach to the definition of power components in three-phase systems under nonsinusoidal conditions.* IEEE Transactions on Instrumentation and Measurement, 1991. **40**(3): p. 568-577.

APPENDIX

APPENDIX A

A.1 Maximum power point tracking (MPPT)

Perturb and Observe (P & O) is a method used to track the maximum power point as shown in the flow chart in Fig. A.1. The power of the new iteration is found by comparing to that of the previous iteration. Depending on whether the power is at the left-hand or right-hand side of the PV curve, the voltage will be increased or decreased respectively by a constant step ΔV. The algorithm will stop when there is no more change in the attainable power.

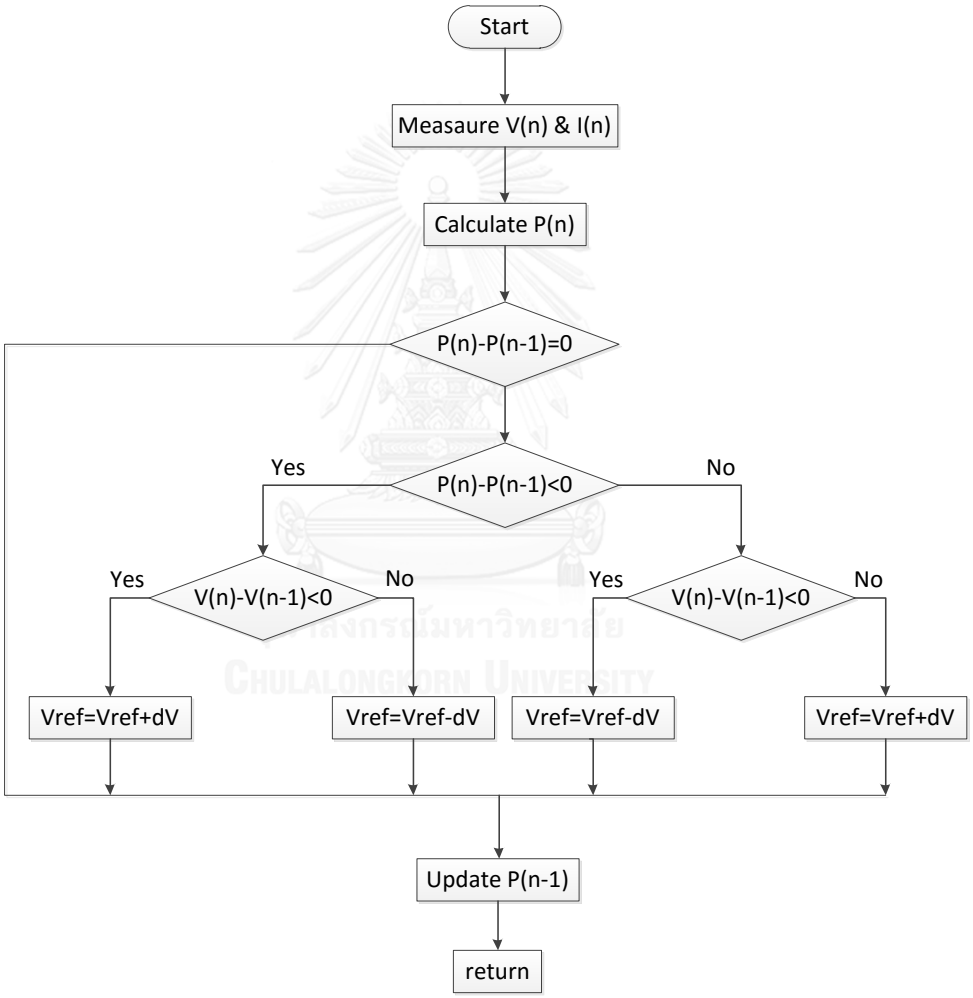

Fig. A.1. Flow chart of the maximum power point tracking.

A.2 Phase-Locked Loop in phasor simulation

In phasor simulation, there is no dynamic response in the system. Therefore, the simulation result will contain only the voltages and currents in the steady state. With this understanding, both positive- and negative-sequence voltage phasors $\mathbf{V}^{+}$ and $\mathbf{V}^{-}$

can be extracted directly based on the symmetrical components as shown in Eqs. (A.1)-(A.2) where $a = e^{j\frac{2\pi}{3}}$, $\mathbf{V}_a, \mathbf{V}_b, \mathbf{V}_c$ are the voltage phasors of *a*, *b* and *c* phases.

$$\mathbf{V}_{+-0} = \left[T_{+-0}\right]\mathbf{V}_{abc} \tag{A.1}$$

$$\begin{bmatrix} \mathbf{V}^+ \\ \mathbf{V}^- \\ \mathbf{V}^0 \end{bmatrix} = \frac{1}{3}\begin{bmatrix} 1 & a & a^2 \\ 1 & a^2 & a \\ 1 & 1 & 1 \end{bmatrix}\begin{bmatrix} \mathbf{V}_a \\ \mathbf{V}_b \\ \mathbf{V}_c \end{bmatrix} \tag{A.2}$$

Inversely from Eq. (A.2), the positive- and negative-sequence voltages can be calculated as shown in Eq. (A.3) and Eq. (A.4), respectively.

$$\begin{bmatrix} \mathbf{V}_a^+ \\ \mathbf{V}_b^+ \\ \mathbf{V}_b^+ \end{bmatrix} = \frac{1}{3}\begin{bmatrix} 1 & e^{j\frac{2\pi}{3}} & e^{j\frac{4\pi}{3}} \\ e^{j\frac{4\pi}{3}} & e^{j\frac{6\pi}{3}} & e^{j\frac{8\pi}{3}} \\ e^{j\frac{2\pi}{3}} & e^{j\frac{4\pi}{3}} & e^{j\frac{6\pi}{3}} \end{bmatrix}\begin{bmatrix} \mathbf{V}_a \\ \mathbf{V}_b \\ \mathbf{V}_c \end{bmatrix} \tag{A.3}$$

$$\begin{bmatrix} \mathbf{V}_a^- \\ \mathbf{V}_b^- \\ \mathbf{V}_b^- \end{bmatrix} = \frac{1}{3}\begin{bmatrix} 1 & e^{j\frac{4\pi}{3}} & e^{j\frac{2\pi}{3}} \\ e^{j\frac{2\pi}{3}} & e^{j\frac{6\pi}{3}} & e^{j\frac{4\pi}{3}} \\ e^{j\frac{4\pi}{3}} & e^{j\frac{8\pi}{3}} & e^{j\frac{6\pi}{3}} \end{bmatrix}\begin{bmatrix} \mathbf{V}_a \\ \mathbf{V}_b \\ \mathbf{V}_c \end{bmatrix} \tag{A.4}$$

A.3 Current-source model of PV generation in phasor simulation

The mathematical current-source model of the PV inverter in phasor simulation is presented in Fig. A. 2. Generally, the per-phase active power of the inverter (P_{abc}) is equal to the total active power at the dc side (P) divided by 3. And finally the inverter current phasor can be found as in Eq. (A.6). It should be noted here that in the simulation the phasor's amplitude is set to be the peak value of the sinusoidal function.

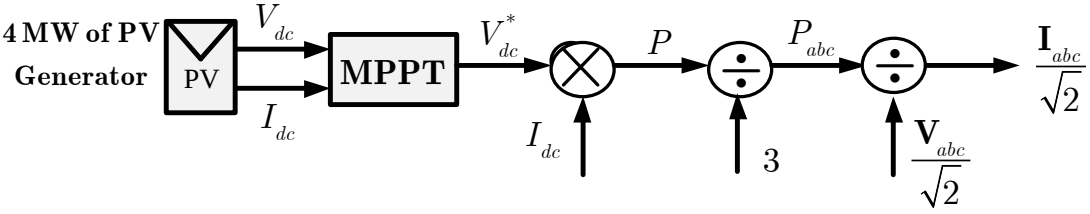

Fig. A. 2. Current-source model of the PV inverter in phasor simulation.

$$P_{abc} = \frac{P}{3} = V_{rms} \cdot I_{rms} = \frac{V_{abc}}{\sqrt{2}} \cdot \frac{I_{abc}}{\sqrt{2}} \quad \text{(A.5)}$$

$$\Rightarrow \mathbf{I}_{abc} = \frac{2}{3} \cdot \frac{P}{V_{abc}} \quad \text{(A.6)}$$

A.4 Phase-Locked Loop in time simulation

Phase-locked loop (PLL) is a method that is used to synchronize two systems. In Fig. A.3, a PLL is used to synchronize between the grid and a PV power plant. The phase angle and frequency of the PLL are adjusted until the instantaneous voltage in the q axis (v_q) becomes zero. The phase angle θ is the position of the d axis as shown in Fig. A.4. Under balanced voltage condition, the PCC voltage will has only the positive-sequence component, and there would be no need to use a low pass filter (LPF) in the PLL to extract the positive-sequent components. However, under unbalanced voltage condition, the PCC voltage will contain both the positive- and negative-sequence components. Therefore, a LPF is necessary to eliminate the negative-sequence component in the signal v_q.

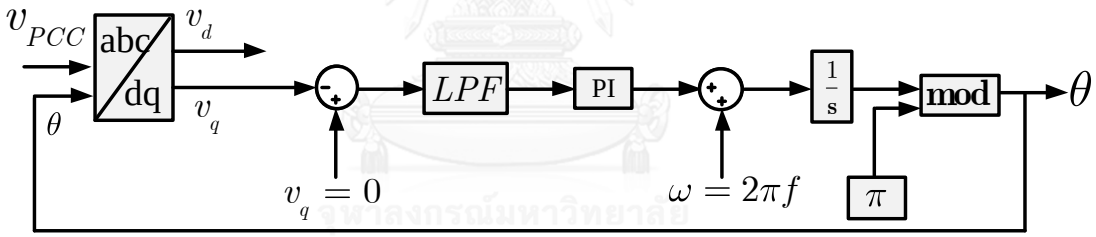

Fig. A.3. Schematic of phase-locked loop.

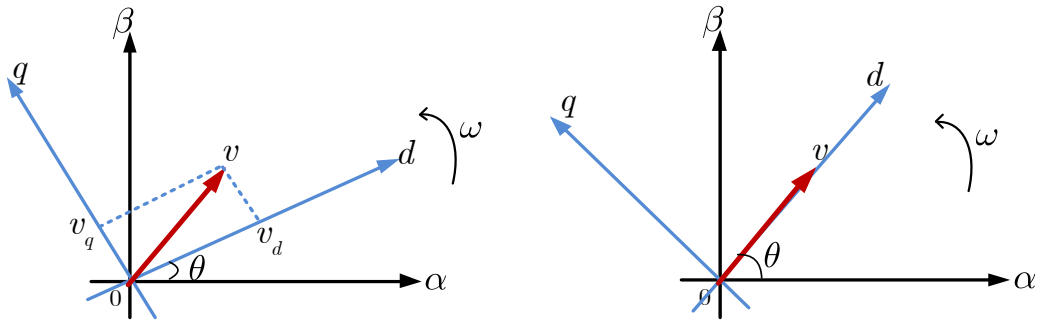

(a) *(b)*

Fig. A.4. The $d-q$ synchronous reference frame. (a) when $v_q \neq 0$. (b) when $v_q = 0$.

Under an unbalanced voltage condition in a three-phase three-wire system, the three-phase voltages will contain only positive and negative sequences, and can be expressed in $\alpha-\beta$ stationary reference as in Eq. (A.7). These positive- and negative-sequence

voltages rotate in the counter-clockwise and clockwise directions, respectively. Therefore, the corresponding synchronous reference frame of the positive sequence (dq^{+}) will rotate with the positive angular velocity ω, while the synchronous reference frame for the negative sequence (dq^{-}) will rotate with a negative angular velocity $-\omega$.

In general, the unbalanced voltage can be expressed in $\alpha-\beta$ reference frame as:

$$v_{\alpha\beta}=\begin{bmatrix}v_{\alpha}\\ v_{\beta}\end{bmatrix}=\mathbf{V}^{+}\begin{bmatrix}\cos(\omega t)\\ \sin(\omega t)\end{bmatrix}+\mathbf{V}^{-}\begin{bmatrix}\cos(-\omega t)\\ \sin(-\omega t)\end{bmatrix} \tag{A.7}$$

where v_{α}, v_{β} are the instantaneous voltages on the $\alpha-\beta$ axes, $\mathbf{V}^{+}, \mathbf{V}^{-}$ are the phasors of the positive- and negative-sequence components. From Eq. (A.7), the instantaneous voltages can be expressed on the $d-q$ rotating reference frames of the positive and negative sequences as v_{dq}^{+}, v_{dq}^{-} shown in Eqs. (A.2)-(A.3).

$$v_{dq}^{+}=\mathbf{V}^{+}\begin{bmatrix}1\\ 0\end{bmatrix}+\mathbf{V}^{-}\begin{bmatrix}\cos(-2\omega t)\\ \sin(-2\omega t)\end{bmatrix} \tag{A.8}$$

$$v_{dq}^{-}=\mathbf{V}^{+}\begin{bmatrix}\cos(2\omega t)\\ \sin(2\omega t)\end{bmatrix}+\mathbf{V}^{-}\begin{bmatrix}1\\ 0\end{bmatrix} \tag{A.9}$$

Since the synchronous reference frame of the PLL uses the $d-q$ rotating frame of the positive sequence, in order to extract only the positive-sequence component the negative-sequence term oscillating at 2ω must be filtered out by a LPF.

The transformations of the three-phase voltages from *abc* to $\alpha-\beta$ stationary reference frame, and from $\alpha-\beta$ stationary reference to $d-q$ rotating reference frame are given in Eq.(A.10) and Eq. (A.11), respectively

- From *abc* reference frame to $\alpha-\beta$ stationary reference frame

$$\begin{bmatrix}\alpha\\ \beta\end{bmatrix}=\sqrt{\frac{2}{3}}\begin{bmatrix}1 & -1/2 & -1/2\\ 0 & \sqrt{3}/2 & -\sqrt{3}/2\end{bmatrix}\begin{bmatrix}a\\ b\\ c\end{bmatrix} \tag{A.10}$$

- From $\alpha-\beta$ stationary reference frame to $d-q$ rotating reference frame

$$\begin{bmatrix}d\\ q\end{bmatrix}=\begin{bmatrix}\cos\theta & \sin\theta\\ -\sin\theta & \cos\theta\end{bmatrix}\begin{bmatrix}\alpha\\ \beta\end{bmatrix} \tag{A.11}$$

A.5 Current-source model of PV generation in time simulation

The mathematical current-source model of the PV inverter for time simulation is presented in Fig. A.5. Generally, the PV inverter will inject only the active power into the grid system, so the ac current from the current source will be at the unity power factor as calculated in Eq. (A.15).

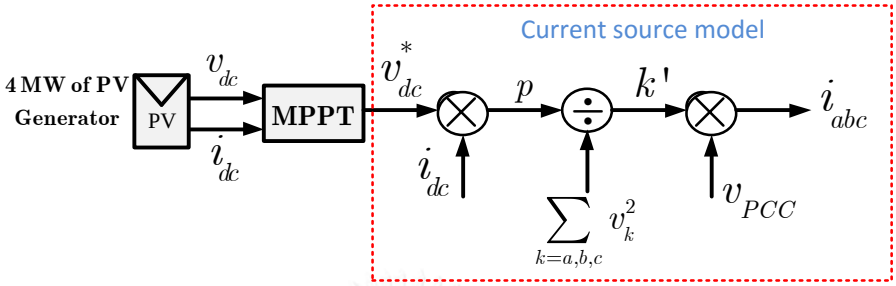

Fig. A.5. Current-source model of the PV inverter for time simulation.

For unity power factor control strategy the instantaneous currents and voltages are in phase as shown in Eq. ((A.12), therefore the instantaneous power on the AC side is given by Eq. (A.13)- (A.14) and is equal to the power *p(t)* of the PV on the dc side. The constant k' can be calculated by Eq. (A.18).

$$\begin{aligned} i_a(t) &= k' \cdot v_a(t) \\ i_b(t) &= k' \cdot v_b(t) \\ i_c(t) &= k' \cdot v_c(t) \end{aligned} \tag{A.15}$$

$$p(t) = v_a(t) \cdot i_a(t) + v_b(t) \cdot i_b(t) + v_c(t) \cdot i_c(t) \tag{A.16}$$

$$= k'\left[v_a^2(t) + v_b^2(t) + v_c^2(t) \right] \tag{A.17}$$

$$\Rightarrow k' = \frac{p(t)}{v_a^2(t) + v_b^2(t) + v_c^2(t)} \tag{A.18}$$

Each line current to be injected to the grid is found to be:

$$i_k(t) = \frac{p(t)}{v_a^2(t) + v_b^2(t) + v_c^2(t)} \cdot v_k(t), \qquad k = a,b,c \tag{A.19}$$

APPENDIX B

Calculation of the transfer function in the unbalanced voltage compensation

From the block diagram in Fig. B. 1, the transfer functions between the references r_d, r_q and the errors e_d, e_q as defined in Eq. (B. 1) can be computed as shown in Eqs. (B. 2)-(B. 5).

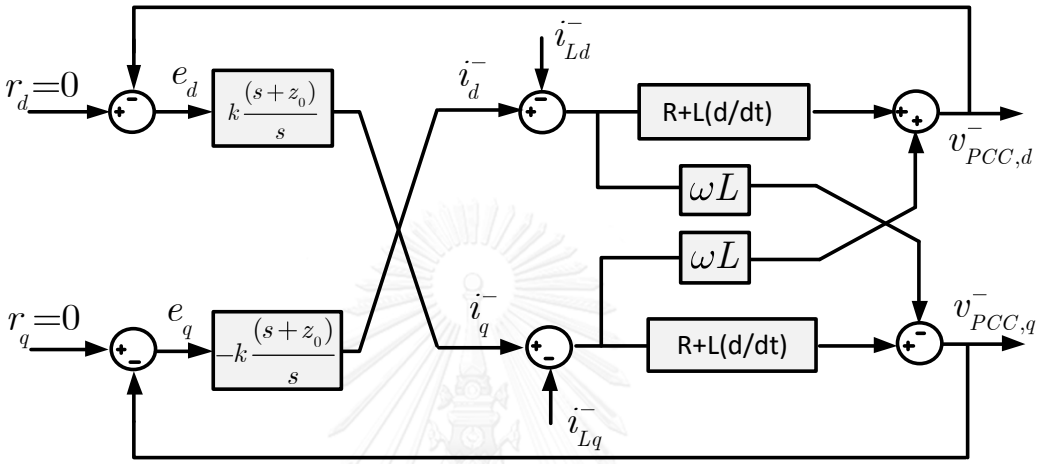

Fig.B.1 . Block diagram of the unbalanced voltage compensation by injection of negative-sequence current.

$$\begin{bmatrix} e_d \\ e_q \end{bmatrix} = \begin{bmatrix} G_{11} & G_{12} \\ G_{21} & G_{22} \end{bmatrix} \cdot \begin{bmatrix} r_d \\ r_q \end{bmatrix} \quad \text{(B. 1)}$$

$$G_{11}(s) = \frac{1 + k\frac{(s+z_0)}{s}(\omega L)}{1 + \left(k\frac{(s+z_0)}{s}\right)^2 (R+sL)^2 + \left(k\frac{(s+z_0)}{s}\right)^2 (\omega L)^2} \quad \text{(B. 2)}$$

$$G_{12}(s) = \frac{-k\frac{(s+z_0)}{s}(R+sL)}{1 + \left(k\frac{(s+z_0)}{s}\right)^2 (R+sL)^2 + \left(k\frac{(s+z_0)}{s}\right)^2 (\omega L)^2} \quad \text{(B. 3)}$$

$$G_{21}(s) = \frac{k\frac{(s+z_0)}{s}(R+sL)}{1 + \left(k\frac{(s+z_0)}{s}\right)^2 (R+sL)^2 + \left(k\frac{(s+z_0)}{s}\right)^2 (\omega L)^2} \quad \text{(B. 4)}$$

$$G_{22}(s)=\frac{1-k\frac{(s+z_0)}{s}(\omega L)}{1+\left(k\frac{(s+z_0)}{s}\right)^2(R+sL)^2+\left(k\frac{(s+z_0)}{s}\right)^2(\omega L)^2} \quad \text{(B. 5)}$$

According to Eq. (B. 2), $G_{11}(s)$ can be finally expressed as shown in Eq. (B. 6)

$$G_{11}(s)=\frac{s^2+k\omega Ls^2+k\omega Lz_0 s}{\left[\begin{array}{l}k^2L^2s^4\left(2RLk^2+2z_0k^2L^2\right)s^3+\left(1+k^2R^2+4RLz_0k^2+k^2z_0^2L^2+k^2\omega^2L^2\right)s^2\\ \left(2k^2R^2z_0+2RLz_0^2k^2+2k^2z_0\omega^2L^2\right)s+\left(k^2z_0^2R^2+k^2z_0^2\omega^2L^2\right)\end{array}\right]} \quad \text{(B. 6)}$$

APPENDIX C

C.1 Time simulation results of voltages and currents in Case 3 and Case 4

Table 24: Voltages and currents at each bus with 2 MW PV and without the injection of negative-sequence current.

	Bus					Three-phase loads			Single-phase loads
	B1	B2	B3	B4	B5	load 1	load2	load3	load4
Vab [kV]	22	23.09	23.74	23.86	24.05	23.09	23.74	23.86	23.86
Vbc[kV]	22	23.26	24.11	24.39	24.58	23.26	24.11	24.39	24.39
Vca [kV]	22	22.96	23.52	23.56	23.74	22.96	23.52	23.56	23.56
Ia [A]	124.6	85.91	43.2	51.97	48.6	27.28	27.9	55.98	17.37
Ib [A]	132.8	90.36	44.17	52.26	48.56	27.64	28.61	57.97	6.283
Ic [A]	138.3	98.97	54.38	51.61	48.57	27.48	28.35	57.26	19.52

Table 25: Voltages and currents at each bus with 2 MW PV and with the injection of negative-sequence current at the instant of 0.5 s.

	Bus					Three-phase loads			Single-phase loads
	B1	B2	B3	B4	B5	load 1	load2	load3	load4
Vab [kV]	22	23.1	23.78	23.92	24.13	23.1	23.78	23.92	23.92
Vbc[kV]	22	23.12	23.82	23.98	24.13	23.12	23.82	23.98	23.98
Vca [kV]	22	23.09	23.77	23.91	24.13	23.09	23.77	23.91	23.91
Ia [A]	131.3	91.28	46.79	56.31	50.79	27.45	28.25	56.96	17.66
Ib [A]	131.9	91.47	46.67	44.9	41.8	27.48	28.31	57.14	6.168
Ic [A]	132.6	92.45	47.76	55.27	53.87	27.47	28.3	57.1	19.68

Table 26: PCC voltages and inverter currents with 2 MW PV before and after the injection of negative-sequence current.

Bus 5 (B 5) before compensation							
Vab [kV]	24.05	V^+ab [kV]	24.15	V^-ab [V]	485	Ia [A]	48.6
Vbc [kV]	24.58	V^+bc [kV]	24.11	V^-bc [V]	485	Ib [A]	48.56
Vca [kV]	23.74	V^+ca [kV]	24.11	V^-ca [V]	485	Ic [A]	48.57
Bus 5 (B 5) after compensation							
Vab [kV]	24.13	V^+ab [kV]	24.13	V^-ab [V]	1.5	Ia [A]	50.79
Vbc [kV]	24.13	V^+bc [kV]	24.13	V^-bc [V]	1.5	Ib [A]	41.8
Vca [kV]	24.13	V^+ca [kV]	24.13	V^-ca [V]	1.5	Ic [A]	53.87

C.2 Phasor simulation results of voltages and currents in Case 1 to Case 4

Table 27: Voltages and currents at each bus with 0 MW PV and without the injection of negative-sequence current (from phasor simulation).

	Bus					Three-phase loads			Single-phase loads
	B1	B2	B3	B4	B5	load 1	load2	load3	load4
Vab [kV]	22	22.4	22.52	22.22	22.27	22.4	22.52	22.22	22.22
Vbc[kV]	22	22.54	22.85	22.72	22.77	22.54	22.85	22.72	22.72
Vca [kV]	22	22.26	22.29	21.95	21.99	22.26	22.29	21.95	21.95
Ia [A]	142.2	117.1	83.15	17.43	0	26.46	26.45	52.13	16.18
Ib [A]	147.2	118	80.09	17.48	0	26.79	27.12	53.98	5.852
Ic [A]	154.8	128.2	91.5	17.34	0	26.63	26.85	53.33	18.19

Table 28: Voltages and currents at each bus with 0 MW PV and with the injection of negative-sequence current at the instant of 0.5 s (from phasor simulation).

	Bus					Three-phase loads			Single-phase loads
	B1	B2	B3	B4	B5	load 1	load2	load3	load4
Vab [kV]	22	22.4	22.54	22.28	22.34	22.4	22.54	22.28	22.28
Vbc[kV]	22	22.42	22.58	22.34	22.35	22.42	22.58	22.34	22.34
Vca [kV]	22	22.39	22.53	22.27	22.34	22.39	22.53	22.27	22.27
Ia [A]	147.6	120.9	84.85	23.55	6.546	26.61	26.77	53.04	16.45
Ib [A]	147.8	120.7	84.3	16.65	6.546	26.64	26.83	53.21	5.746
Ic [A]	148.8	121.9	85.52	13.44	6.546	26.63	26.82	53.19	18.33

Table 29: PCC voltages and inverter currents with 0 MW PV before and after the injection of negative-sequence current (from phasor simulation).

Bus 5 (B 5) before compensation							
Vab [kV]	22.27	V^+ab [kV]	22.34	V^-ab [V]	455.9	Ia [A]	0
Vbc [kV]	22.77	V^+bc [kV]	22.35	V^-bc [V]	455.9	Ib [A]	0
Vca [kV]	21.99	V^+ca [kV]	22.34	V^-ca [V]	455.9	Ic [A]	0
Bus 5 (B 5) after compensation							
Vab [kV]	22.34	V^+ab [kV]	22.35	V^-ab [V]	5.415	Ia [A]	6.546
Vbc [kV]	22.35	V^+bc [kV]	22.35	V^-bc [V]	5.415	Ib [A]	6.546
Vca [kV]	22.34	V^+ca [kV]	22.35	V^-ca [V]	5.415	Ic [A]	6.546

Table 30: Voltages and currents at each bus with 600 kW PV and without the injection of negative-sequence current (from phasor simulation).

	Bus					Three-phase loads			Single-phase loads
	B1	B2	B3	B4	B5	load 1	load2	load3	load4
Vab [kV]	22	22.64	22.94	22.78	22.87	22.64	22.94	22.78	22.78
Vbc[kV]	22	22.78	23.28	23.29	23.38	22.78	23.28	23.29	23.29

Vca [kV]	22	22.5	22.71	22.49	22.58	22.5	22.71	22.49	22.49
Ia [A]	136.1	106.8	70.26	23.23	15.42	26.74	26.94	53.42	16.59
Ib [A]	142.1	108.6	67.92	23.75	15.42	27.08	27.62	55.32	5.998
Ic [A]	149.2	118.5	79.31	23.21	15.42	26.91	27.36	54.66	18.64

Table 31: Voltages and currents at each bus with 600 kW PV and with the injection of negative-sequence current at the instant of 0.5 s (from phasor simulation).

	Bus					Three phase loads			single loads
	B1	B2	B3	B4	B5	load 1	load2	load3	load4
Vab [kV]	22	22.64	22.96	22.83	22.94	22.64	22.96	22.83	22.83
Vbc [kV]	22	22.66	23.01	22.9	22.95	22.66	23.01	22.9	22.9
Vca [kV]	22	22.63	22.95	22.82	22.94	22.63	22.95	22.82	22.82
Ia [A]	141.9	111	72.36	29.52	18.26	26.89	27.27	54.35	16.86
Ib [A]	142.3	110.9	71.87	18.16	9.145	26.93	27.34	54.54	5.889
Ic [A]	143.2	112.1	73.11	23.98	20.76	26.92	27.32	54.51	18.79

Table 32: PCC voltages and inverter currents with 600 kW PV before and after the injection of negative-sequence current (from phasor simulation).

Bus 5 (B 5) before compensation							
Vab [kV]	22.87	V^+ab [kV]	22.94	V^-ab [V]	467.3	Ia [A]	15.42
Vbc [kV]	23.38	V^+bc [kV]	22.94	V^-bc [V]	467.3	Ib [A]	15.42
Vca [kV]	22.58	V^+ca [kV]	22.94	V^-ca [V]	467.3	Ic [A]	15.42
Bus 5 (B 5) after compensation							
Vab [kV]	22.94	V^+ab [kV]	22.94	V^-ab [V]	5.55	Ia [A]	18.26
Vbc [kV]	22.95	V^+bc [kV]	22.94	V^-bc [V]	5.55	Ib [A]	9.145
Vca [kV]	22.94	V^+ca [kV]	22.94	V^-ca [V]	5.55	Ic [A]	20.76

Table 33: Voltages and currents at each bus with 2MW PV and without the injection of negative-sequence current (from phasor simulation).

	Bus					Three-phase loads			Single-phase loads
	B1	B2	B3	B4	B5	load 1	load2	load3	load4
Vab [kV]	22	23.09	23.73	23.85	24.04	23.09	23.73	23.85	23.85
Vbc[kV]	22	23.25	24.1	24.38	24.57	23.25	24.1	24.38	24.38
Vca [kV]	22	22.95	23.51	23.55	23.73	22.95	23.51	23.55	23.55
Ia [A]	124.4	85.74	43.12	51.8	48.5	27.27	27.88	55.93	17.36
Ib [A]	132.6	90.15	44	52.13	48.5	27.62	28.59	57.92	6.279
Ic [A]	138.1	98.8	54.22	51.48	48.5	27.47	28.33	57.22	19.51

Table 34: Voltages and currents at each bus with 2MW PV and with the injection of negative-sequence current at 0.5 s (from phasor simulation).

	Bus					Three-phase loads			Single-phase loads
	B1	B2	B3	B4	B5	load 1	load2	load3	load4
Vab [kV]	22	23.1	23.78	23.91	24.11	23.1	23.78	23.91	23.91
Vbc[kV]	22	23.12	23.82	23.98	24.12	23.12	23.82	23.98	23.98
Vca [kV]	22	23.09	23.77	23.9	24.12	23.09	23.77	23.9	23.9
Ia [A]	131.1	91.01	46.57	56.25	50.8	27.44	28.23	56.92	17.66
Ib [A]	131.6	91.16	46.37	44.99	41.98	27.47	28.3	57.11	6.167
Ic [A]	132.4	92.26	47.58	55.34	53.97	27.46	28.29	57.09	19.68

Table 35: PCC voltages and inverter currents with 2MW PV before and after the injection of negative-sequence current (from phasor simulation).

Bus 5 (B 5) before compensation							
Vab [kV]	24.04	V^+ab [kV]	24.11	V^-ab [V]	489.2	Ia [A]	48.5
Vbc [kV]	24.57	V^+bc [kV]	24.11	V^-bc [V]	489.2	Ib [A]	48.5
Vca [kV]	23.73	V^+ca [kV]	24.11	V^-ca [V]	489.2	Ic [A]	48.5
Bus 5 (B 5) after compensation							
Vab [kV]	24.11	V^+ab [kV]	24.12	V^-ab [V]	5.82	Ia [A]	50.8
Vbc [kV]	24.12	V^+bc [kV]	24.12	V^-bc [V]	5.82	Ib [A]	41.98
Vca [kV]	24.12	V^+ca [kV]	24.12	V^-ca [V]	5.82	Ic [A]	53.97

Table 36: Voltages and currents at each bus with 4 MW PV and without the injection of negative-sequence current (from phasor simulation).

	Bus					Three-phase loads			Single-phase loads
	B1	B2	B3	B4	B5	load 1	load2	load3	load4
Vab [kV]	22	23.55	24.57	25.02	25.33	23.55	24.57	25.02	25.02
Vbc[kV]	22	23.74	24.97	25.58	25.88	23.74	24.97	25.58	25.58
Vca [kV]	22	23.43	24.35	24.71	25	23.43	24.35	24.71	24.71
Ia [A]	113.2	63.87	19.54	94.05	92.15	27.82	28.87	58.68	18.22
Ib [A]	124.3	73.46	32.06	94.28	92.15	28.19	29.61	60.77	6.588
Ic [A]	126.9	77.87	31.86	93.61	92.15	28.05	29.36	60.04	20.47

Table 37: Voltages and currents at each bus with 4 MW PV and with the injection of negative-sequence current (from phasor simulation).

	Bus					Three-phase loads			Single-phase loads
	B1	B2	B3	B4	B5	load 1	load2	load3	load4
Vab [kV]	22	23.57	24.62	25.08	25.4	23.57	24.62	25.08	25.08
Vbc[kV]	22	23.59	24.67	25.15	25.41	23.59	24.67	25.15	25.15
Vca [kV]	22	23.56	24.61	25.07	25.41	23.56	24.61	25.07	25.07
Ia [A]	120.7	70.96	26.67	97.32	94.09	28	29.24	59.71	18.52
Ib [A]	121.6	71.65	27.71	86.65	85.11	28.03	29.31	59.91	6.469
Ic [A]	122.1	72.4	27.98	98.35	97.65	28.03	29.3	59.88	20.64

Table 38: PCC voltages and inverter currents with 4 MW PV before and after the injection of negative-sequence current (from phasor simulation).

Bus 5 (B 5) before compensation							
Vab [kV]	25.33	V^+ab [kV]	25.4	V^-ab [V]	513.2	Ia [A]	92.15
Vbc [kV]	25.88	V^+bc [kV]	24.4	V^-bc [V]	513.2	Ib [A]	92.15
Vca [kV]	25	V^+ca [kV]	24.4	V^-ca [V]	513.2	Ic [A]	92.15
Bus 5 (B 5) after compensation							
Vab [kV]	25.4	V^+ab [kV]	25.41	V^-ab [V]	6.08	Ia [A]	94.09
Vbc [kV]	25.41	V^+bc [kV]	25.41	V^-bc [V]	6.08	Ib [A]	85.11
Vca [kV]	25.41	V^+ca [kV]	25.41	V^-ca [V]	6.08	Ic [A]	97.65

VITA

Lysorng OENG was born in Battambang, Cambodia in 1990. She graduated from Preah Monivong high school in 2009 and pursued her bachelor's degree at Institute of Technology of Cambodia. In 2014, she received her bachelor's degree in electrical engineering and granted a scholarship from AUN/Seed-net(JICA) to continue her Master's degree at Chulalongkorn University in August 2014. She conducted her research in Power Electronic Research Lab in the field of Smart Grids and Renewable Energy.